THE EFFECTS OF ORGANIC GASES ON ATOMIC SPECTROMETRIC SIGNALS IN THE ICP

by

Jeffrey S. Bolton

Dissertation submitted to the Faculty of the
Virginia Polytechnic Institute and State University
in partial fulfillment of the requirements for the degree of

Doctor of Philosophy

in

Chemistry

Approved:

Gary L. Long, Chairman

Raymond E. Dessy

John G. Mason

George Sanzone

Larry T. Taylor

August, 1988

THE EFFECTS OF ORGANIC GASES ON ATOMIC SPECTROMETRIC SIGNALS IN THE ICP

by

Jeffrey S. Bolton

Committee Chairman: Gary L. Long
Chemistry

(ABSTRACT)

Over the past several decades, the inductively coupled plasma (ICP) has become one of the analytical chemists most popular tools. The principle use of the ICP has been as an excitation cell for atomic emission spectrometry (AES). More recently, it has been used as an atomization cell for atomic fluorescence spectrometry (AFS). Since the ICP is an energetic source, the vaporization process is efficient. This high temperature promotes transitions of the analyte and the argon support gas making spectral interference a problem. To alleviate this problem in AFS, it was necessary to look higher in the plasma tail, now the entrainment of oxygen and the formation of metal oxides was thought to be occurring. It was proposed that the addition of an organic gas may reduce the metal oxides, thus increasing the free atom concentration. The addition of propane produced enhancements of AFS signals in the ICP.

In this study, the addition of propane and butane depressed many AES signals. In an attempt to elucidate a

mechanism for the observed discrepancies, electron number density, excitation temperature, ion temperatures, atomic emission and atomic absorption measurements were considered. The system used enabled observations to be made on the effects of organic species in the plasma without altering the analyte transport efficiency.

Using atomic absorption, scatter free data was obtained for the effects of propane on the ground state atom population, and it was observed to increase the ground state atom concentration for all elements attempted, with the exception of silver. With slurry introduction into the ICP, it was possible to control the composition of the plasma tail plume. The results from the slurries indicated that molecular formations can occur in the ICP. Finally, it was determined that a relationship between excitation energy and the effects of propane existed, and the increased ground state was due to propane hindering the excitation process of the plasma.

ACKNOWLEDGEMENTS

It has been said, this is the most difficult section of a dissertation to write, therefore it was saved until last. Not that it is difficult to thank people, but it is important not to forget anyone. First, I must thank my parents for giving me the support and the desire necessary to embark upon the long journey of education. Also, a special thanks to for having the confidence that I sometimes lacked, and for providing the sometimes required recreation time.

This research would have never been accomplished without the enthusiasm for plasma *spectrometry*, and the patience of Dr. Gary Long. Thanks go to you Dr. Long for the gentle push that was sometimes necessary to meet deadlines, and for the many scientific and personal conversations.

To the plasman, each of you helped to generate ideas for this work in you own way; I thank you, , , and . , a special thanks for your data acquisition program, and for helping me set up this word processor. , thanks for your sometimes brutal honesty, also aiding with the preparation of this work.

To my friends at Virginia Tech, its impossible to make it alone, thanks for being there, especially and . Also, thanks go to for spending time proofing and correcting much of the grammar in this dissertation.

Thanks go to for your expertise in making ICP torches, without your skill of working with quartz, our research funds would have dried up long ago.

This dissertation is dedicated to , I could not have accomplished it without your endless support.

Finally, it is necessary to thank the financial supporters of this work: PRF, DOI-BOM, Virginia Core Research, Baird Corp, and of RF Plasma.

TABLE OF CONTENTS

PAGE

Acknowledgements iv

List of Tables ix

List of Figures x

1. Introduction 1

Characteristics of the ICP 2

ICP Interferences 3

ICP Sample Versatility 4

The Addition of Organics into the ICP 5

The Need for ICP Diagnostics 6

2. Equipment 13

ICP 13

Generator and Matching Network 13

ICP Torch 17

Pencil Plasma 18

Sample Introduction 18

Gas Flow System 21

Spectrometer 23

Data Acquisition 27

Data Storage and Plotting 28

3. Atomic Emission 29

Experimental 29

Results and Discussion 30

Plasma Temperature 30

Electron Number Density..... 37
Analyte Ionization..... 40
Reduction of Metal Oxide..... 44
Atomic Emission Profiles..... 45
Mechanism of Signal Depression..... 59
4. Atomic Emission of Refractory Slurries..... 62
Sample Introduction..... 62
Results and Discussion..... 66
Temperature and Electron Number Density..... 66
Metal Oxide Formation..... 67
Molecular Formation Reactions..... 69
Physical Alteration of the ICP..... 78
Conclusions..... 83
5. Atomic Absorption..... 86
Experimental Setup..... 88
Excitation Source..... 90
Detection System..... 91
Data Collection and Presentation..... 92
Results and Discussion..... 93
Conclusions..... 109
6. Energy Studies..... 111
Experimental..... 111
Results and Discussion..... 113
ICP Power reduction..... 113
Modified Long Torch..... 118

Thermodynamic Equilibrium..... 125

Ionization Temperature..... 127

Energy Reduction..... 135

Transition Metals..... 141

Plasma Energy Density..... 146

7. Conclusions..... 151

Future Studies..... 156

References..... 158

Appendices

A Data acquisition program to take atomic emission profiles..... 163

B Fe excitation temperature using the slope method..... 166

C Proof for scatter (Fluorescence vs. Absorption)... 169

D Atomic absorption translation stage..... 171

E HCL pulsing supply..... 172

F Data acquisition program for atomic absorption profiles..... 173

G Ion temperature program..... 176

Vita..... 178

LIST OF TABLES

TABLE		PAGE
I	Typical ICP Operating Parameters	15
II	Iron Temperature Constants	31
III	Condensed Atomic Emission and Absorption Results	110
IV	Spectral Data of Ionic and Atomic lines	132
V	Local Thermodynamic Equilibrium Ion to Atom Ratios	133
VI	Calculated Ionization Temperatures	134
VII	Atomic Data Using Propane for the Group IIa Atom Emission	138
VIII	Atomic Data Using Propane for the Group IIa Ion Emission	140
IX	Atomic Data Using Butane for the Group IIa Atom Emission	143
X	Atomic Data Using Butane for the Group IIa Ion Emission	145
XI	Atomic Data for the Transition Metals	148

LIST OF FIGURES

FIGURE		PAGE
1	Plot of mass of droplets versus the droplet diameter; the cut-off diameter is labele D_c.....	10
2	Block diagram of the ICP setup.....	14
3	Schematic of a long sleeve torch.....	18
4	Schematic of a Meinhard nebulizer and a Scott type spray chamber.....	20
5	Diagram of primary, secondary, and tertiary droplet formation/separation.....	22
6	Plot of transmission versus wavelength for a fused silica fiber optic bundle.....	25
7	Plot showing how to obtain the excitation temperature spectroscopically.....	34
8	Actual scan of a 1000 ppm Fe solution, showing the wavelengths used to determine the excitation temperature.....	35
9	Excitation temperature throughout the plasma tail plume, circles are with the argon backfiller and boxes are with 20 cc/min propane..	36
10	Profile of a 50 ppm Na solution at 589.0 nm where the circles represent data points with the argon backfiller, and boxes represent data points with the addition of 20 cc/min propane....	43
11	Profile of a 500 ppm Y solution at 410.2 nm where the circles represent data points with the argon backfiller, and boxes represent data points with the addition of 20 cc/min propane....	46
12	Profile of a 50 ppm YO solution at 597.2 nm where the circles represent data points with the argon backfiller, and boxes represent data points with the addition of 20 cc/min propane....	48
13	Profile of a 250 ppm La solution at 545.5 nm where the circles represent data points with the argon backfiller, and boxes represent data points with the addition of 20 cc/min propane....	49

14 Profile of a 50 ppm Al solution at 396.2 nm where the circles represent data points with the argon backfiller, and boxes represent data points with the addition of 20 cc/min propane.... 51

15 Profile of a 50 ppm Ba solution at 553.5 nm where the circles represent data points with the argon backfiller, and boxes represent data points with the addition of 20 cc/min propane.... 53

16 Profile of a 50 ppm Cr solution at 425.4 nm where the circles represent data points with the argon backfiller, and boxes represent data points with the addition of 20 cc/min propane.... 55

17 Profile of a 50 ppm Ca solution at 422.7 nm where the circles represent data points with the argon backfiller, and boxes represent data points with the addition of 20 cc/min propane.... 56

18 Profile of a 50 ppm Mg solution at 285.2 nm where the circles represent data points with the argon backfiller, and boxes represent data points with the addition of 20 cc/min propane.... 58

19 Schematic of a Babington nebulizer and a Jarrel Ash type spray chamber..... 64

20 Profile of a 250 ppm La solution at 441.8 nm where the circles represent data points with the argon backfiller and the diamonds represent data points with 20 cc/min oxygen..... 68

21 Profile of a 1000 ppm Ti solution at 334.2 nm where the circles represent data points with the argon backfiller and the diamonds represent data points with 20 cc/min oxygen..... 70

22 Profile of a 2000 ppm titanium carbide slurry at 334.2 nm where the circles represent data points with the argon backfiller, the diamonds represent data points with the addition of 20 cc/min propane, and the triangles represent data points with the addition of 20 cc/min oxygen..... 72

23 Profile of a 2000 ppm titanium oxide slurry at 334.2 nm where the circles represent data points with the argon backfiller, the diamonds represent data points with the addition of 20 cc/min propane, and the triangles represent data points with the addition of 20 cc/min oxygen..... 74

24 Profile of a 2000 ppm tungsten carbide slurry at 407.4 nm where the circles represent data points with the argon backfiller, the diamonds represent data points with the addition of 20 cc/min propane, and the triangles represent data points with the addition of 20 cc/min oxygen..... 76

25 Profile of a 2000 ppm tungsten oxide slurry at 407.4 nm where the circles represent data points with the argon backfiller, the diamonds represent data points with the addition of 20 cc/min propane, and the triangles represent data points with the addition of 20 cc/min oxygen..... 77

26 Profile of a 2000 ppm aluminum oxide slurry at 396.2nm where the circles represent data points with the argon backfiller, the diamonds represent data points with the addition of 20 cc/min propane, and the triangles represent data points with the addition of 20 cc/min oxygen..... 79

27 Profile of a 1000 ppm aluminum solution at 396.2 nm where the circles represent data points with the argon backfiller, the diamonds represent data points with the addition of 20 cc/min propane, and the triangles represent data points with the addition of 20 cc/min oxygen..... 81

28 Oxygen flowrate study on the aluminum oxide slurry..... 82

29 Working curves of aluminum oxide slurries at 396.2 nm where the circles represent data points with the argon backfiller, the diamonds represent data points with the addition of 20 cc/min propane, and the triangles represent data points with the addition of 20 cc/min oxygen..... 84

30 Mechanisms for emission, absorption and fluorescence..... 87

31 Atomic absorption setup..... 89

32 Emission and absorption profiles for 100 ppm Ca at 422.7 where circles are with the argon backfiller and the triangles are with 20 cc/min propane..... 95

33 Emission and absorption profiles for 500 ppm Cu at 327.4 nm where circles are with the argon backfiller and the triangles are with 20 cc/min propane..... 97

34 Emission and absorption profiles for 1000 ppm Ba at 455.4 nm where circles are with the argon backfiller and the triangles are with 20 cc/min propane..... 99

35 Emission and absorption profiles for 1000 ppm Ba at 553.5 nm where circles are with the argon backfiller and the triangles are with 20 cc/min propane..... 101

36 Emission and absorption profiles for 500 ppm Ni at 352.4 nm where circles are with the argon backfiller and the triangles are with 20 cc/min propane..... 102

37 Emission and absorption profiles for 100 ppm Li at 670.7 nm where circles are with the argon backfiller and the triangles are with 20 cc/min propane..... 105

38 Emission and absorption profiles for 500 ppm K at 766.5 nm where circles are with the argon backfiller and the triangles are with 20 cc/min propane..... 106

39 Emission and absorption profiles for 1000 ppm Ag at 328.1 nm where circles are with the argon backfiller and the triangles are with 20 cc/min propane..... 108

40 Schematic of a modified long sleeve torch..... 112

41 Barium atom and ion lines at 1 kW, 1 kW with propane, and 850 W without propane..... 114

42 Profile of atom to ion ratios for Ca where the circles represent ratios with the argon backfiller and the triangles represent data points with 20 cc/min propane..... 117

43 Profile for 100 ppm Ca(II) at 393.3 nm the circles represent data points with the addition of the argon backfiller and the boxes represent data points with the addition of 20 cc/min propane..... 119

44 Profile for 100 ppm Ca(I) at 422.7 nm the circles represent data points with the addition of the argon backfiller and the boxes represent data points with the addition of 20 cc/min propane..... 121

45 Excitation temperature for the modified torch using 1000 ppm Fe the circles represent data points with the addition of the argon backfiller and the boxes represent data points with the addition of 20 cc/min propane..... 122

46 Calcium atom and ion lines at 60 mm above the induction coil for a long sleeve and a modified torch..... 124

47 The effect of Na on Ca atom (the circles) and ion (the triangles)..... 128

48 The effect of Na on Ca atom (the circles) and ion (the triangles) with the addition of 20 cc/min propane..... 129

49 Ratio of atom intensities for the group IIa with propane..... 137

50 Ratio of ion intensities for the group IIa with propane..... 139

51 Ratio of atom intensities for the group IIa with butane..... 142

52 Ratio of ion intensities for the group IIa with butane..... 144

53 Ration of atom intensities for several transition metals with propane..... 147

54 The effect of organics on the shape of the plasma ball..... 149

55 Schematic diagram of the AAS translation system..... 171

56 Schematic diagram of the HCL pulsing supply..... 172

Chapter 1

Introduction

The analytical chemist has been challenged for many years to find a technique to perform rapid, inexpensive and accurate quantitative and qualitative analysis of many different types of samples. For a number of years flame atomic absorption spectrometry (AAS) was the most popular and widely accepted technique for routine analyses. Although flame AA has parts per million (ppm) limits of detection for many elements, it is inherently a single element technique [1]. With the need to perform routine multielement analysis a more suitable technique was indicated. Inductively coupled plasma (ICP) atomic emission spectrometry (AES) was shown to be more capable of doing multielement analysis and rapidly replaced other techniques [2]. The ICP was used most commonly for aqueous samples, since organics tended to cause interferences. The addition of organic gases into the inductively plasma has been shown to cause changes in atomic spectrometric signals. Even though the ICP possesses many of the characteristics of the ideal technique, it is not perfect.

The purpose of this dissertation was to study the effects that organic species have on atomic spectrometric signals in the ICP. This was accomplished by the use of organic gases in conjunction with diagnostic techniques.

The methods utilized were atomic emission and atomic absorption spectrometry. Spatial profiles of analyte species with and without the addition of organic gases were used to elucidate a possible mechanism for the observed effects. Excitation temperatures and electron number densities were also used to characterize the effects with reference to physical and chemical interferences.

Characteristics of the ICP

Inductively coupled plasma atomic emission spectrometry meets many of the requirements for an ideal technique. The detection limits of the ICP range from 0.1 to 100 ng/mL for the majority of elements in the periodic table. The use of ultrasonic nebulizers rather than the typical pneumatic nebulizer can lower these detection limits by a factor of 3 to 10 [3-5]. There are currently other techniques used that will lower the detection limits of a few elements, such as hydride generation and desolvation systems [6]. The linear dynamic range with the ICP is 5 to 6 orders of magnitude for many elements [7]. This large working range makes it possible to look at trace, major, and minor components in a single sample without the need to make dilutions to optimize each constituent. With the ICP it is possible to analyze most of the elements on the periodic table rapidly and with

little difficulty.

The precision obtained with the ICP usually resides between 0.5 and 2.0 percent relative standard deviation [8]. There are two major sources of fluctuation in the signal output: fluctuations in the RF power input, and noise which arises from the nebulizer. The input power has been reported to cause a 1% fluctuation in signal output from a 0.1% fluctuation in input power [9]. Fluctuation in the nebulizer system arises from changes in the aerosol delivery gas, nebulizer sample uptake rate, and/or back pressure in the nebulizer chamber [10]. The power source error can be reduced by more accurately regulating the input power, and the nebulizer errors can be reduced by using a mass flow controller to regulate gas flows.

ICP Interferences

Most analytical techniques suffer from interferences, and the ICP is no exception. The interferences to which the ICP is susceptible fall into two major categories: matrix interferences and spectral interferences. Matrix interferences can be lessened or alleviated if the proper operating conditions are chosen. The ICP has been shown to be much less susceptible to interelement matrix interferences than many other similar techniques [11]. This insensitivity is due to relatively high temperature,

the inert gas environment, and the long residence time of the sample in the plasma. Due to the ICPs high temperature, most elements exhibit extremely rich emission spectra making spectral interferences quite troublesome [12]. It is possible to alleviate some of the spectral interferences by using a high resolution monochromator, but this alternative can be very expensive. Another technique for minimizing the problem of spectral interference is to use an alternative emission line for the analysis.

ICP Sample Versatility

The ICP is very versatile when it comes to analyzing different samples, but the majority are in solution form. This technique is the most accepted form of analysis. The samples are usually introduced into the plasma with a concentric or a crossflow nebulizer. The concentric type nebulizer suffers from three problems: short-term noise, long term drift, and low sample transport efficiency (1-3%) [13]. The crossflow nebulizer suffers from these same problems and is more expensive then the concentric nebulizer [14].

With the ICP, it is possible to analyze solids. The technique used for solids analysis is slurry injection, in which a suspension or slurry of the insoluble solid is prepared and directed into the plasma using a high solids

nebulizer such a the Babington [15-17]. The problems associated with solids analysis are lower sample transport efficiency and increased noise due to the size of the slurry particles.

Sample volumes necessary to produce enough signal for discrimination are usually small, and so is the quantity of solid needed to create the solution. Typical sample flow rates are 1 mL/min using a pneumatic nebulizer. Since many elements can be studied under similar operating conditions, it is possible to analyze many routine samples per hour.

The Additions of Organics into the ICP

Since the ICP was determined to be an excellent atomization and ionization source, it was only natural that investigators attempted to look at metal concentrations in organic solutions. The first to examine the ICP for its utility with organics was Truit et al. [18] and they conducted their studies in the ultraviolet-visible region of the spectrum, looking at simple hydrocarbons using atomic emission spectrometry. In their work, it was determined that the ICP could be used to observe the swan transitions C_2 (469.7 to 563.5nm). This observation was accomplished for several compounds, including some with a single carbon atom (methane, carbon tetrachloride, methyl

iodide, chloroform, carbon monoxide and carbon dioxide) for which the swan transitions were still observed, indicating molecular formations between the carbon atoms must be occurring. Transitions for CN were also observed for these compounds, indicating molecular formations between carbon and nitrogen were also occurring. Truit et al. noted an absence of CO and CO_2 emission lines in the plasma but postulated their existence.

The next group to study organics in the plasma was Alder and Mermet [19]. They looked at emissions from Zr, Hf and Zn in argon and in argon-methane plasmas. They did not observe enhancements from the methane in the emission intensities of Zr and Hf, indicating the plasma had already sufficiently dissociated these compounds. Unlike what had been postulated, LaO showed no effect upon the addition of methane. They had expected the LaO to be reduced by the free carbon in the plasma. To look for an explanation for this result a temperature investigation was attempted for the carbon containing plasma but it was inconclusive.

More recently, Caruso and co-workers [20] looked at ICP atomic emission spectrometry as a way to determine trace metals in organic solvents versus their equivalents in aqueous solutions. This work was done in an attempt to find a better method of detecting trace metals in high performance liquid chromatography effluens. This group

created the aerosol by means of a frit type nebulizer, which has a higher transport efficiency then do the more common Meinhard concentric or cross flow nebulizers [21]. One of the first observations that was noticed from their work was the addition of organic solvents into the plasma tended to increase the reflected power. Thus, some of the applied power was not making it to the plasma but being wasted by returning to the RF generator. The effects of adding an organic solvent, methanol, to the plasma were observed by looking at changes in the intensity of a Cd emission line. It was noted although an increase in transport efficiency was occurring with higher concentrations of methanol, depressions were observed in the Cd emission signals. Similar phenomena have been observed by other researchers working with the aspiration of organic solvents into the ICP [22-24]. More recently, determinations of non metals in organic solvents have been accomplished by several research groups [25-27]. It was determined by Blades et al. that by adopting the correct working conditions (high power levels and low sample uptake rates) the non-metals could be detected without matrix interferences. However, low power and normal solvent uptake rates do cause matrix interferences to occur.

The Need for ICP Diagnostics

It is necessary to understand what is occurring in the ICP, upon the addition of the organics, in order to better utilize this source. Are the changes observed due to the carbon atoms from the organics, the amount of carbon atoms in the plasma (transport efficiency), reactions occurring with the carbon atoms, or possible plasma perturbations? Using organic solvents is not the way to determine such a mechanism, because organic solvents have been observed to increase sample transport efficiency without enhancing the atomic signals. Different results have been observed upon the addition of organic gases to the ICP [28,29]. This discrepancy is an indication that organic solvents and gases are acting differently in the ICP. Using the Nukijama-Tanasawa expression it is possible to see why there may be a difference between organic solvents and gases with respect to transport efficiency of the sample to the plasma. The organic solvents transport efficiency will be altered, therefore its results should not be compared to those of aqueous samples.

$$d_o = \frac{585}{V}\left(\frac{s}{p}\right) + 597\,\frac{n}{(s\,p)^{0.5}}\left(1000\,\frac{Q_l}{Q_g}\right)$$

where:

d_o = mean droplet diameter (um)

V = velocity of gas (m/s)

s = surface tension of liquid (dyne/cm)

p = density of liquid (g/cm^3)

Q_l = flow rate of liquid (cm^3)

Q_g = flow rate of gas (cm^3)

As can be seen from the expression, the droplet size formed in a nebulizer is related to many of the physical parameters of the solvent. Therefore, it is not possible to make accurate comparisons of organic versus aqueous solutions simply on the basis of droplet size. The droplet size has greater effects later in the analyte transport process. Every spray chamber has specific characteristics, including a particular droplet cut off diameter [30]. This means that at a certain droplet diameter the sample will not make it to the plasma but instead will be lost down the drain, as can be seen in Figure 1. For the aqueous versus organic problem, it can be seen that organic solvents tend to make smaller droplets giving them a higher transport efficiency to the plasma.

Another way to look at the effects of organics in the ICP would be by the addition of an organic gas. By using a gas, it is possible to use aqueous samples for all experiments. If an organic gas is added to the spray chamber it will change the pressure in the chamber,

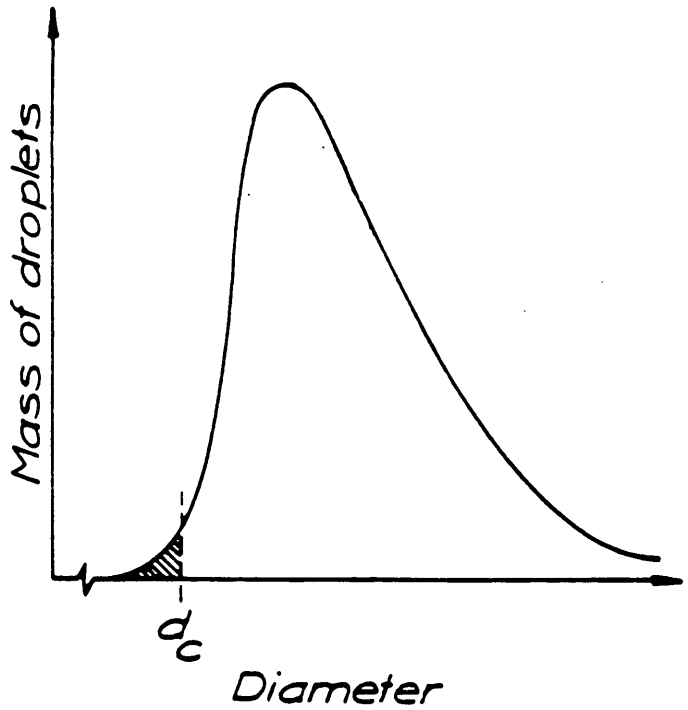

Figure 1. Plot of mass of droplets versus the droplet diameter; the cut-off diameter is labeled D_c.

possibly altering the droplet formation, and it will change the velocity of the aerosol traveling to the plasma. By changing the velocity of the aerosol, the effective droplet diameter cut off will be altered and the analyte transport efficiency will be changed. Unlike with an organic solvent, these problems can be alleviated simply by adding a fill gas to the plasma when the organic gas is not being added. It will be possible to maintain the transport efficiency at a constant value, with the spray chamber cut off diameter remaining constant. Another advantage of this system is that the residence time (the time the analyte is in contact with the plasma ball) will also remain constant. Holding all of these parameters constant will allow a true evaluation of the effects of organic species on spectrometric signals in the ICP, unlike what has previously been accomplished with organic solvents and organic gases. To help elucidate a possible mechanism for the enhancements that have been observed with atomic fluorescence the plasma was studied by changes observed in atomic emission signals, atomic absorption signals, atomic fluorescence signals, electron number densities, and plasma temperatures.

The experimental setup that was used for most emission experiments and the experimental parameters will be discussed in detail in chapter 2. In chapter 3, the

effects observed upon the addition of propane into the pencil plasma, on atomic emission spectrometric signals is discussed. This discussion deal with the problems observed with respect to excitation temperature, electron number density, and possible molecular formations. The aspect of molecular formations is examined in greater detail in chapter 4. The addition of refractory slurries to the plasma was accomplished by using a Babington nebulizer. There is a discussion on the effects to the spectrometric signals observed upon the addition of propane or oxygen. In chapter 5, atomic absorption measurements that were taken in the pencil plasma using a disassembled Baird atomic fluorescence module are discussed. These measurements were taken to obtain relatively scatter free information about the atomic ground state populations with and without the addition of propane. These experiments were accomplished to determine if the enhancements observed in AFS were due to scatter or to an increase in the ground state. In the final chapter, several different ratios of atomic emission signal intensities (ion to atom, ion to ion and atom to atom) are discussed, with and without the addition of propane to obtain information on the energy effects of organic gases on various energetic populations in the plasma tail plume.

Chapter 2

Equipment

ICP

The center of an atomic spectrometric system is the excitation source. This source must be capable of promoting the desolvation, vaporization and dissociation of the analyte species. An Inductively Coupled Plasma (ICP), which is efficient for the above processes, was used for this study (for a block diagram of the system see Figure 2). An ICP consists of a Radio Frequency (RF) generator, a matching network, an induction coil to transfer the energy from the system to a sample, and a torch and spray chamber system to contain the high temperature plasma and to deliver the analyte species to the plasma for atomization. In the following sections, these aspects of the ICP operation will be described in further detail. For a list of operating parameters see Table I.

Generator and Matching Network

For this work, a Plasma Therm HFS-2000D RF generator was used. This generator was conservatively rated at 2000 W output power. The generator used a crystal which oscillated at 13.56 MHz and a frequency doubling network to obtain a 27.12 MHz operating frequency. The output was

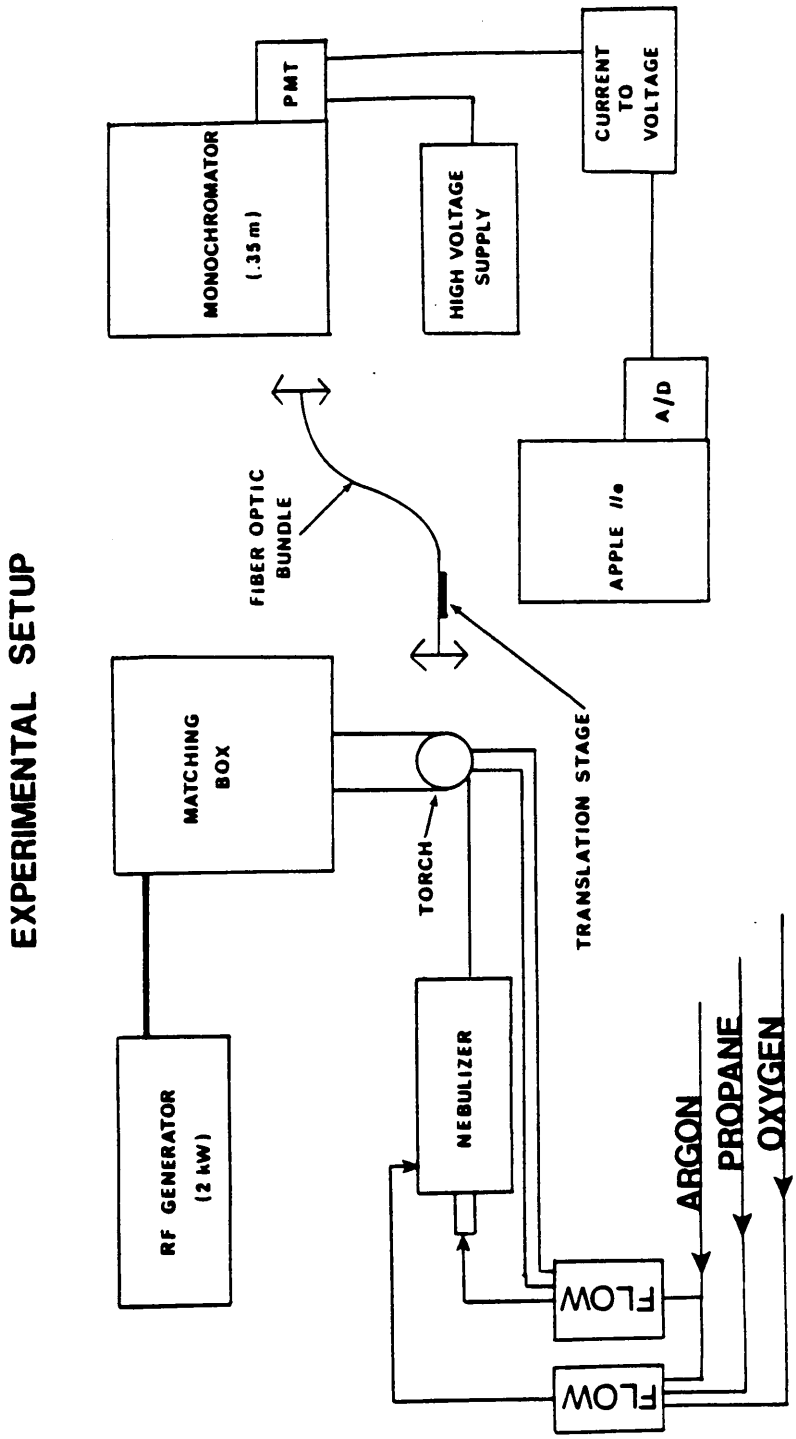

Figure 2. Block diagram of the ICP setup.

Table I - Typical ICP Operating Parameters

Incident RF power	1000 watts
Reflected RF power	0 watts
Tangential argon flow	10 L/min
Auxiliary argon flow	0 L/min
Nebulizer argon flow	2 L/min
Propane flow	20 mL/min
Filler argon flow	22 mL/min
Nebulizer uptake rate	1 mL/min
Current to voltage converter sensitivity	variable
Photomultiplier voltage	variable

generated at this frequency because of Federal Communications Commission (FCC) regulations. The system consisted of a crystal oscillator driving a buffer, which in turn drove a power amplifier. The oscillator and the buffer were the exciter portion of the RF unit. The signal must be matched to the torch and the sample so a 50 ohm impedance was sensed. To accomplish this, the network utilized variable vacuum capacitors for both tuning and loading [31]. In this study, a power setting of 1000 W incident RF was used, and with the system properly matched 0 W reflected power was observed. In order to maintain a constant output power an automatic power control network was engaged. An operational amplifier that was driven by the diode detector was sensitive to only the incident radio frequency power operated as a differential amplifier. The output of the incident power detector was fed through a voltage divider to the non-inverting input of the operational amplifier. A variable voltage was obtained from the center arm of the ten-turn incident power control, and it was fed to the inverting input of the operational amplifier. The operational amplifier compared these two voltages and produced an output proportional to their ratio. The output of the operational amplifier was used to control the output from the generator. After generating the RF signal it was necessary to transfer the energy to

the sample.

An induction coil was used to transfer the energy into the plasma. The induction coil (load coil) was a three turned piece of 1/8 inch outer diameter (o.d.) silver plated copper tubing. The inside diameter of the turns is 25 mm, which allowed ample room to fit a 22 mm o.d. quartz torch through the center. The induction coil was attached at one end to the RF output of the matching network and to ground at the other end.

ICP Torch

The torch was a Fassel type with an extended sleeve (see Figure 3) [32,33]. The torch consisted of three concentric quartz tubes with the innermost tube (1.0 mm inner diameter [i.d.] at the tip) delivering the aerosol to the plasma. The second tube was an auxiliary tube (i.d of 13.0 mm and an o.d. of 15.0 mm) that maintained the plasma above the aerosol delivery tube. The outermost tube (18.0 mm i.d with a 22.0 mm o.d.) confined the plasma and centered it in the torch. The extended sleeve enabled the formation of a unique type of plasma known as the "pencil plasma" used for most of the studies in this work. This plasma was typically formed by reducing the tangential and the auxiliary flows and by increasing the nebulizer flow to maintain a stable plasma. For a standard ICP torch (not an

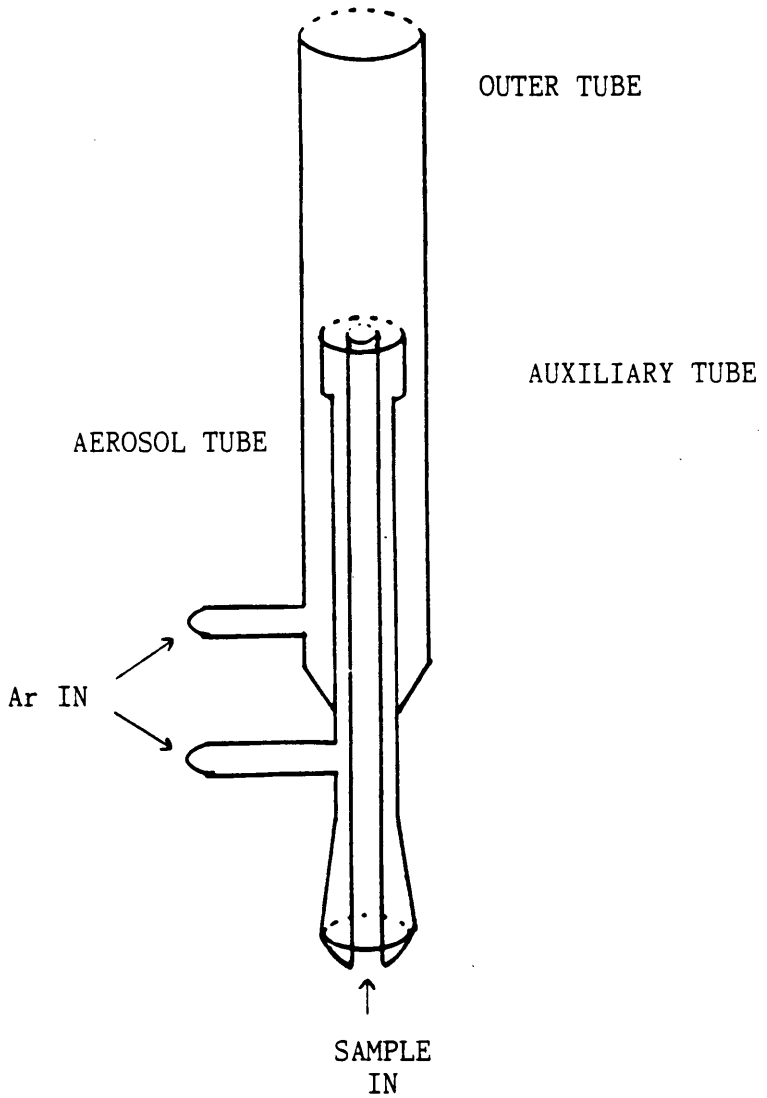

Figure 3. Schematic of a long sleeve torch.

extended sleeve) common flow rates for a stable plasma are 12-19 L/min of argon for the tangential flow, 0.5-1.0 L/min for the auxiliary flow, and 1.0 L/min for the aerosol flow [34].

Pencil Plasma

The formation of the pencil plasma required the normal flow rates be altered, an extended sleeve torch must be used, and must be moved higher in the the induction coil then normal, with the auxiliary tube placed between the first and second turns of the induction coil. The tangential flow rate was 8-10 L/min, no auxiliary flow was used, and the aerosol flow rate was 2.0 L/min. This aerosol flow maintained the plasma off of the auxiliary tube. A reduced power setting of 1 kW was used instead of the normal 2.0-2.5 kW power.

Sample Introduction

Sample introduction was accomplished by the most common method: use of a pneumatic nebulizer in conjunction with a Scott type spray chamber [5-7]. A Meinhard TA2-40 concentric nebulizer was used for this work (see Figure 4). It should be noted that the TA2-40 nebulizer was a special order part and that the actual part was a TA1-16 (a nebulizer that delivers 1.0 L/min argon at 16 PSI). The

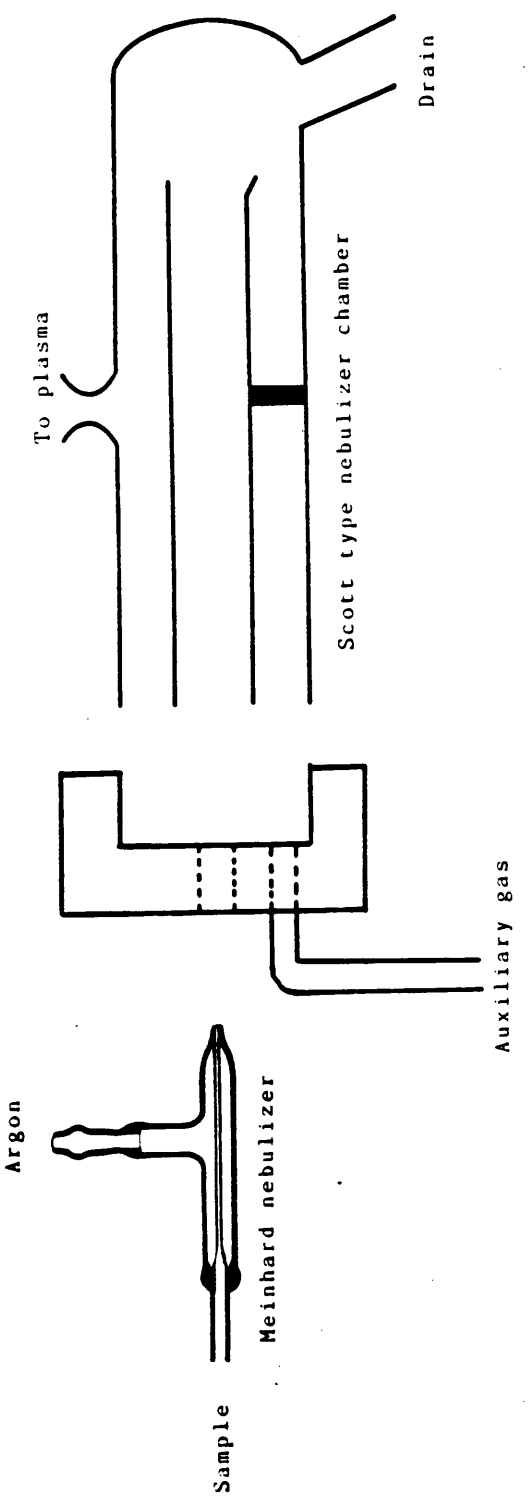

Figure 4. Schematic of a Meinhard nebulizer and a Scott type spray chamber.

Scott type spray chamber was used to narrow the droplet size distribution that reaches the plasma. To accomplish this distribution several methods were used (see Figure 5). Droplets first impacted on the central tube of the chamber and then on the end wall of the chamber where secondary droplet formation occurred narrowing the range of droplet sizes. The third step in droplet segregation/formation employed by the Scott type chamber was tertiary separation. This process used inertia to allow larger droplets to pass through the orifice and smaller droplets to be carried along with the argon to the plasma. This type of aerosol production was 1-3 % efficient with the remainder of the sample removed as waste [30].

Gas Flow System

The argon used in this system was delivered by a two stage regulator, that was set to deliver 60 PSI. The nebulizer flow was re-regulated by another two stage regulator to 40 PSI giving 2L/min argon and 1mL/min sample uptake using the TA2-40. There were three other flow meters used: one for the tangential flow, another for auxiliary flow, and a third for the sample gas (propane or argon). The third meter was one of the unique aspects of this system because it allowed the effects of the organic species to be studied without altering other plasma

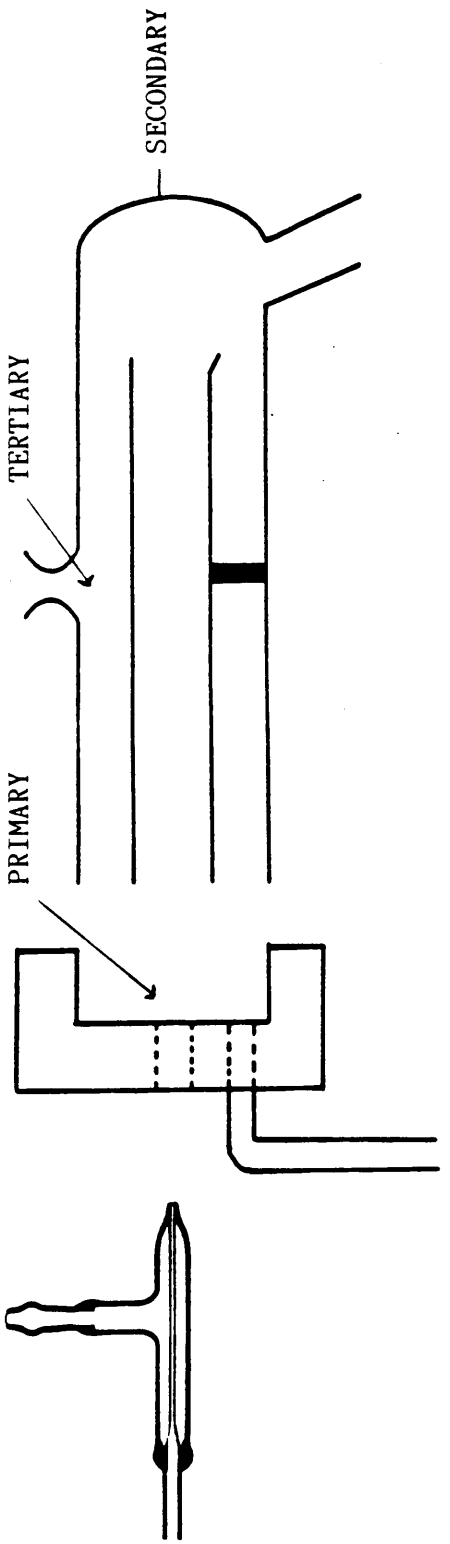

Figure 5. Diagram of primary, secondary, and tertiary droplet formation/separation.

parameters. The third meter was connected to a directional valve, which made it is possible to study the effects of propane or some other organic gas as well as argon. The addition of argon, when not adding an organic gas, allowed the transport efficiency of the sample to the plasma to remain constant. The argon maintained a constant pressure in the nebulizer chamber constant, thus maintaining a constant droplet size according to the Nukijama/Tanasawa expression. Each nebulizer chamber has a characteristic droplet size cut off point, so by maintaining a constant droplet size, the transport efficiency of the sample to the plasma remains constant. Also, the added argon flow keeps the analyte residence time in the plasma constant. If this parameter is not held constant, there would be changes in the plasma processes of analyte desolvation, vaporization, and dissociation. Altering these processes would make the analysis on the effects of organic species in the plasma much more difficult, if not impossible.

Spectrometer

With this work, it was important to look at spatial profiles of atomic signals to observe changes in signal intensity as a function of height in the plasma tail plume. This measurement aided in the formulation of possible excitation, de-excitation, or quenching mechanisms

occurring in the plasma tail due to the addition of organic species into the plasma. A system described by Hieftje et al. that translated the entire plasma torch was first utilized and found unacceptable for our particular needs [38]. The system resulted in excessive RF radiation being released throughout the laboratory, saturating the detection electronics. The plasma stability was also noted to suffer in this demounted configuration due to unacceptably high levels of reflected RF power. Therefore, it was necessary to try an alternative method, and for simplicity a fiber optic system was designed and used.

The first consideration for choosing a fiber optic bundle was the wavelength range that needed to be covered. For this study, the range was 200 to 700 nm. Fused silica fiber optic bundles fulfilled this requirement (see Figure 6) [39]. In this work, it was necessary to look at separate points in the plasma and to transmit the light to a monochromator. To accommodate this requirement it was necessary to place focusing lenses on the ends of the fused silica bundle. The fused silica bundle was an Oriel circular bundle that was 2.0 mm in diameter and 2 feet in length. The individual fibers were threaded through the bundle housing in a random manner, thus resulting in an incoherent beam. The two lenses fit into a probe that was attached onto the ends of the fiber bundle. The first lens

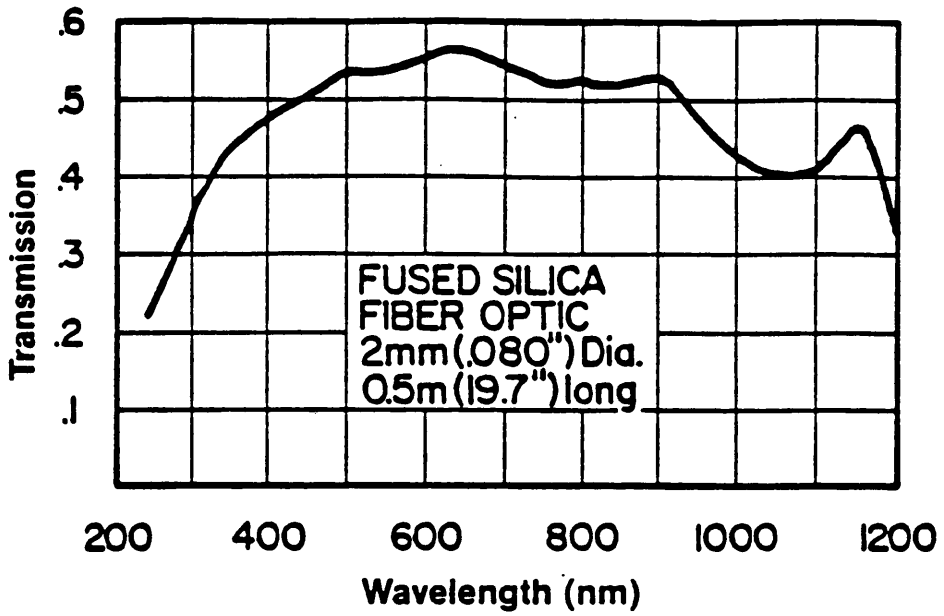

Figure 6. Plot of transmission versus wavelength for a fused silica fiber optic bundle.

was a 19 mm f/1.7 used for collimating the light and the second lens was an f/4.5 that was used for focusing the light to a point 50 mm away from it. The first lens took the divergent light from the end of the fiber bundle and collimated it and the second lens took the collimated light and focused it to a point. To translate the fiber bundle, a 4 inch translation stage from NRC was used in conjunction with a micrometer made in house, that moved the bundle 1 mm for each revolution.

The light from the bundle was focused onto the slits of a McPherson (model 270) 0.35 M monochromator. The model 270 was a single-pass Czerny-Turner mounting with folding mirrors to provide entrance and exit beams on a common optical axis. The effective aperture ratio was f/6.4 and the focal length is 350 mm. When the slits were closed to a width of 5 microns and an aperture disk was used to limit the height to 1 mm the resolution was 0.3 angstrom [40]. Depending upon the wavelength, the reciprocal dispersion was approximately 20 angstroms per mm at the exit slit. The scanning mechanism was a sine-bar and precision leadscrew assembly driven by a 0.1 angstrom per step stepping motor. A 5-digit counter read directly in angstroms with 0.2 angstrom divisions.

To detect the light as it was separated by the monochromator an RF shielded housing was used with a

photomultiplier tube (PMT). The PMT used was red sensitive (Hamamatsu model 1P28A). The shielding was necessary to insure that the induced current in the PMT was due to photons and not due to stray RF from the system. A high voltage supply (Pacific Instruments model 204-10) was used to operate the PMT. This power supply was capable of delivering up to 2010 volts and 10 milliamps of current. It was possible to to control the voltage to 1 volt with resolution and resetability. The power supply had drift which was less than 0.01% for eight hours, and was regulated to change less than 0.002% for a 10% change in the line voltage with or without a load connected [41].

Data Acquisition

Current from the PMT must be converted to a voltage by way of a current to voltage converter (I/V). The current to voltage converter used with this work was a Heath model EU-703-31. This unit has a zero to 1.0V output which can run a chart recorder or go directly into a computer interface. There are four separate sensitivities that the unit could be operated, for current inputs ranging from 1 X 10^{-6} amps to 1 X 10^{-9} amps.

Typically, the output of the I/V converter was used to feed the input of an analog to digital (A/D) converter. The A/D converter was a dual slope integrating 12 bit A/D

converter from Interactive Microware, Inc (IMI). The entire data acquisition system was on an Apple IIe computer using IMI's "Adalab" interface card. The A/D converter subsystem reads voltages from the Heath I/V converter with precision of 0.025% (12 bits) and an overall accuracy better than 0.1% [42]. The system had jumper-selectable voltage ranges of +/- 4V, +/- 2V, +/- 1V, and +/-0.5V. The output of the Heath I/V converter was 1.0V therefore the +/- 1V setting on the Adalab card was used. A software program was designed that allowed data to be taken on command. See Appendix A

Data Storage and Plotting

All the obtained data was background corrected by the above mentioned software and then the net signal was stored on disk for later manipulation. After the data was stored it was plotted using software purchased from Interactive Microware Inc. The data was than replotted by hand to make it more aesthetically pleasing. Each plot of data contains a representitive error bar for a minimum of 95% confidence.

CHAPTER 3

Atomic Emission

The effect of propane on atomic emission signals of aqueous samples is discussed in this section. Propane has been shown to cause enhancements in atomic fluorescence signals by several groups [28,29]. The use of atomic emission spectrometry will help to elucidate a possible mechanism for the enhancements that were observed in atomic fluorescence spectrometry. Originally, the enhancements were thought to be occurring by a chemical reaction of metal oxides formed in the plasma tail with free carbon from the propane giving a free metal atom and a carbon oxide:

$$MO + C \rightleftarrows M + CO_X \quad (1).$$

Experimental

All of the chemical reagents used in this section were reagent grade, and the water was deionized. Stock solutions of Ba, Ca, Mg, Al, Cu, Na, Fe, Cr, La, and Y were all 1000 parts per million (ppm) and were prepared following standard procedures [43]. Volumetric dilutions of these solutions were made to obtain the desired concentrations. The gases used were Airco analytical grade argon, Airco 99.5% pure propane and Airco grade 2.6 oxygen

which was 99.6% pure. The experimental apparatus was described in chapter 2.

Results and Discussion

Plasma temperature

Since propane is a combustible gas, it is possible that the addition of propane into the ICP may cause a change in the plasma temperature. If the plasma excitation temperature is altered, then the atomic emission signals are expected to change. To study this effect, the excitation temperature of the pencil plasma was determined with and without the addition of propane at a height of 60-100 mm above the induction region of the plasma. The method used to determine the excitation temperature was the slope method using the relative emission intensities of 10 Fe lines. This spectroscopic method was primarily used since it does not disturb the plasma. Each line has a particular wavelength of transition (λ), an excitation energy of the emitting level (E_q), a statistical weight of the emitting level (g_q) and a transition probability (A_{pq}). All of these parameters can be used in conjunction with the relative emission intensity of the respective Fe lines to determine the excitation energy (see Table II for Fe constants) [44].

The relative emission intensities of these lines were

Table II - Iron Temperature Constants

λ(nm)	E_q (cm^{-1})	g_q	A_{qp}
367.992	27167	9	0.0138
370.557	27395	7	0.0328
371.994	26875	11	0.163
372.256	27560	5	0.0505
373.487	33695	11	0.886
373.713	27167	9	0.143
374.826	27560	5	0.0904
374.949	34040	9	0.744
375,824	34329	7	0.611
376.379	34547	5	0.523

measured and by using the expression listed below relating emission intensity to level population that has been substituted into a Boltzmann function to determine the excitation temperature T_{exc} [45,46]. Strictly speaking, this method is only valid for sources in local thermal equilibrium [47,48]. If the source is not in local thermal equilibrium then the temperature derived is only applicable to the energy levels of the thermometric species used to derive it.

$$I_{pq} = (1/4Pi)\ A_{pq}\ h\ V_{pq}\ n_p\ B_{pq}$$

Substituted into this Boltzmann function:

$$n_p = n_a[g_p/Z_a(T)]\exp(-E_p/kT)$$

giving:

$$I_{pq} = (1/4pi)n_a[g_p/Z_a(T)]A_{pq}\ h\ V_{pq}\ \exp(-E_p/kT)$$

rearrange and take ln of both sides:

$$\ln[I_{pq}/(g_pA_{pq}V_{pq})] = -E_p/kT + \ln[n_a lh/(4piZ_a(T))]$$

where:

I_{pq} = intensity of the emitted radiation field

l = the path length of the source

A_{pq} = the transition probability for the pq transition

h = Plancks constant

V_{pq} = frequency of the pq transition

n_p = the population of level p

n_a = the total concentration of atom a

B_{pq} = probability that the photons will escape from the emitting volume without being reabsorbed. For optically thin sources this value is 1.

g_p = the statistical weight of level p

$Z_a(T)$ = is the partition function of atom a

E_p = excitation energy of level p

By plotting the $\ln(J_{qp}/g_q A_{qp} V_{qp})$ where J_{qp} is the relative intensity of the transition versus E_q a straight line with a slope equal to $-1/kT_{exc}$ is obtained (see Figure 7).

For this work, a 1000 ppm Fe solution was used, and the monochromator slits were closed down to 25 microns to allow sufficient resolution (see Figure 8 for an actual scan). The excitation temperature was determined to be between 3500 K and 3100 K throughout the entire plasma tail from 60 to 100 mm above the induction region, as can be seen in Figure 9. No statistical difference was observed

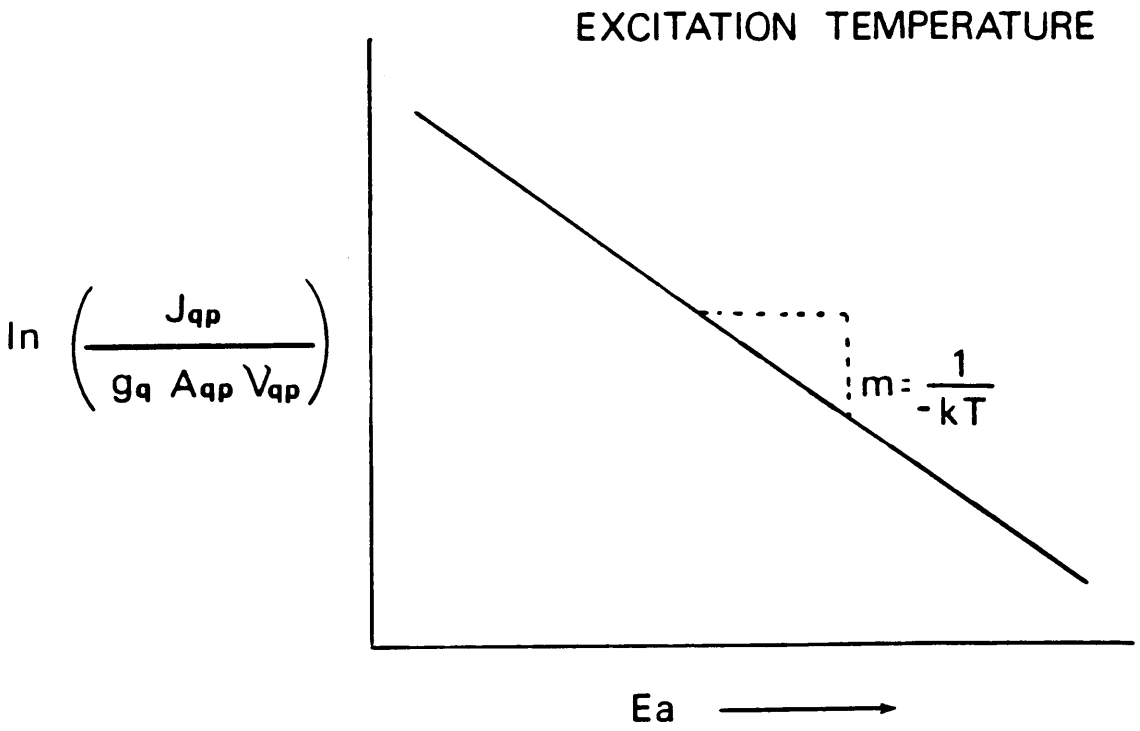

Figure 7. Plot showing how to obtain the excitation temperature spectroscopically.

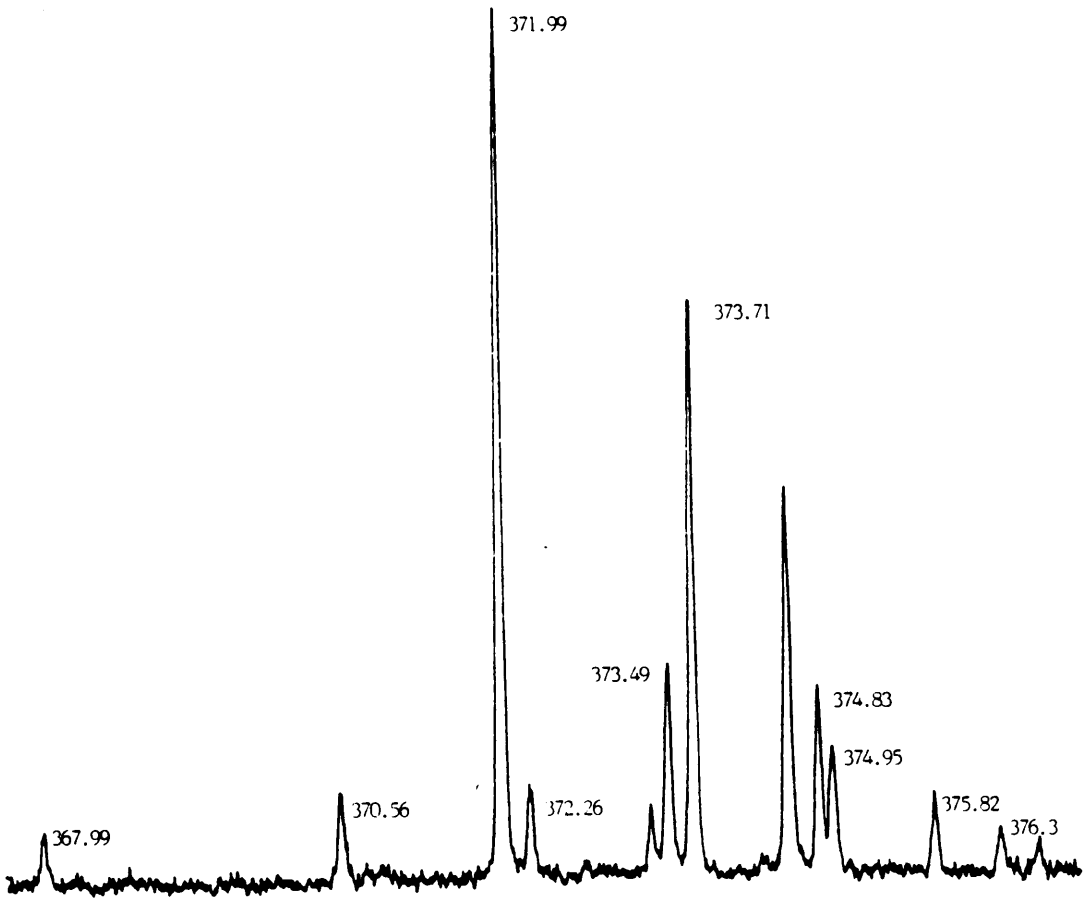

Figure 8. Actual scan of a 1000 ppm Fe solution, showing the wavelengths used to determine the excitation temperature

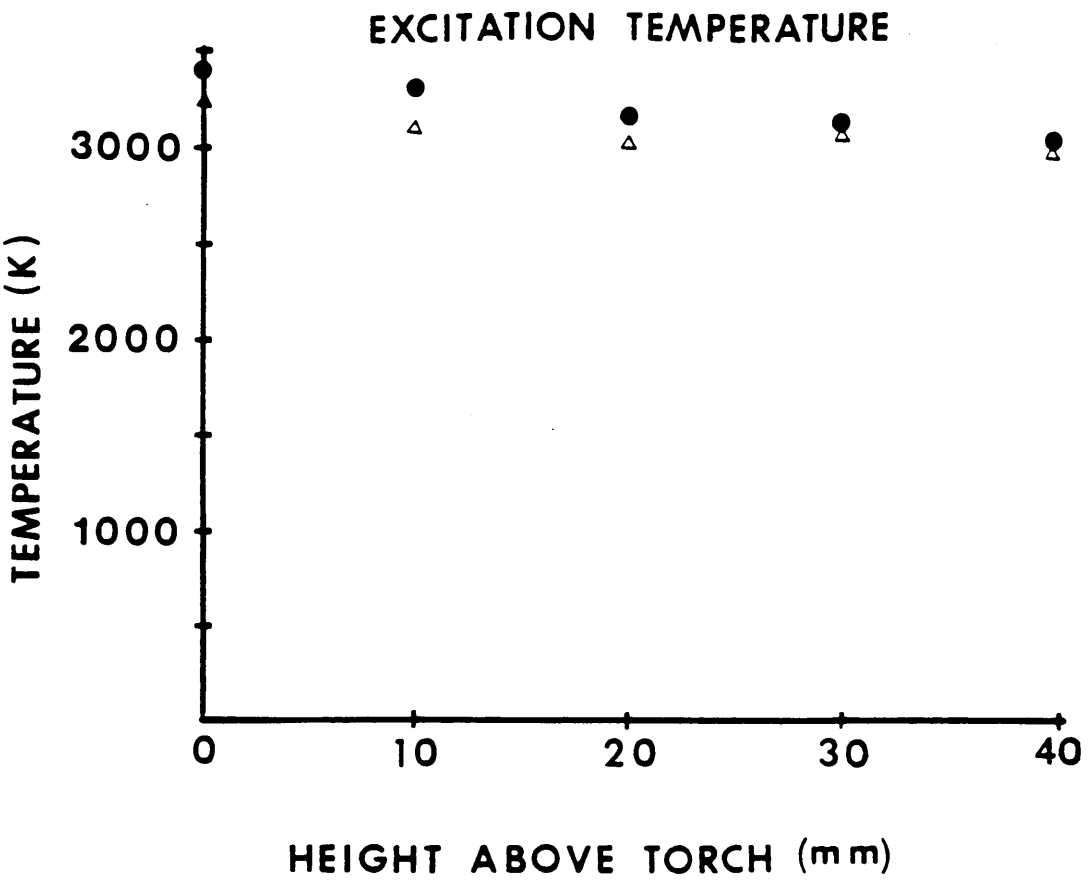

Figure 9. Excitation temperature throughout the plasma tail plume, circles are with the argon backfiller and boxes are with 20 cc/min propane.

for the excitation temperature with and without the addition of propane since each temperature measurement was determined to have between 2-4% relative error. These results suggest that the excitation temperature was not significantly altered by the addition of propane.

Electron Number Density

The electron number density (n_e) is a measure of the degree of ionization of a plasma or other source. The electron number density is very important, as is the excitation temperature, because it gives information on the extent of thermal equilibrium in the plasma. Local thermal equilibrium is said to occur when the electron number density is between 10^{15} electrons/cc and 10^{21} electrons/cc [49,50].

There are numerous techniques for determining the electron number density. One such technique is to the Saha-Eggert Ionization Equilibrium. This method requires the determination of relative emission line intensities from successive ionization stages, generally for the neutral atom and singly ionized species. When these intensities are combined with the known equilibrium relationships between spectral emission and temperature, the Saha-Eggert expression can be used to determine the n_e [51,52].

Another more preferred method, is the use of Stark broadening of the H_B line (486.13 nm). Stark broadening arises from perturbations of the energy levels of an emitting (or absorbing) species by an electric field. This electric field is formed as a consequence of the motions and concentrations of surrounding charged particles. The popularity of this technique arises from the simplicity of using a singly ionized species for the n_e determinations. The choice of using the hydrogen beta line (H_B) as the line of preference for n_e calculations is: (a) freedom from spectral interferences from the plasma; (b) the range of half widths anticipated (0.1 to 0.5 nm) and the relative intensities observed for this line are sufficient to allow accurate measurements at various heights above the induction region of the plasma; (c) there is extensive information available about the Stark broadening of this line for many temperatures and n_e values and; (d) greater accuracy is generally associated with Stark calculations for the hydrogen beta line than for other atomic lines. The most commonly accepted expression for n_e was developed by C.R. Vidal [53]:

$$n_e(R) = 7.9658 \times 10^{12} [\lambda_{1/2}(R)/\alpha_{1/2}]^{3/2}$$

where:

$\lambda_{1/2}(R)$ = the radial full width of the H_B line after deconvolution of the instrument half width

$\alpha_{1/2}$ = reduced half width parameter

The reduced half width parameter is directly related to the observed half width and is a function of both excitation temperature and electron number density. For this work, accurate values of n_e were unable to be determined since the 0.35 M monochromator could only provide a reciprocal linear dispersion of 2 nm/mm, thus making it impossible to precisely deconvolute the H_B half width. Therefore, the values for n_e obtained cannot be compared with values obtained elsewhere nor can they be described as absolute. However, the values can be used to determine changes in this particular system, and to note if there were any changes in electron number density. Another way to describe the results on n_e is to call them relative electron number densities. Since relative electron number densities will be used for comparison, it is possible to use a simplified expression for n_e [49].

$$n_e = C(n_e, T)(\lambda_{1/2})^{3/2}$$

where:

C = a constant which depends on the electron number density and the excitation temperature

$\lambda_{1/2}$ = full width at half maximum

For this expression two values exist for C: 3.84×10^{14} when the electron number density is 10^{14} and the excitation temperature is below 5000 K, and 3.68×10^{14} when the electron number density is 10^{15} and the excitation temperature is above 5000 K. For this work, the excitation temperature was determined to be around 3500 K, and the first value for C was used. The half width of the H_B line was observed to be 0.35 nm with the addition of the argon backfiller gas, and 0.43 nm with the addition of 20 cc/min propane. These values lead to relative electron number densities 2.4×10^{15} electrons/cc and 3.3×10^{15} electrons/cc, respectively.

Analyte Ionization

The normal viewing range for the pencil plasma is a minimum of 60 mm above the induction coil, unlike the viewing height for a normal plasma which can extend down to the the induction coil. As was previously mentioned, the excitation temperature was shown to be between 3500 to 3100 K in the viewing region of the pencil plasma. This temperature is greatly reduced as compared to typical

excitation temperatures for standard plasmas at a lower viewing height. The electron number density for the pencil plasma should also be reduced as compared with that of the standard ICP. In this cooler less energetic region of the plasma the role of the electrons is expected to be analyte ion recombination reactions rather than excitation due to ion impact. Elements which possess low ionization energies (also known as easily ionizable elements or EIE's) are usually fully ionized in the normal analytical zone of the plasma. A significant increase in the electron number density should result in a significant increase in the free atom state of the EIE higher in the plasma tail, resulting in an increased atomic emission signal:

$$M^{O} \rightleftarrows M^{+} + e- .$$

If the introduction of propane significantly alters the electron number density of the pencil plasma, then a change in the atomic emission of the neutral atom is expected. An increase in the electron number density should also result in a decreased number of ions in the plasma tail plume and an increased number of ground state atoms, resulting in an increased atomic emission signal. The electron number density of the plasma determined by Stark broadening of the hydrogen beta line was 2.4×10^{15} electrons/cc without the

addition of propane and 3.3 X 10^{15} electrons/cc. These values are expected to be high due to the lack of resolution of the instrument. The actual electron number densities are thought to be about 1 X 10^{14}, but these calculated values will be sufficient for comparison of the effects with and without propane [47,51,52,54,55].

To evaluate this increase in the relative electron number density (REND) on analyte ionization, an EIE was used. The atomic emission signals were observed with and without the addition of 20 cc/min propane into the aerosol gas. If there was a significant increase in the electron number density then a significant increase in the atomic emission for the EIE should also be observed. A 50 ppm solution of sodium was used for this experiment at the atomic emission wavelength for the Na atom of 589.0 nm. In Figure 10 the emission profiles of Na(I) can be observed with and without the addition of propane. The circles represent data points without the addition of propane and the boxes represent data points with the addition of 20cc/min propane. At low observation heights (<20mm above the top of the torch or 80mm above the induction coil) no significant difference was observed for the atomic emission of Na(I) indicating no significant increase in the electron number density at that height. There was a slight enhancement observed in the Na(I) emission at higher

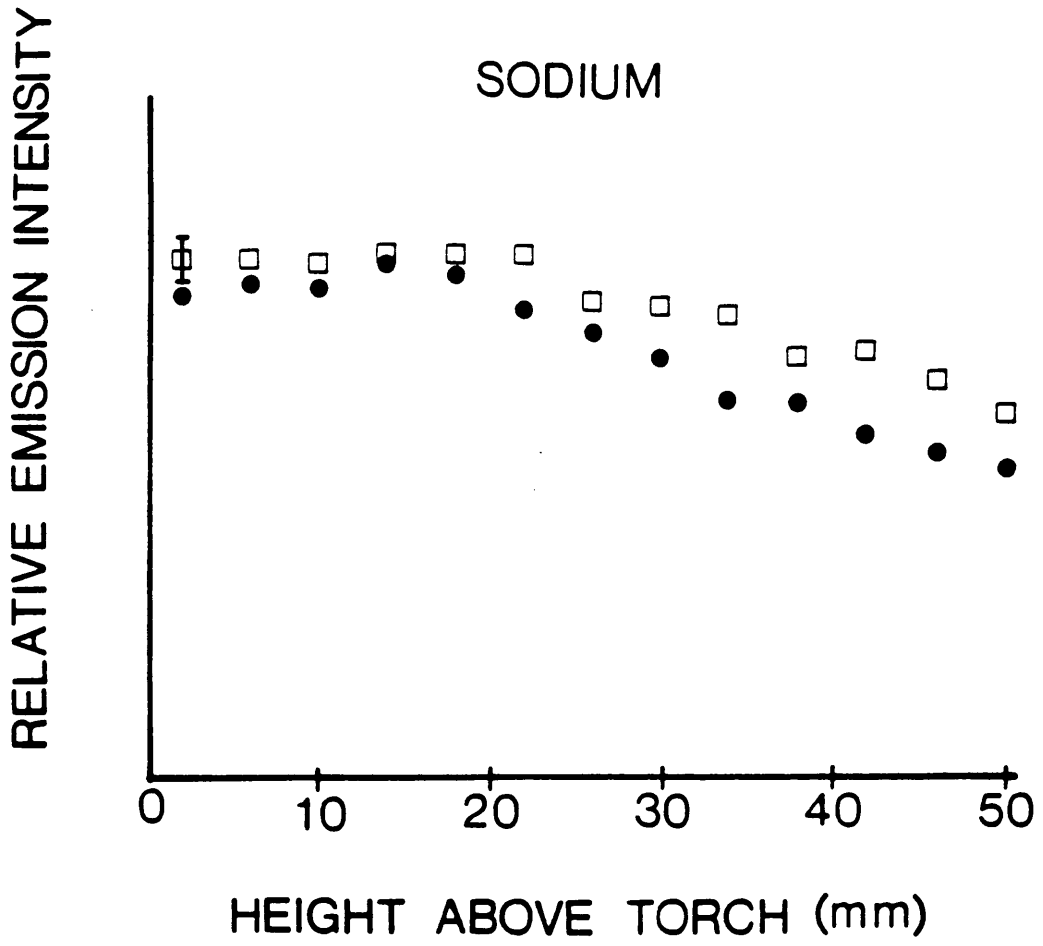

Figure 10. Profile of a 50 ppm Na solution at 589.0 nm where the circles represent data points with the argon backfiller, and boxes represent data points with the addition of 20 cc/min propane.

viewing heights (approximately 10%). This small enhancement of the EIE emission suggested that the electron number was increasing but that it did not significantly affect the analyte ionization, and could not be responsible for the large enhancements of refractory elements previously observed with atomic fluorescence spectrometry.

Reduction of Metal Oxide

The addition of propane into the pencil has been shown not to significantly affect the Fe excitation temperature or the analyte ionization. Therefore, the enhancements observed in atomic fluorescence spectrometry were possibly due to some other mechanism. It was postulated that the addition of propane into the pencil plasma may be reducing the metal oxides to give a greater free metal atom population. The pencil plasma being much cooler than a standard plasma is a good environment for oxygen entrainment and molecular formations. Thus, in a favorable oxide environment the enhancements in atomic signals would logically be thought to come from the reduction of metal oxides by the free carbon atoms from the propane. This argument is synonymous for the increase in signal of strong oxide formers in flame AAS. By using a fuel rich flame enhancements were observed in the absorbance signals.

Atomic Emission Profiles

To evaluate this reduction mechanism in the pencil plasma, emission profiles were collected for several refractory and non-refractory elements comparing the pencil plasma with and without the addition of propane. The profiles cover observation heights from 0 mm above the extended sleeve torch to a height of 50 mm above the top of the torch. This corresponds to measurements from a height of 60 mm above the induction coil to a point 110 mm above the load coil. By scanning this region much information can be obtained on the effects of propane on analyte emission. Also, the effect of propane on the maximum signal intensity can be observed, and its effect on analyte vaporization and dissociation can be noted by observing a shift in the signal maximum.

The first element to be presented is yttrium. Yttrium is a refractory element and forms a very stable oxide in the plasma tail. The oxide emission is a strong line for yttrium and should offer valuble information toward the mechanism. The dissociation energy of yttrium oxide is 7.3 eV. This plasma emission profile is for a 500 ppm solution of yttrium, depicted in Figure 11. The atom line at 410.2 nm was used for this profile. The circles represent data points with the addition of an argon backfiller to maintain plasma conditions, and the boxes

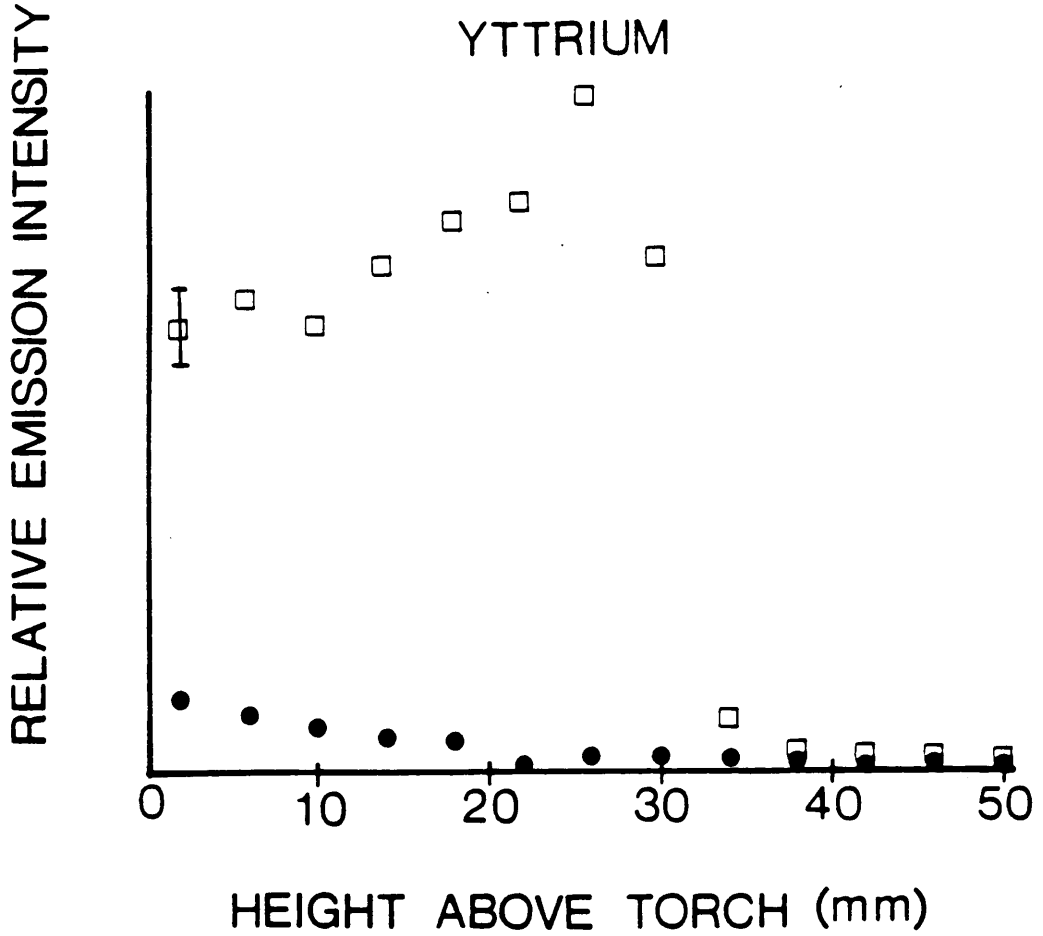

Figure 11. Profile of a 500 ppm Y solution at 410.2 nm where the circles represent data points with the argon backfiller, and boxes represent data points with the addition of 20 cc/min propane.

represent data points with the addition of 20 cc/min propane. This profile shows that the yttrium atom emission was greatly enhanced by the addition of propane. To help elucidate the mechanism, the yttrium oxide emission must also be observed. It was expected, if the enhancement in the yttrium atom was due to the reduction of metal oxides, then the yttrium oxide line should depress upon the addition of propane. In Figure 12 a 50 ppm solution of yttrium was used to observe the yttrium oxide transition at 597.2 nm. Again, the circles represent data with the argon, and boxes represent data with the addition of propane. It was observed that the addition of propane caused a depression in the metal oxide transition. For yttrium, an enhancement in the atom emission signal and a depression in the oxide emission signal support the metal oxide reduction mechanism.

Another refractory element closely related to yttrium, that was expected to show similar results upon the addition of propane was lanthanum. Lanthanum oxide has a dissociation energy of 8.2 eV. It was necessary to look at plasma profiles of lanthanum atom emission and of lanthanum oxide emission. The profile shown in Figure 13 was a 250 ppm lanthanum solution for the atom transition occurring at 545.5 nm. The same data representations are used, where data with the argon backfiller is represented by the

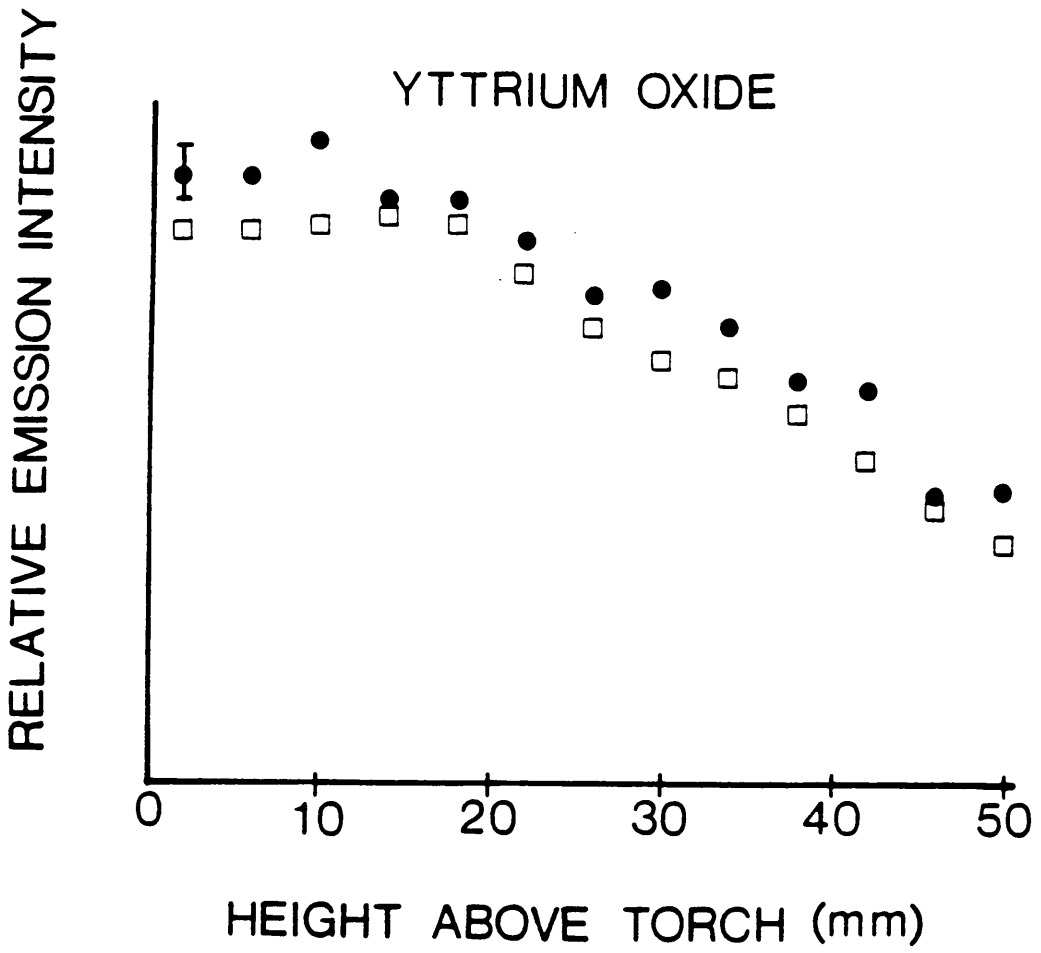

Figure 12. Profile of a 50 ppm YO solution at 597.2 nm where the circles represent data points with the argon backfiller, and boxes represent data points with the addition of 20 cc/min propane.

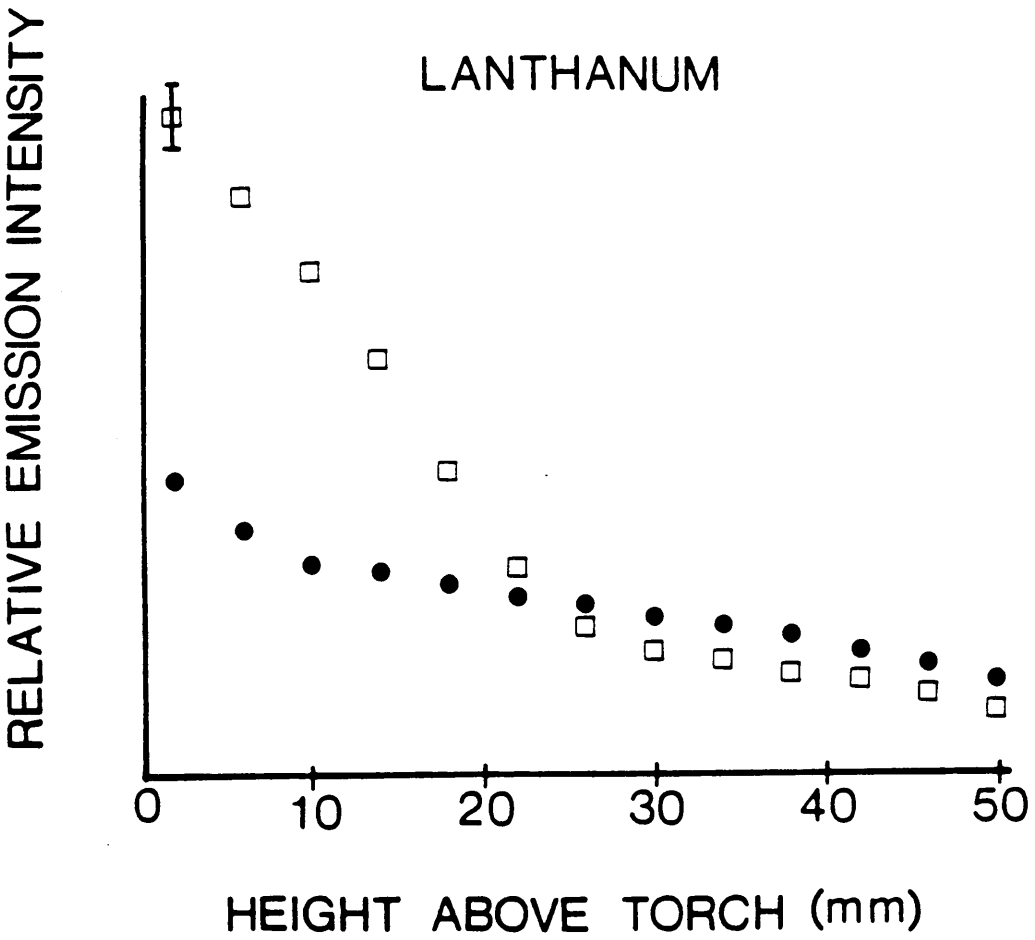

Figure 13. Profile of a 250 ppm La solution at 545.5 nm where the circles represent data points with the argon backfiller, and boxes represent data points with the addition of 20 cc/min propane.

circles and the addition of propane is represented by boxes. The lanthanum atom showed the same initial enhancement that was observed for yttrium, but higher in the plasma a slight depression was observed. The data for the lanthanum oxide was not as clear as for yttrium oxide, however, these results still appear to support the metal oxide reduction mechanism.

A refractory element that has previously shown enhancements in AFS signals upon the addition of propane was aluminum. The dissociation energy of aluminum oxide is 4.6 eV, which is much lower than the previous elements. The plasma emission profiles for a 50 ppm solution of aluminum with the atom emission occurring at 396.2 nm can be observed in Figure 14. It can be seen that the addition of propane (represented by boxes) caused an enhancement to the signal versus the argon back filler (represented by circles). It was not possible to obtain an aluminum oxide transition signal using this system. However, the aluminum atom signal was observed to exhibit a normal emission profile. The higher the analyte goes in the plasma tail, the cooler the environment becomes, thus less energy is transferred from the plasma to the analyte species. This reduction in energy was observed by the decrease in aluminums atomic emission which occurs. The addition of propane alters this normal decrease in emission. As can be

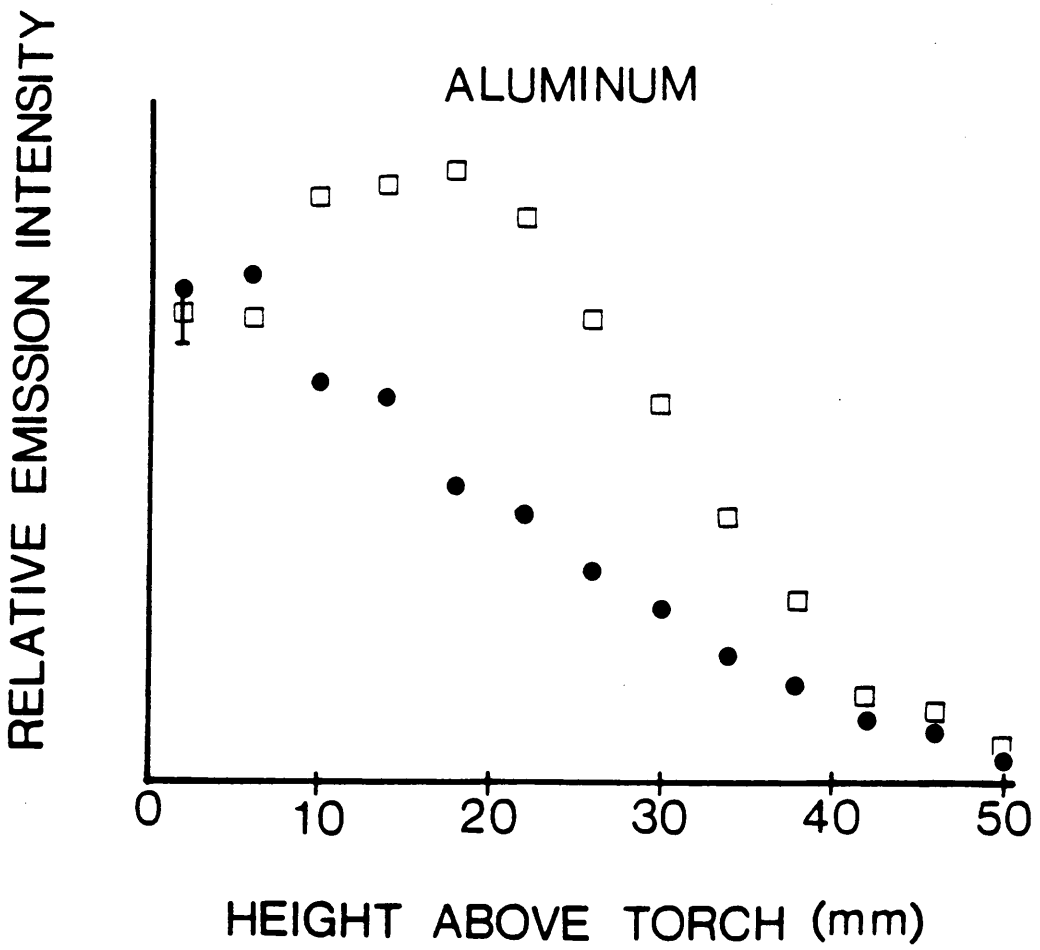

Figure 14. Profile of a 50 ppm Al solution at 396.2 nm where the circles represent data points with the argon backfiller, and boxes represent data points with the addition of 20 cc/min propane.

observed in Figure 14, the point of maximum signal intensity was shifted to a region higher in plasma tail plume. This suggests that the addition of propane causes desolvation and vaporization of the aluminum to occur higher in the plasma than normal. Another possible interpretation of this observation is the decrease in the aluminum signal was due to the formation of aluminum oxide, and the propane reduced the aluminum oxide to aluminum atom and CO. The second interpretation supports the mechanism of metal oxide reduction by propane.

Barium is expected to show similar results to aluminum, since their metal oxide dissociation energies are close. The dissociation energy for barium oxide is 5.3 eV. The plasma emission profiles for barium with and without the addition of propane can be seen in Figure 15. The profile was for a 50 ppm barium solution for the atom transition occurring at 553.5 nm. The boxes represent data points with the addition of 20 cc/min propane and show a large enhancement over the circles which represent data points with the argon backfiller. Again, it was observed that propane affected the position of maximum signal intensity. As was observed for aluminum, barium shows a maximum signal higher in the plasma tail than it did with the argon. This enhancement may be a result of the reduction of the barium oxide by free carbon.

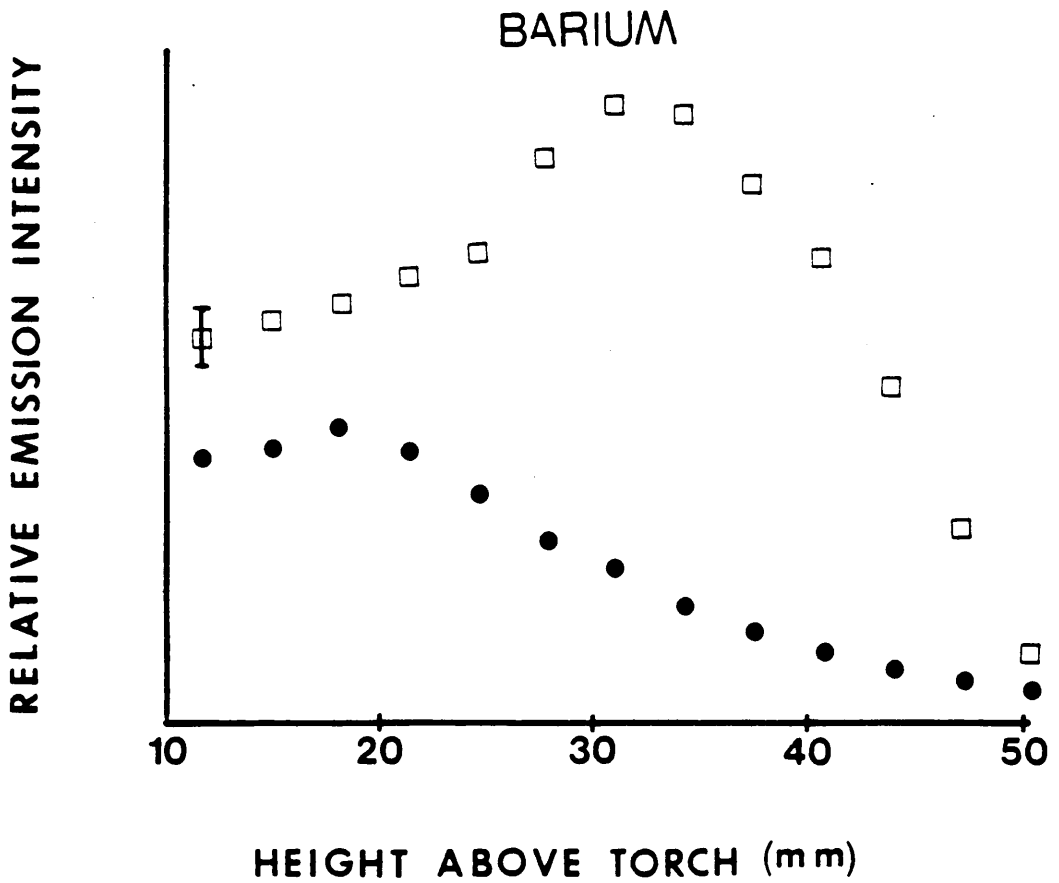

Figure 15. Profile of a 50 ppm Ba solution at 553.5 nm where the circles represent data points with the argon backfiller, and boxes represent data points with the addition of 20 cc/min propane.

Another element which has been observed to exhibit enhancements upon the addition of propane to the plasma was chromium. The addition of propane to a 50 ppm solution of chromium was observed to cause a 2-fold enhancement of the atomic emission signal for the chromium atom at the 425.4 nm transition as can be seen Figure 16. The data with the addition of propane (represented by boxes) appeared to show a consistent enhancement mimicking the atom emission profile with the argon, rather than shifting the position of the maximum signal. This observation was not expected since the dissociation energy of chromium oxide is 4.74 eV, which falls directly between that of aluminum and barium oxides. It was thought that the chromium profile would appear similarly to that of aluminum and barium, but the enhancement still defends the postulated mechanism of metal oxide reduction by propane.

Calcium was used as a diagnostic test element by many researchers and was also examined. The effects of propane on calcium signals for AFS have been observed by several groups working on AFS techniques, and propane was observed to caused a 2 fold enhancement in calcium AFS signals at a wavelength of 422.7 nm. In this work, calcium was also studied, but it was found not to agree with the previous AFS observations. As can be seen from Figure 17, the addition of propane (represented by the boxes) was observed

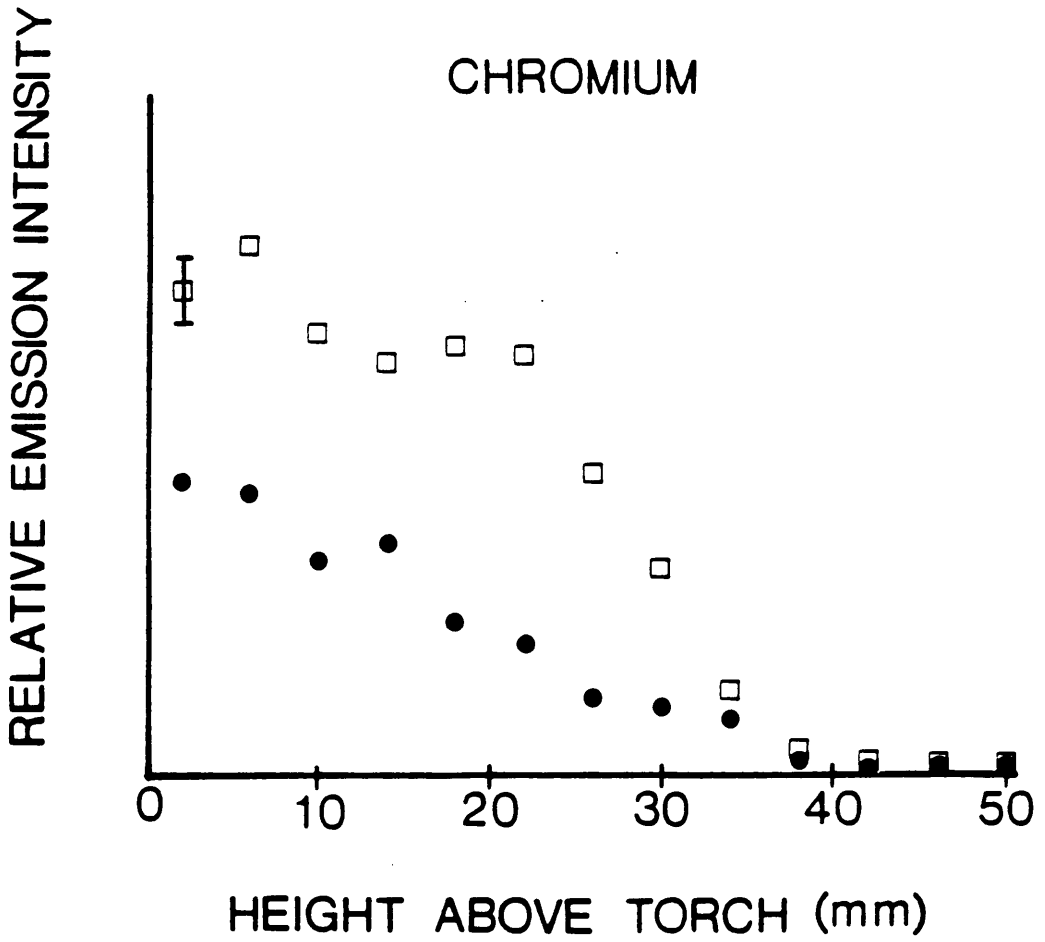

Figure 16. Profile of a 50 ppm Cr solution at 425.4 nm where the circles represent data points with the argon backfiller, and boxes represent data points with the addition of 20 cc/min propane.

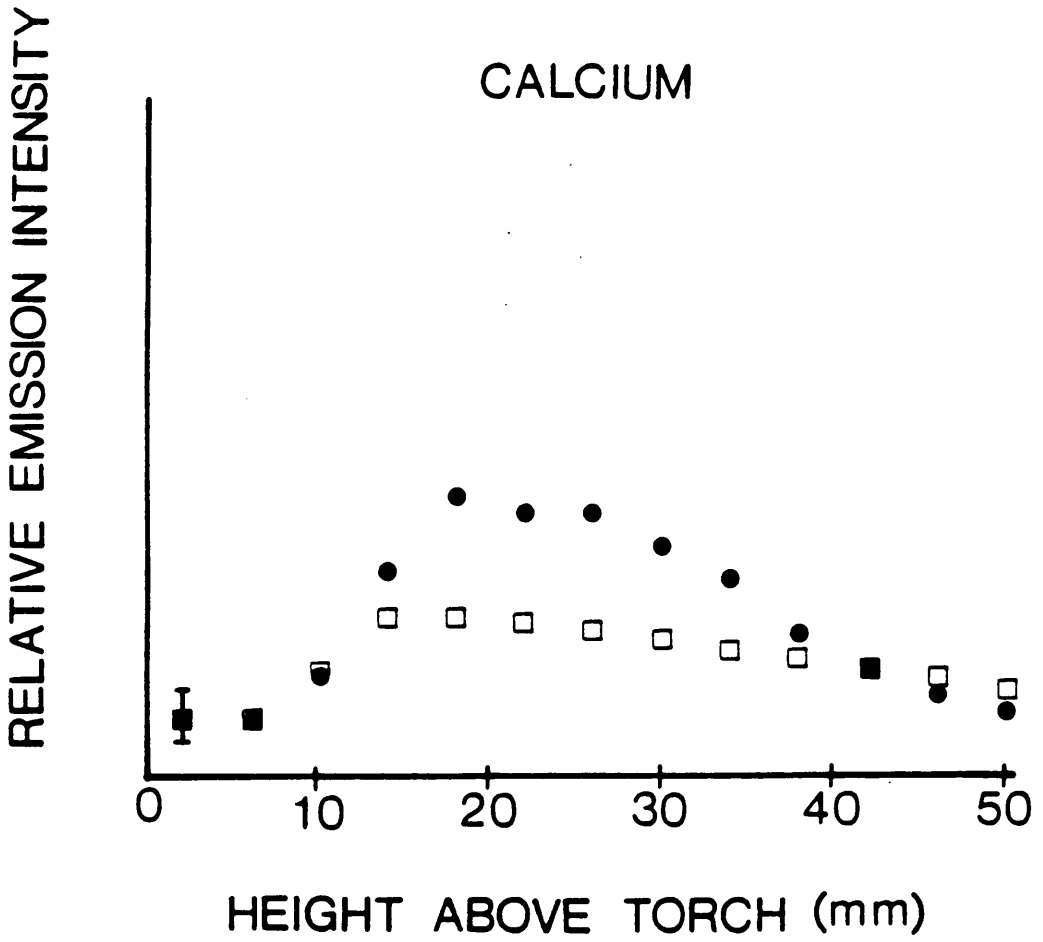

Figure 17. Profile of a 50 ppm Ca solution at 422.7 nm where the circles represent data points with the argon backfiller, and boxes represent data points with the addition of 20 cc/min propane.

to cause a depression in calcium atomic emission at the 422.7 nm transition. With this data, there was a contradiction of what was expected to occur upon the addition of propane. Calcium has a strong oxide transition, therefore it was possible to observe the effects of propane on the calcium oxide signal. The addition of propane was observed to cause a depression in the calcium oxide emission. This observation may be indicating that the changes in the metal atom emission signal intensities were not related to the metal oxide signal intensities. To gain a more complete picture on the effects of propane on calcium signals, its effects on the calcium ionic transition at 393.3 nm was observed. The calcium ion exhibited a similar effect as the calcium atom, yet the ionic depression was more severe.

Magnesium also forms a stable oxide with a dissociation energy of 3.8 eV. See Figure 18, where the addition of propane (represented by the boxes) was observed to cause a severe depression in the magnesium atom emission of a 50 ppm solution at the 285.2 nm wavelength. Other elements were noted to give similar results. Iron observed a 50% depression of the atom emission signal upon the addition of propane. A larger depression (up to 80%) in the atom emission signal was noted for copper. It was observed that the profiles of elements exhibiting

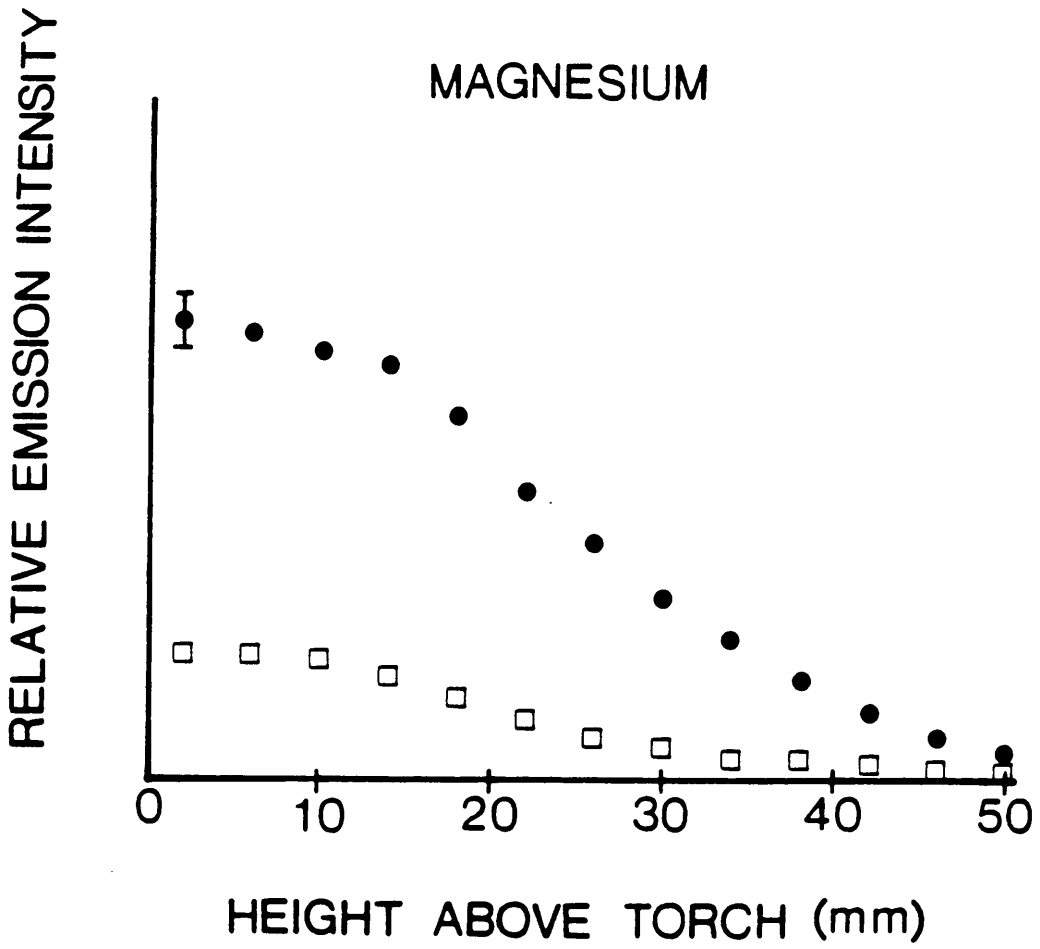

Figure 18. Profile of a 50 ppm Mg solution at 285.2 nm where the circles represent data points with the argon backfiller, and boxes represent data points with the addition of 20 cc/min propane.

depressions converged by the end of the 50 mm profile.

Mechanism of Signal Depression.

The effects of propane on the emission signals of calcium, magnesium, iron, and copper are not consistent with the previous results observed for AFS signals. These results suggest that the vapor phase reaction of metal oxide reduction may not predominate for these elements. A possible explanation for these discrepancies was the formation of metal carbides in the plasma tail plume or a deactivation of the analyte excited state possibly by the free carbon or by some other carbon radical.

The reduction of the atomic signal may be attributed to a competing reaction occurring with free carbon atoms. The reaction could be between elemental carbon from propane and the metal atoms in the plasma to form a metal carbide compound:

$$M + xC \longrightarrow MC_x$$

The carbides are well known refractory compounds which have been found to form in temperatures over 4000 K [56-58]. These temperatures are certainly achieved in the induction region and low in the plasma tail plume even in the pencil

plasma. Through the formation of a metal carbide compound, the analyte concentration would be depleted and would lead to a reduced emission signal. However, such a reduction in the free atomic metal concentration should also result in a decrease in the AFS signal observed upon the addition of propane. AFS signals are susceptible to scattering, but for these metal carbides to promote Rayleigh scattering in the plasma tail plume, a significant amount of carbide aggregation must occur. The high number of collisions and the short amount of time for these collisions to occur greatly decreases the probability that this is the only mechanism. However, the formation of metal carbides may still be the mechanism that explains the depressions observed for some elements. It is not clear why Ca, Cu, Fe, and Mg are affected by carbide formation while Y, La, Cr, Ba, and Al remain unaffected by this process.

The second mechanism that may explain the depressions observed with atomic emission and support the enhancement of atomic fluorescence signals of these elements with the addition of propane is the deactivation of excited metal analyte species through a non-radiative process. In using AES as a diagnostic tool for observing the effects of propane on analyte signals in the pencil plasma, it was presumed, since the Fe excitation temperature was determined to be unaffected and the electron number density

was shown not to alter analyte ionization, that the excitation process or the excited state populations would not be altered by the addition of propane. Thus, carbon would be expected to only change the total metal atom concentration by molecular dissociation or formation reactions. If through the collisional process the excited state concentration of the analyte species was reduced, the emission signal, which is related to the excited state concentration would also decrease. On the other hand, this reaction could also result in a signal enhancement for AFS because the excited state is populated by radiative means and the carbon species could be providing a greater initial ground state population. The AFS measurements could be enhanced by metal oxide reductions to promote an increase in total metal atom concentration in the plasma and/or the deactivation of excited state analyte species to increase the ground state analyte atom population. These two mechanisms must be studied separately and in greater detail to explain the anomalies observed between AES and AFS signals.

Chapter 4

Atomic Emission of Refractory Slurries

Propane was shown in the previous chapter to alter atomic emission signals differently than it does atomic fluorescence signals in the pencil plasma. To help elucidate a mechanism to explain the observed discrepancies, the previously proposed, metal oxide reduction and metal carbide formation, mechanisms were examined. The first mechanism tested for plausibility in this chapter is the molecular formation reaction of metal carbides upon the addition of propane to the pencil plasma. One possible way to study the carbide in the plasma is adding it directly into the plasma, thus controlling the composition of the plasma tail plume. The metal carbides and oxides used in this work will be solids that are insoluble in water and the sample delivery process was accomplished by the use of a high solids nebulizer, more specifically a Babington nebulizer [15].

Sample Introduction

The Babington nebulizer was used for the sample analysis of the slurries and the aqueous solutions in order to compare the results. One of the major requirements of the nebulizer was that it must deliver 2 L/min argon

through the nebulizer in order to sustain a pencil plasma. The way the Babington nebulizer works is a slurry (water with suspended solid sample particles) is pumped by a peristaltic to an orifice, where it runs down a glass tube. The aerosol argon is forced through a smaller orifice on the same glass tube. When the aerosol argon contacts the flowing slurry an aerosol is created. This aerosol is directed into an impaction bead where secondary droplet formation occurs. The sample goes directly to the plasma and does not undergo tertiary droplet formation (see Figure 19).

The Babington nebulizer was used in conjunction with a Jarrel Ash type spray chamber. This chamber increase the sample transport to the plasma, since the transport of solids and solutions from the Babington is inherently less than a solutions from a concentric nebulizer, due to an increased in mean droplet diameter [30]. This spray chamber has a higher transport efficiency than that of the Scott type nebulizer chamber, because it has a larger droplet cut-off diameter. The range of droplet sizes from the Jarrel Ash type chamber is much greater, thus raising the level of plasma noise due to sample introduction.

This system was modified for the addition of propane similarly as was the Scott type spray chamber in conjunction with the Meinhard nebulizer. A side arm was

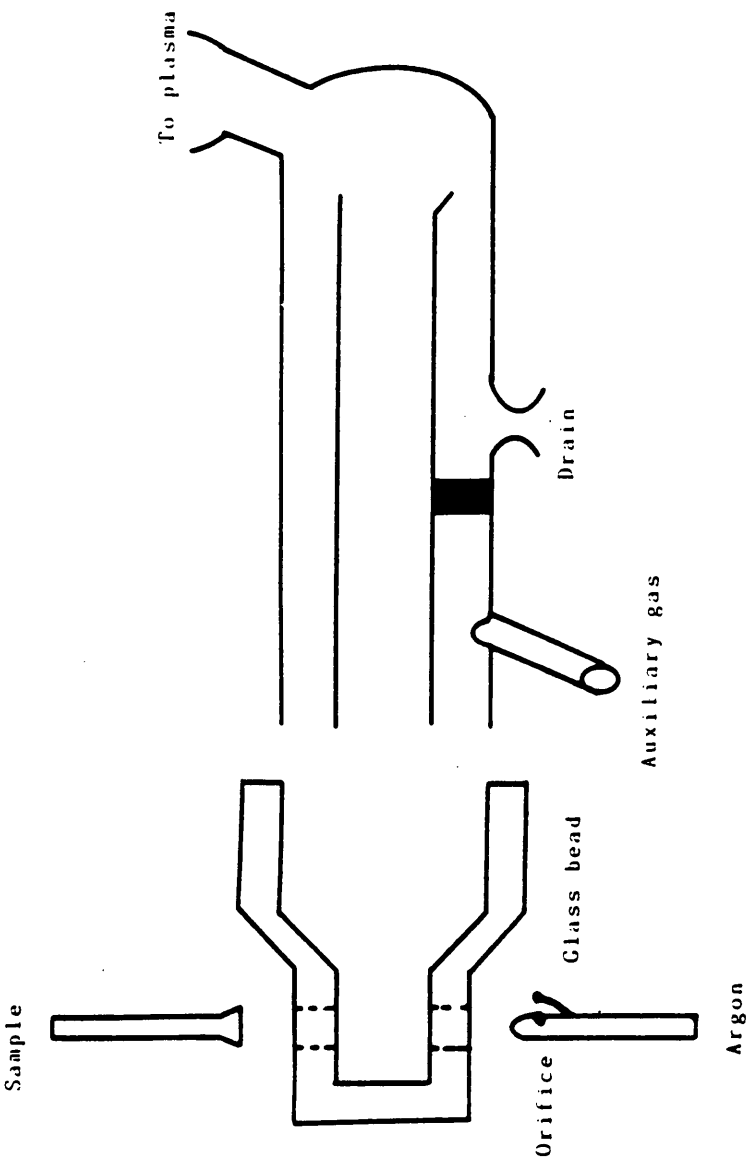

Figure 19. Schematic of a Babington nebulizer and a Jarrel Ash type spray chamber

attached directly to the spray chamber in order that propane could be added directly to the aerosol gas. When propane was not being analyzed argon was added to maintain all of the plasma parameters. The addition of the backfiller argon again gave a point of reference for a comparison of the effects of propane.

The propane was proposed to cause the formation of metal carbides in the pencil plasma by reaction with free metal atoms. To study this type of reaction, the effects of propane and oxygen on slurries of metal oxides, metal carbides and solutions of the same elements were examined. The effects of oxygen on the oxide lines of yttrium and lanthanum were used to study oxide formation, since both of these elements are known to have intense oxide emission lines. It was expected that if molecular reactions are occurring, the spectrometric signals of the various elemental and molecular species will be altered by the addition of excess reagents such as carbon and oxygen. If the equilibrium concentrations are changing it was also expected that the changes will be reflected in their emission signals.

Proposed reactions:

$$M + O \longrightarrow MO \quad (1)$$

$$M + C \longrightarrow MC \quad (2)$$

$$MO + C \longrightarrow M + CO \quad (3)$$

$$MC + O \longrightarrow M + CO \quad (4)$$

Results and Discussion

Temperature and Electron Number Density

The effects of oxygen on temperature and electron number density must first be conducted to determine if physical parameters are altered. By using the 10 line method, the addition of 20 cc/min oxygen raised the Fe excitation temperature from 3350 K to 3500 K. This change was within the limits of the error, therefore no statistical difference in temperature resulted. The electron number density was calculated to be 2.4×10^{15} with and without the addition of oxygen. These values were determined by using the Stark broadening effect on the hydrogen beta line. The lack of change observed in the excitation temperature and the electron number density

indicated that the plasma conditions were not being altered by the addition of oxygen and it would be possible to look at the molecular formation reactions occurring by monitoring the atomic spectrometric signals. It has previously been shown, the effect of propane on the excitation temperature on and electron number density in the pencil plasma is not significant. Again, it is important to note that the values of excitation temperature and electron number density should only be used for comparison within this work due to the limitation in resolution of the 0.35 M monochromator.

Metal Oxide Formation

The effect of adding oxygen to the plasma containing La is shown in Figure 20. The emission wavelength of lanthanum oxide is 441.8 nm. The circles represent data points with the addition of the argon back filler and the diamonds represent data points with the addition of 20 cc/min oxygen. It can be observed that the lanthanum oxide was enhanced with the addition of oxygen as predicted by reaction 1. It is also noted that the two emission profiles tend to converge at a point 25 mm above the top of the torch. This convergence is believed to occur at the point where sufficient oxygen from the surroundings has diffused into the plasma tail plume, masking the effects of

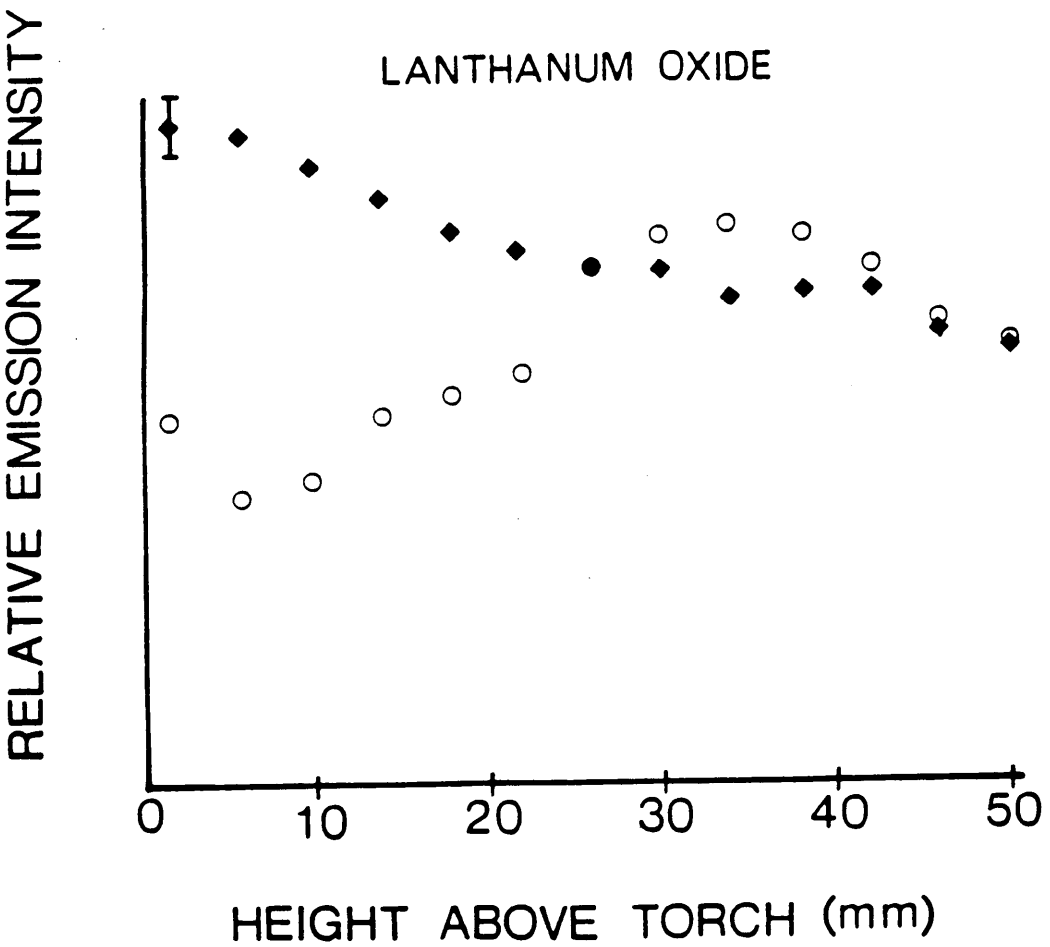

Figure 20. Profile of a 250 ppm La solution at 441.8 nm where the circles represent data points with the argon backfiller and the diamonds represent data points with 20 cc/min oxygen.

the added oxygen. The same effects were observed for a yttrium sample, as expected from their similar chemistry. These two elements were chosen specifically for their intense metal oxide emission lines that can be easily monitored. Results from this experiment indicate that molecular formations in the pencil plasma are possible.

Molecular Formation Reactions

The slurries used in the following experiments were 2000 ppm weight/volume. Therefore, the carbide and oxide of the samples contained the same weight/volume of the metal atom in question. The effects of oxygen, propane, and the argon filler were examined on slurries of the oxides and carbides, and the solutions of the respective samples. The slurries were prepared by adding the sample directly to water from the sample bottle with no pretreatment of the sample. The particle sizes were listed as being less than 10 microns in diameter [59].

The effect of adding propane to the plasma on a refractory metal is shown in Figure 21. A 1000 ppm solution of titanium was examined with propane, oxygen and an argon backfiller at the 334.2 nm transition. The circles represent data with the argon backfiller, the triangles represent data with the addition of 20 cc/min oxygen and the diamonds represent data with the addition of

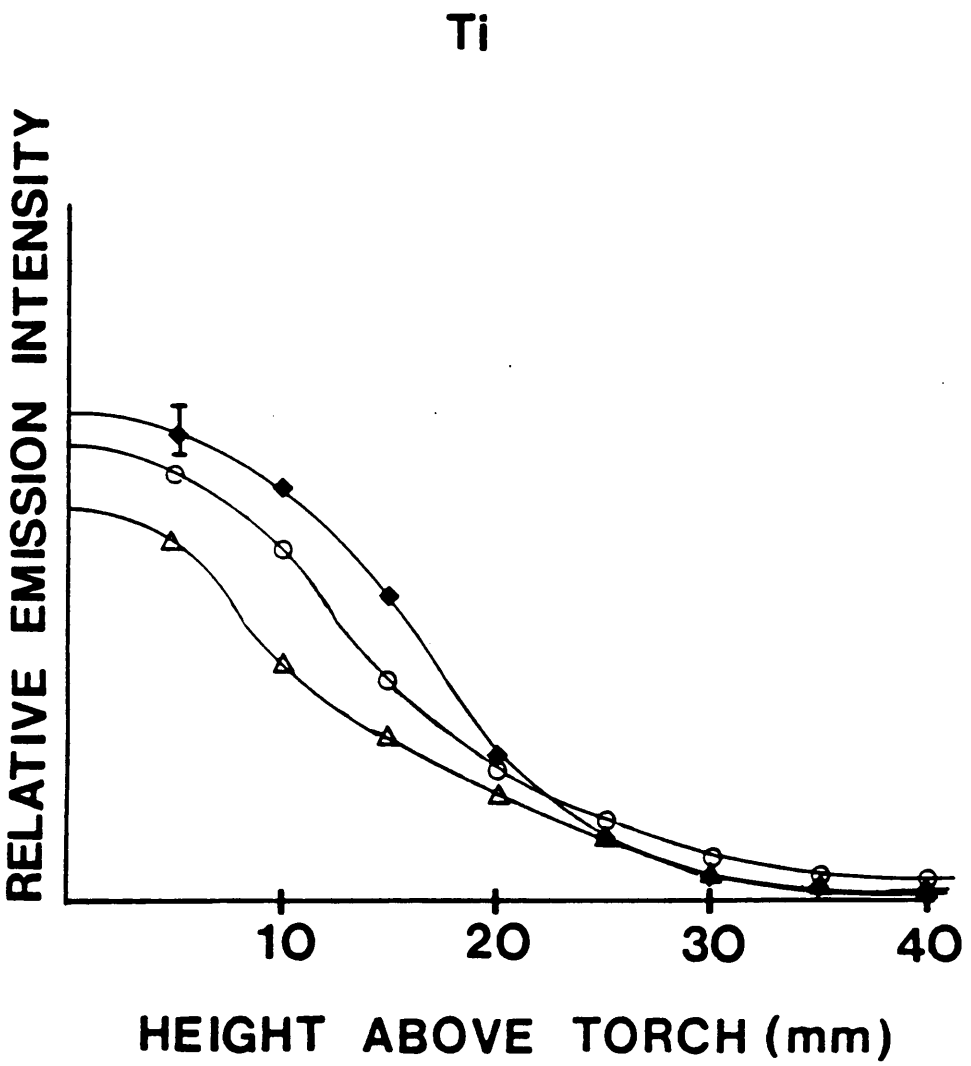

Figure 21. Profile of a 1000 ppm Ti solution at 334.2 nm where the circles represent data points with the argon backfiller and the diamonds represent data points with 20 cc/min oxygen.

20 cc/min propane. It can be observed that the titanium solution profile shows an enhanced emission signal with the addition of propane and a depression with the addition of oxygen. Since the bond formation energy for the oxide is 157 kcal/mol and the bond formation energy for the carbide is 104 kcal/mol titanium is more likely to form an oxide than a carbide [60]. This data follows the predictions in that titanium reacts with the oxygen to form titanium oxide, depleting the concentration of free titanium atoms. This depletion results in a depression of the atomic emission signal, as compared to that of a titanium solution with the argon back filler. The enhancement observed upon the addition of propane can be explained by reasoning that oxygen from the dissociation of water or from atmospheric entrainment may be reacting with titanium to give titanium oxide. Therefore, propane may be reacting with the titanium oxide to give CO and free titanium atoms, which will enhance the atomic emission from the titanium atoms as can be seen in reaction 3. As the titanium sample travels higher into the plasma tail plume, all of the signals converge giving little diagnostic information.

In Figure 22, the atomic emission profiles for the titanium carbide sample can be observed. The circles represent data points with the addition of the argon backfiller, the diamonds represent data points with the

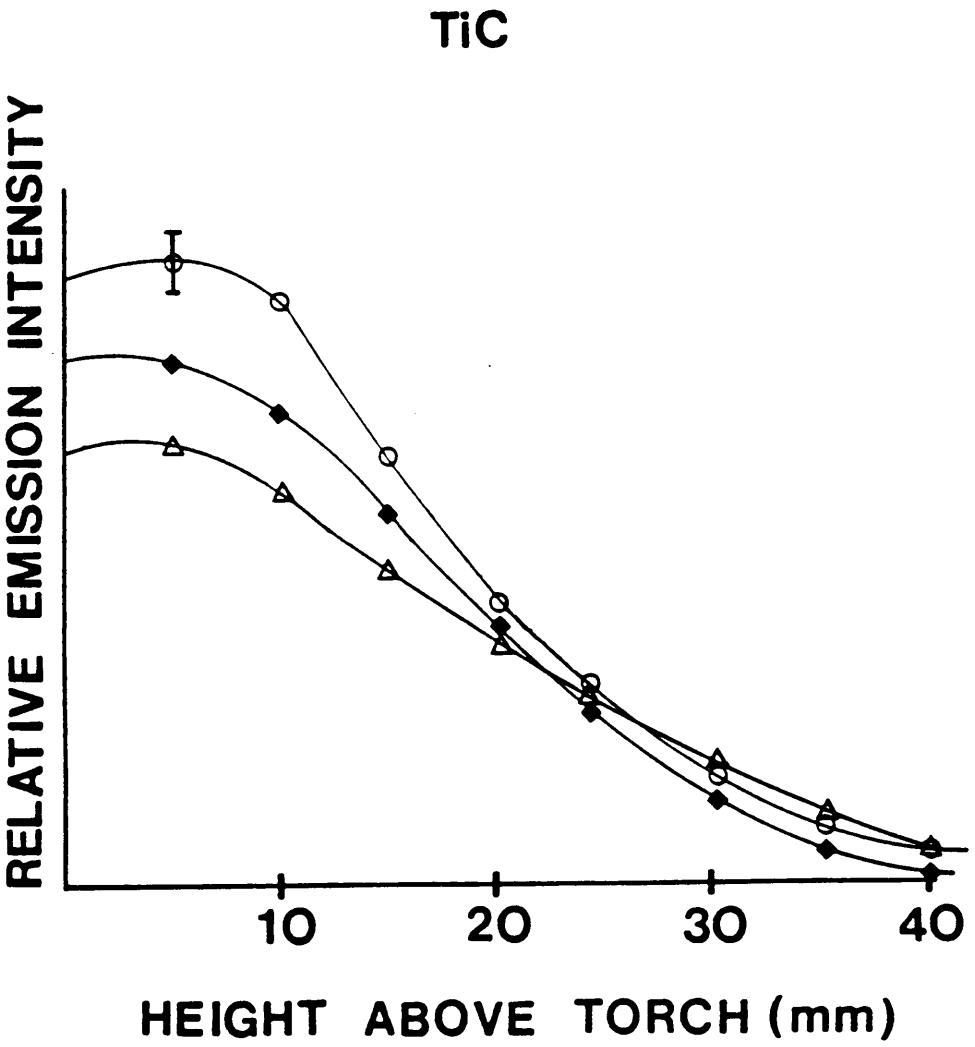

Figure 22. Profile of a 2000 ppm titanium carbide slurry at 334.2 nm where the circles represent data points with the argon backfiller, the diamonds represent data points with the addition of 20 cc/min propane, and the triangles represent data points with the addition of 20 cc/min oxygen.

addition of 20 cc/min propane, and the triangles represent data points with the addition of 20 cc/min oxygen. The recovery of signal versus a solution of titanium was 10% for the slurry. These profiles show that the addition of propane caused a depression in the titanium atom signal from the dissociation of titanium carbide. This depression was predicted by reaction 2. The addition of 20 cc/min oxygen did not cause the results predicted by reaction 4, but instead may be explained by bond formation energies. Titanium carbide is dissociated by the plasma to give vapor phase titanium and carbon. The added oxygen may not have reacted solely with the carbon to form CO and give an enhanced titanium atom signal, but also with the titanium to form titanium oxide.

A titanium oxide slurry was also analyzed and its profiles can be seen in Figure 23. The circles represent data points with the addition of the argon backfiller, the diamonds represent data points with the addition of 20 cc/min propane, and the triangles represent data points with the addition of 20 cc/min oxygen. The addition of propane or oxygen causes depressions in the atomic emission signal of the titanium atom line. The addition of oxygen was predicted to cause a depression in the atomic emission of the metal oxide as indicated by reaction 1. It was predicted by reaction 3 that the addition of propane to the

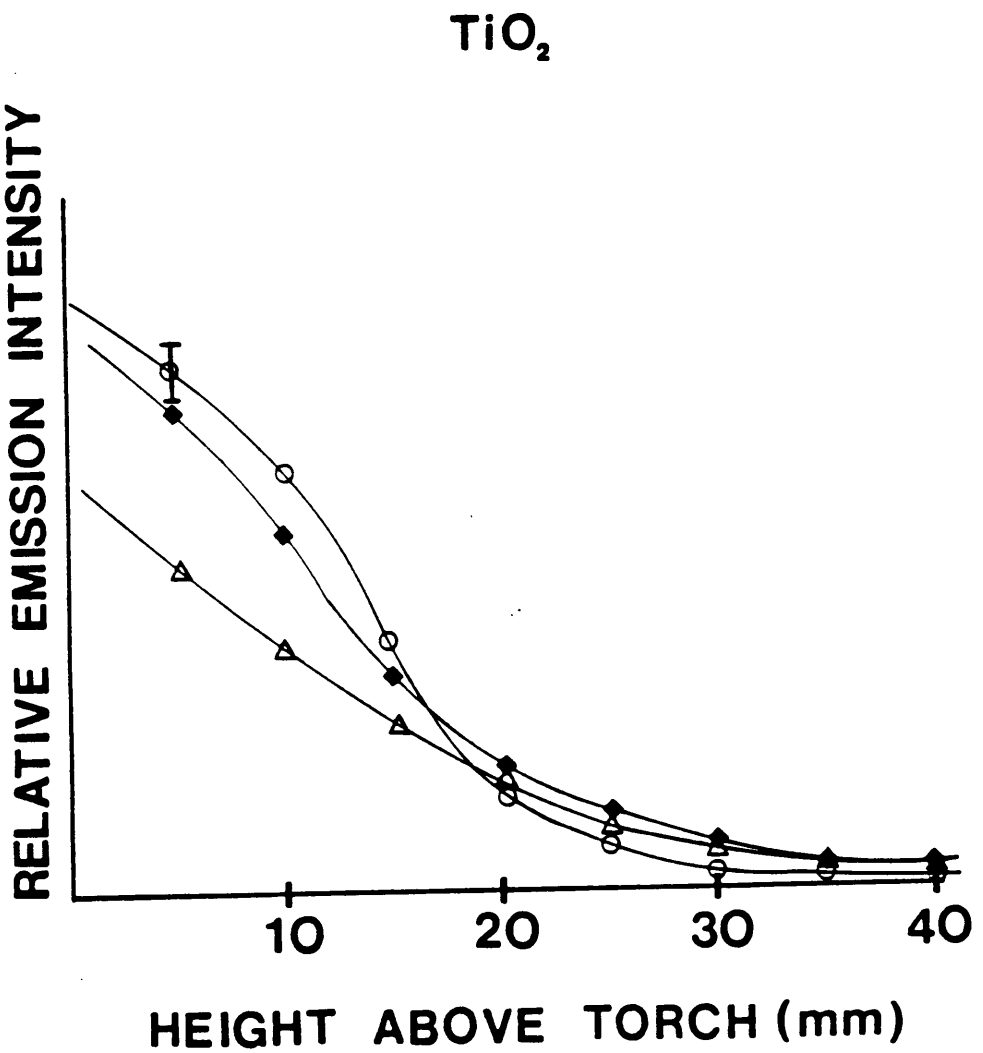

Figure 23. Profile of a 2000 ppm titanium oxide slurry at 334.2 nm where the circles represent data points with the argon backfiller, the diamonds represent data points with the addition of 20 cc/min propane, and the triangles represent data points with the addition of 20 cc/min oxygen.

metal oxide slurry would cause an enhancement in the atomic emission of the metal atom, but again this was not observed. The propane depression of the atomic emission may be caused by the free atom reacting with carbon as in reaction 2, to reduce the free atom population.

Unlike titanium, tungsten appeared to more closely follow the predicted reactions for atom enhancements. In Figure 24 it can be seen that the addition of oxygen (the triangles) to a tungsten carbide slurry caused an enhancement in the tungsten atomic emission at 407.4 nm. This result was predicted by reaction 4. The addition of 20 cc/min propane (the diamonds) to the plasma caused a depression in the atomic emission signal of the tungsten atom line, as predicted by reaction 2. It can be noted that the emission profiles of the slurries for tungsten carbide merged higher in the plasma tail plume.

The profiles for tungsten oxide also behaved according to the predicted reactions as can be seen in Figure 25. The addition of propane to the 2000 ppm slurry of tungsten oxide showed an enhancement throughout the entire plasma profile. The addition of 20 cc/min oxygen did not originally show a depression in the metal atom emission signal, as was predicted by reaction 1. Instead, as the tungsten oxide went higher into the plasma tail plume a depression was recognized. The results for tungsten and

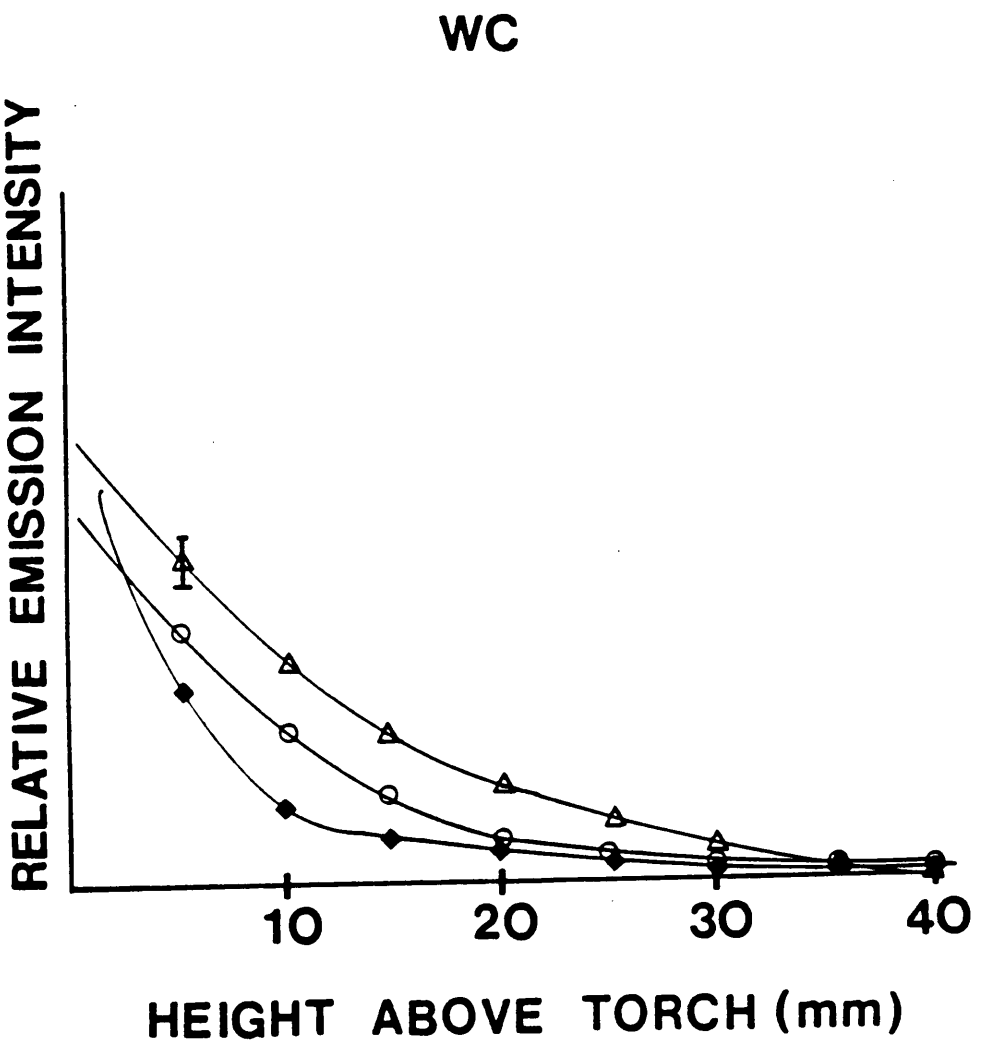

Figure 24. Profile of a 2000 ppm tungsten carbide slurry at 407.4 nm where the circles represent data points with the argon backfiller, the diamonds represent data points with the addition of 20 cc/min propane, and the triangles represent data points with the addition of 20 cc/min oxygen.

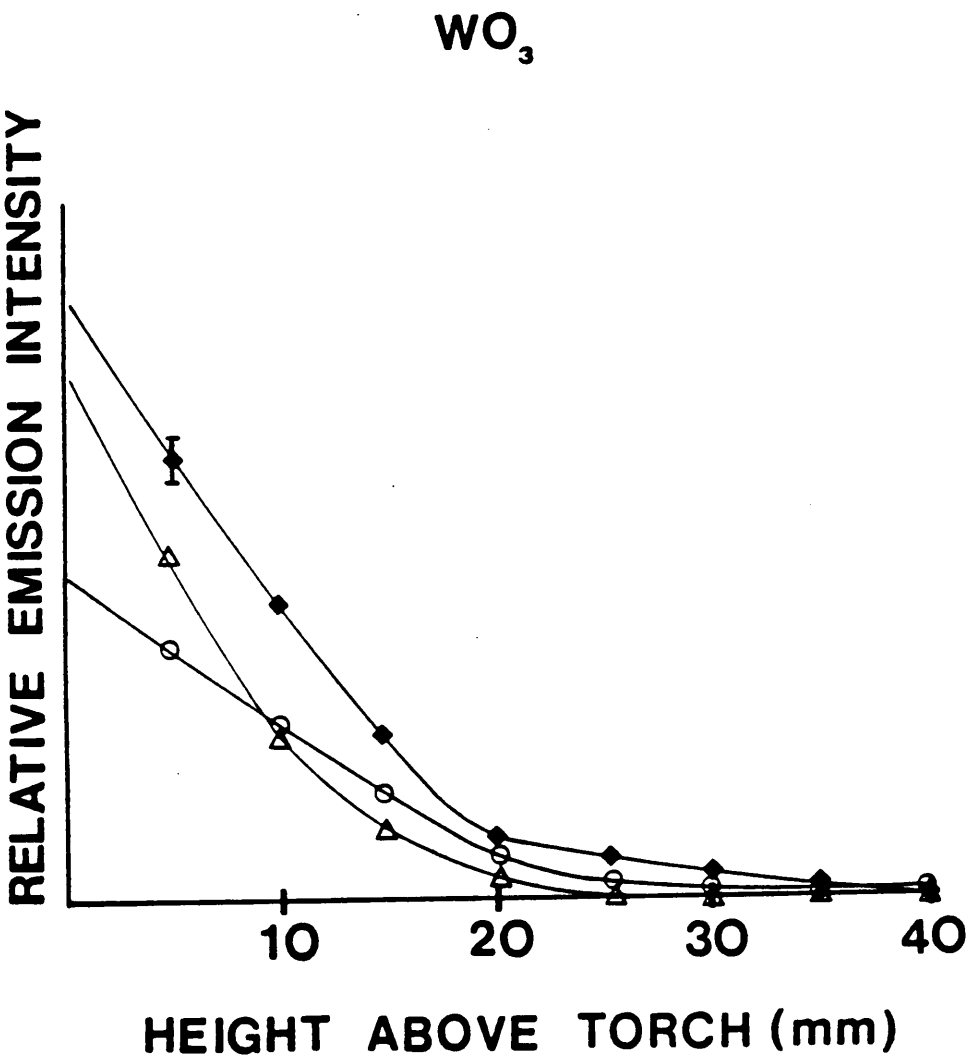

Figure 25. Profile of a 2000 ppm tungsten oxide slurry at 407.4 nm where the circles represent data points with the argon backfiller, the diamonds represent data points with the addition of 20 cc/min propane, and the triangles represent data points with the addition of 20 cc/min oxygen.

titanium support the hypothesis that molecular formation reactions are responsible for signal depressions in the plasma with the addition of propane.

Physical Alteration of the ICP

The plasma profiles at 396.2 nm for a 2000 ppm aluminum oxide slurry can be seen in Figure 26. The addition of 20 cc/min propane (the diamonds) gave an enhancement throughout the entire plasma profile, as was predicted by reaction 3. The addition of 20 cc/min oxygen (the triangles) did not show the effect that was predicted. Unexpectedly, the addition of oxygen showed an enhancement in the aluminum atom emission signal. This enhancement could not easily be explained by a simple molecular formation reaction. The addition of oxygen to the aluminum oxide would be expected to cause a depression in the aluminum oxide slurry atom emission by increasing the formation of the aluminum oxide. However, this was not the case for the aluminum oxide slurry. The addition of oxygen appeared to cause a physical change in the plasma rather than a molecular formation to occur in the plasma. The use of an aluminum carbide slurry to help explain this anomaly was not possible since aluminum carbide reacts vigorously with water. In order to explore this observation, it was

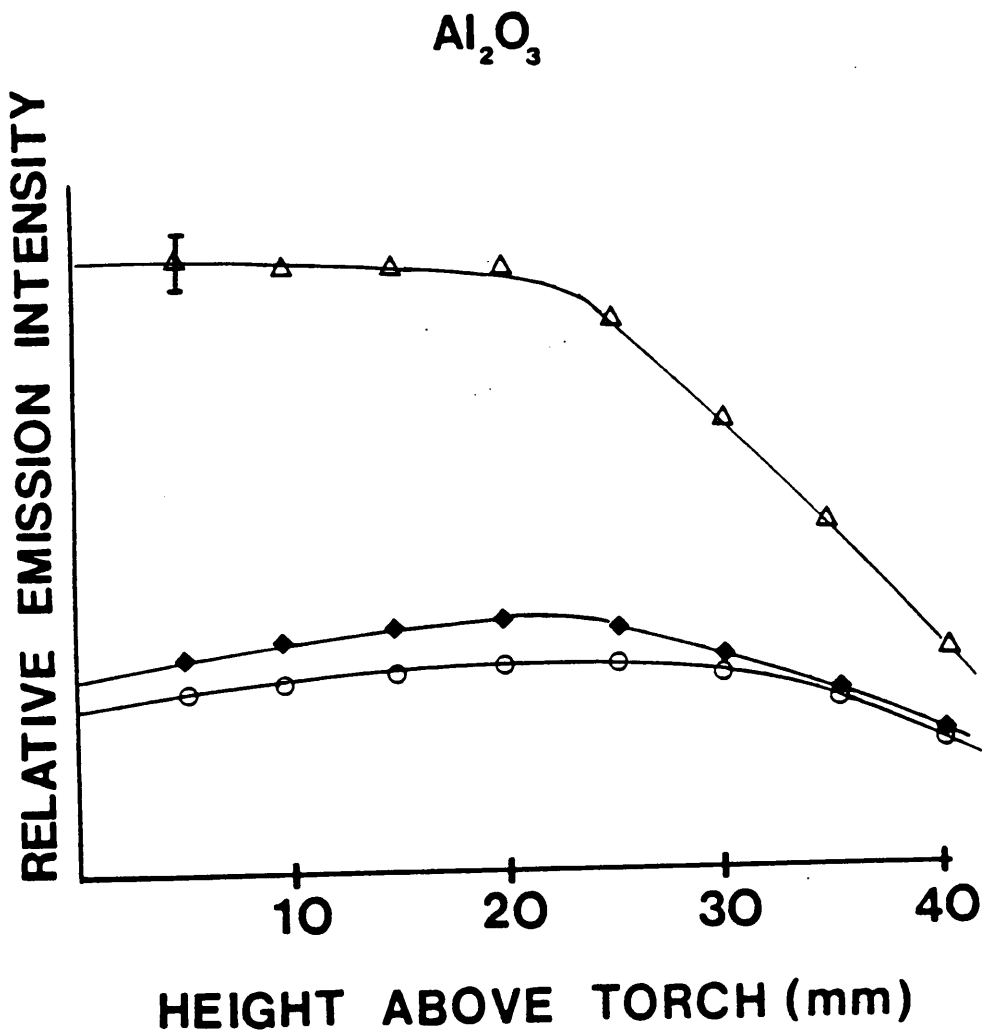

Figure 26. Profile of a 2000 ppm aluminum oxide slurry at 396.2 nm where the circles represent data points with the argon backfiller, the diamonds represent data points with the addition of 20 cc/min propane, and the triangles represent data points with the addition of 20 cc/min oxygen.

necessary to observe the effects of both propane and oxygen on a 1000 ppm solution of aluminum. As can be seen in Figure 27, the addition of propane appears to slightly enhance the aluminum atom emission signal as compared to the signal with the argon backfiller. This was predicted by reaction 3. However, as with the aluminum oxide slurry, the aluminum solution signal is unexpectedly enhanced with the addition of 20 cc/min oxygen. This addition of oxygen would be thought to promote the formation of aluminum oxide in both cases, resulting in a depression of the aluminum atom atomic emission rather than the observed enhancements.

To help explain this observation, an experiment to show the relationship between the enhancement of the aluminum atom signal and the amount of oxygen added was conducted. As can be seen in Figure 28, there appears to be a relationship between the addition of oxygen and the relative emission intensity of the aluminum atom. It can be seen that the addition of up to 60 cc/min oxygen enhanced the aluminum atom signal. This experiment was run with the addition of argon and the signal intensity was noted to decrease slightly with increased flow rates, with a characteristic drop in signal intensity at 70 cc/min.

Another experiment performed to elucidate the mechanism of signal enhancement. The effects of changing the concentration of the aluminum oxide slurry and

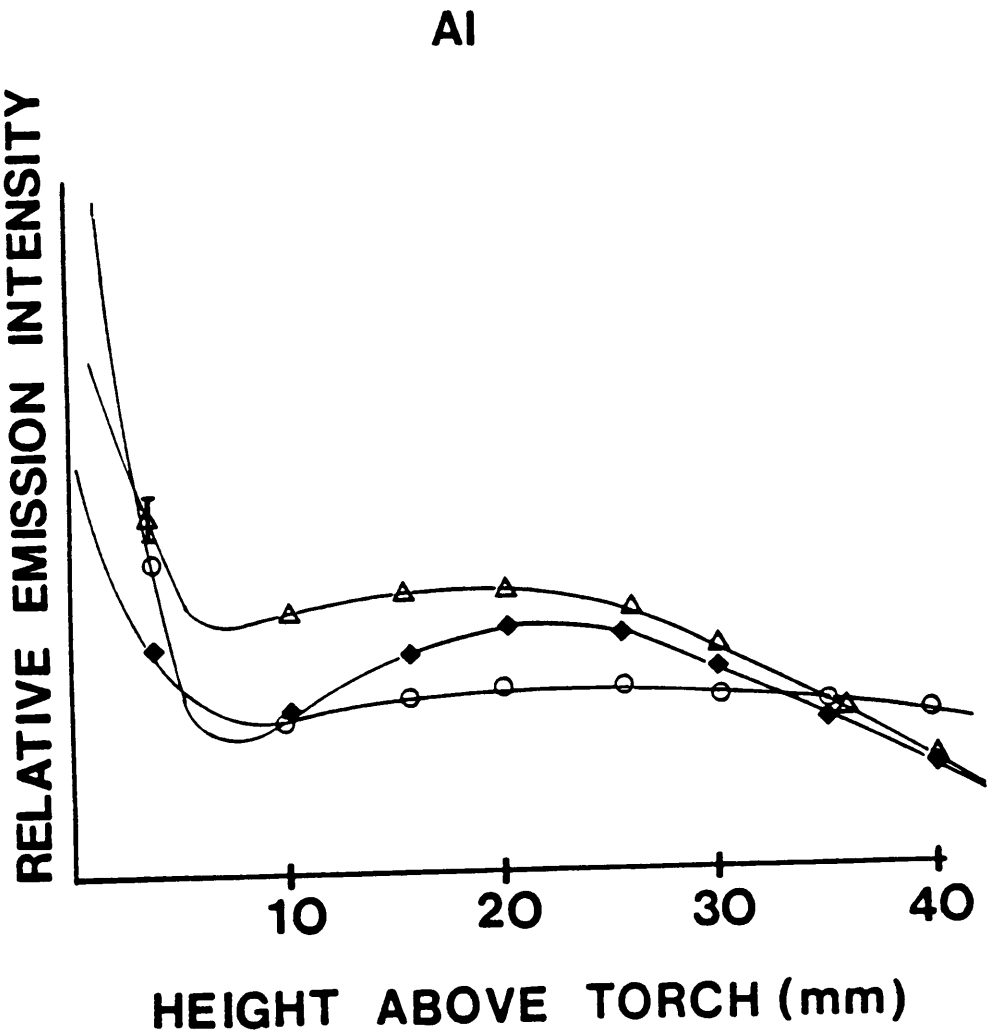

Figure 27. Profile of a 1000 ppm aluminum solution at 396.2 nm where the circles represent data points with the argon backfiller, the diamonds represent data points with the addition of 20 cc/min propane, and the triangles represent data points with the addition of 20 cc/min oxygen.

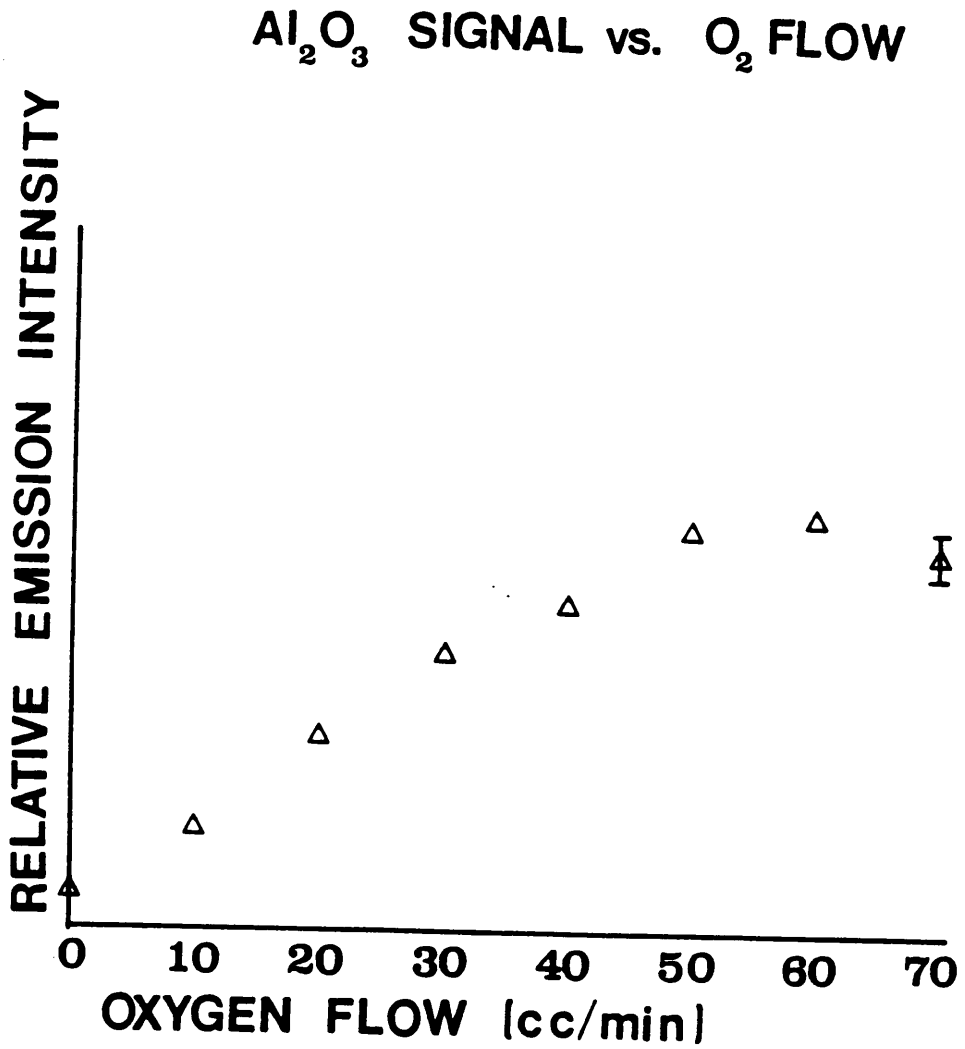

Figure 28. Oxygen flowrate study on the aluminum oxide slurry

maintaining the flow rates of the oxygen or the propane. In Figure 29, it is shown that there was a consistent relative enhancement in the working curve with the addition of 20 cc/min oxygen (the triangles). Also, noted by the linearity of the curve with respect to that of the aluminum atom signal with the argon backfiller. It is also important to note that the addition of propane also caused a similar effect. There does not appear to be a dependence upon the analyte concentration with respect to the observed enhancements. However, there does appear to be a direct relationship between the amount of oxygen or propane added to the plasma and the signal enhancement.

Conclusions

The results of these slurry experiments indicate that molecular formation reactions in the pencil plasma are plausible, but they do not appear to be the predominant mechanism occurring to affect the atomic signals. As shown above, the nature and the magnitude of magnitude of the effects of propane or oxygen on the atom signal can not be well correlated to the strength of the metal oxide or the metal carbide bond strengths. There was no effect of analyte concentration on the relative enhancements observed for the aluminum oxide slurry upon the addition of propane or oxygen, but there was an effect from the flow rate of

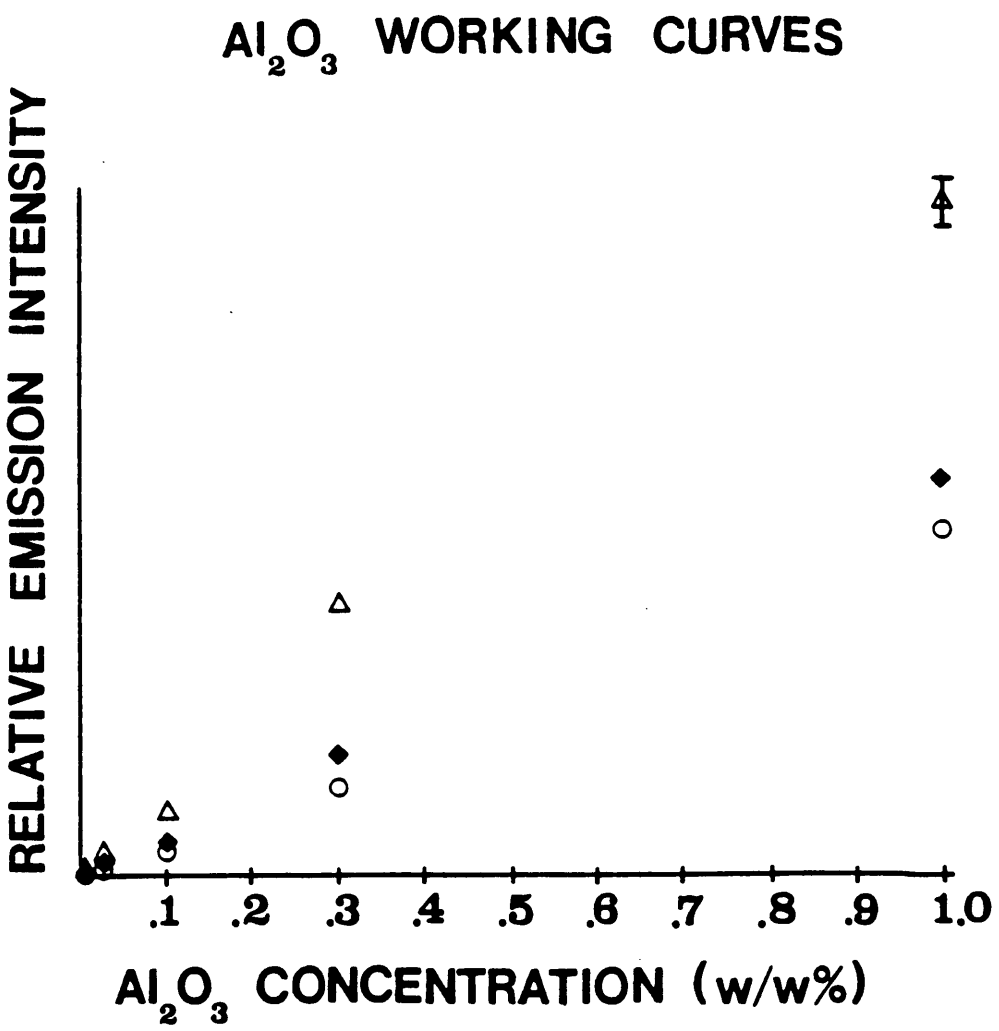

Figure 29. Working curves of aluminum oxide slurries at 396.2 nm where the circles represent data points with the argon backfiller, the diamonds represent data points with the addition of 20 cc/min propane, and the triangles represent data points with the addition of 20 cc/min oxygen.

the auxiliary gas on the enhancements indicating that the plasma itself is being affected. Thus, the large enhancements that are observed in atomic fluorescence spectrometry using propane probably do not solely result from the reduction of metal oxides.

Chapter 5
Atomic Absorption

The introduction of metal oxide and metal carbide slurries was used for diagnostic studies to gain information into the possible mechanism for the observed discrepancies between atomic emission and fluorescence in the pencil plasma. With the slurries, molecular formation reactions (i.e. metal oxide) appear to be occurring in the tail plume of the pencil plasma. However, there also appears to be a reduction mechanism based on energy transfer to the analyte occurring in this region.

To further examine the effects of propane on atomic spectrometric signals and to develop a mechanism explaining the discrepancy observed between atomic fluorescence spectrometry and atomic emission spectrometry, it is necessary to examine the ground state atom population. As can be seen in Figure 30, the ground state atom population can be probed by either atomic fluorescence or by atomic absorption spectrometry [8]. For both of these techniques, the ground state atom is radiatively populated to an excited level by an external source. This source can be a xenon arc lamp, a laser, or a hollow cathode lamp. With atomic emission, the plasma must also provide the energy to thermally excite the ground state atoms. In this study,

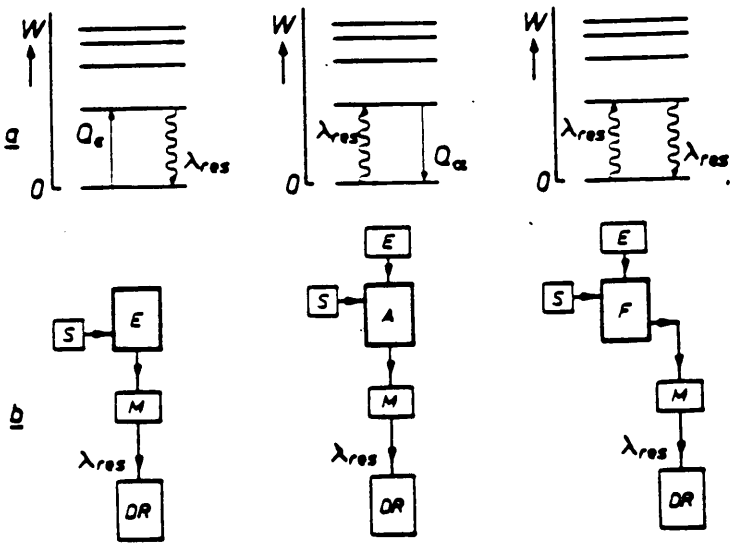

Figure 30. Mechanisms for emission, absorption and fluorescence.

hollow cathode lamps (HCL) were used as the excitation source for atomic absorption spectrometry.

The use of atomic absorption to examine the ground state should not be as severely affected by scatter as is atomic fluorescence and should give information about changes in ground state population with the addition of propane and. With atomic fluorescence, only a small percentage of the light absorbed is detected as fluorescence. In AAS, the total absorbance can be detected. The amount of light being scattered should remain constant in both the absorption and fluorescence studies, but the relative amount of scatter will be greater in the fluorescence studies as compared to the absorbance work. For our system, using f#2 lenses placed 6" away from the plasma, atomic fluorescence is 240 times more severely affected than is atomic absorption (see Appendix C) [61,62].

Experimental Setup

The system used for this study must be translatable throughout the plasma tail plume. See Figure 31 for a block diagram of the setup. The first method involved the translation of the plasma itself, but as was previously described, this would not be a simple task. Therefore, a method to translate the atomic absorption system with

EXPERIMENTAL SETUP

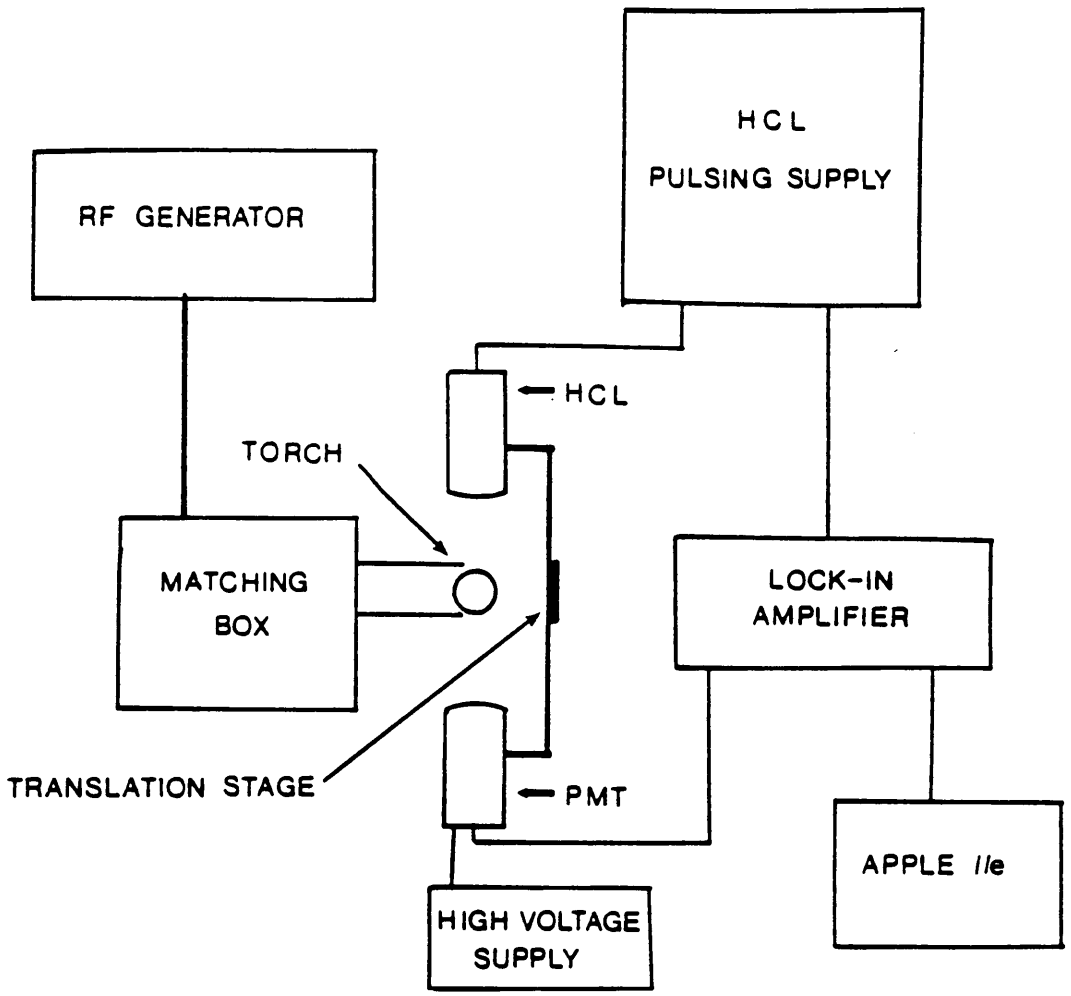

Figure 31. Atomic absorption setup

respect to the plasma was necessary. To accomplish this task a Baird atomic fluorescence module was dismantled and assembled to resemble an atomic absorption system (see Appendix D for the schematic). The source was placed a 180 degrees to the detector. The translation was accomplished using a translation stage from NRC with the module attached, and a thumb wheel micrometer for the motion.

Excitation Source

The source was an adjustable hollow cathode lamp housing, with a hollow cathode lamp (HCL) inside, taken from the Baird fluorescence system. An f#2 lens was used which gave a one to one image of the HCL six inches from the lens, in the center of the plasma tail plume. The detection system consisted of another f#2 lens placed 6 inches from the plasma tail plume which took the signal from the plasma and imaged it onto a photomultiplier tube (PMT). An interference filter was used to restrict the wavelengths of light that would reach the PMT to allow selectivity with reference to the samples.

To resolve the absorption from the background emission it was necessary to use a modulated source. Therefore, it was possible to separate the ac and dc components of the signal. Many times, it would be simplest to place a light chopper in the incident beam, but in this case it would be

difficult to translate the assembly throughout the plasma tail plume. Another way to modulate the light was necessary, so a pulsing system was designed which would turn the HCL on and off at regular intervals. This system consisted of three components. The first component was a high voltage supply from Heath that delivered 400 volts DC at 100 mA. The 400 volts were maintained inside of the pulsing network but the current was regulated by another part of the system. The signal was set by a waveform generator that gave a square wave signal at 12 Hz. This frequency was chosen since the output of the HCL still resembled a square wave. As the frequency was increased beyond 12Hz the lamp appeared more like dc source than a square wave. The third section of the pulsing system brought the waveform generator and the high voltage supply together, and was used to regulate when the current could flow through the lamp. Hence, the actual pulses in the lamp were caused by the current switching from 0 milliamps to 15 milliamps at 400 V dc in a square wave pattern. (See Appendix E)

Detection System

The detection system consisted of the PMT, the filters previously described, a fast current to voltage converter, and a lock-in amplifier. The current to voltage converter

was an EG&G model 5002. This I/V converter could be used with frequencies between 0.5Hz to 200kHz, and currents ranging from 100 nA to 1.0 mA. The non-linearity was typically 0.01%. The output voltage had a maximum of 17V peak to peak [63]. This was hooked directly to a model 5104 lock-in amplifier by EG&G. This amplifier had a useful range from 5Hz to 20kHz. The maximum input voltage was +/-200V dc. The output voltage is +/- 10V full scale [64]. It was possible to adjust the phase sensitivity of this amplifier to obtain the maximum signal deflection and to compensate for delays in the lamp current.

Data Collection and Presentation

The output voltage was obtained in the same fashion as described previously for atomic emission signals with the Apple IIe computer and the Adalab interface card.
The data in this chapter was obtained under nearly identical conditions in order to more accurately describe the effects of propane. Each set of data will consist of two plasma profiles, with the dots representing data points with the argon backfiller, and the triangles represent data points with the addition of 20 cc/min propane. This is consistent for both the atomic emission profiles and for the atomic absorption profiles. The atomic emission

profiles were obtained by using the demounted Baird fluorescence system to have a basis of comparison for the atomic absorption profiles. Each point represents a three second integration of signal with the respective background subtracted off for the atomic emission profiles. The atomic absorption profiles were obtained using a different data acquisition program. This program stored the background signal intensity (transmittance of the blank) for each data point. Then it stored the sample signal intensity (transmittance of the signal). After both profiles, background and signal, were obtained an absorbance value was calculated for each pair of transmittances (see Appendix f). Concentrations of analytes used in each absorption experiment were in the linear portion of the atomic absorption working curve, and corresponded to the same concentrations used for the atomic emission profiles. The profiles encompassed a distance from 10 mm above the top of the torch (70 mm above the induction coil) up to 50 mm above the torch (110 mm above the induction coil). The profiles began at 10 mm above the torch due to the size of the fluorescence module.

Results and Discussion

Much work has previously been accomplished with calcium with respect to atomic fluorescence and atomic

emission with the addition of propane, and it gave anomalous results. Therefore, calcium was selected to be the starting point for the atomic absorption study. A 100 ppm calcium solution was observed to be in the linear portion of the atomic absorption working curve, therefore it was used to examine the effects of propane on atomic absorption signals. The wavelength used was that of the calcium atom at 422.7 nm, which was consistent with previous calcium data. It can be seen in Figure 32 that the 100 ppm calcium solution has an absorbance slightly less than 0.3 absorbance units (represented by the circles) and upon the addition of 20cc/min propane (represented by the triangles) this absorbance increased. As the absorption profile was enhanced by the addition of propane, the calcium emission profile (represented by the triangles) was depressed in signal intensity. This effect was indicating the ground state atom concentration was enhanced by the addition of propane while the excited state population was somehow being depopulated through a non-radiative process. This observation helps to explain why enhancements were observed for calcium atomic fluorescence signals upon the addition of propane while atomic emission signals were depressed. Another important observation that can be made was the Baird fluorescence module operating in the atomic emission mode observed a

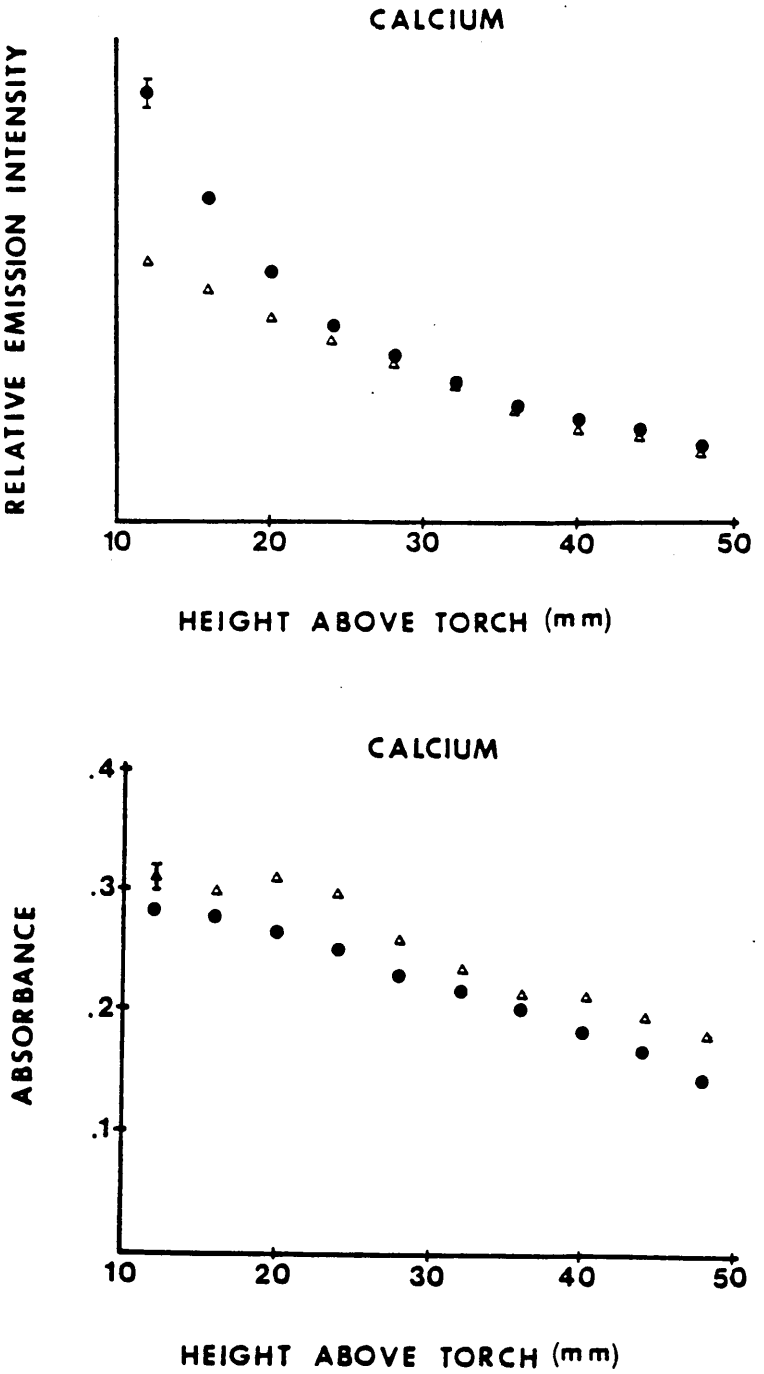

Figure 32. Emission and absorption profiles for 100 ppm Ca at 422.7 where circles are with the argon backfiller and the triangles are with 20 cc/min propane.

depression in atomic emission as did our system set up with a monochromator.

Copper has previously been observed to show depressions in atomic emission signal intensity upon the addition of propane into the pencil plasma. Copper was observed to exhibit linearity in its atomic absorption working curve with a 500 ppm copper solution directly in the center of the linearity. Therefore, it was used for this study. The copper atom wavelength used was 327.4 nm, and was used for both the atomic absorption and the atomic emission profiles. Again, the dots are data points with the argon backfiller and the triangles are data points with the addition of 20 cc/min propane. It can be seen in Figure 33 that the addition of the propane has caused between a 15-20% enhancement in the atomic absorption profile for copper throughout the entire plasma tail plume. At the same a 35-40% depression in the copper atomic emission profile extended throughout the entire pencil plasma tail plume. As was observed previously with copper atomic emission profiles, the addition of propane decreased the signal intensity. This observation indicates the depressions observed with the addition of propane are not an artifact of the previously used system. The copper profiles are indicating the the addition of propane increased the ground state atom population while decreasing

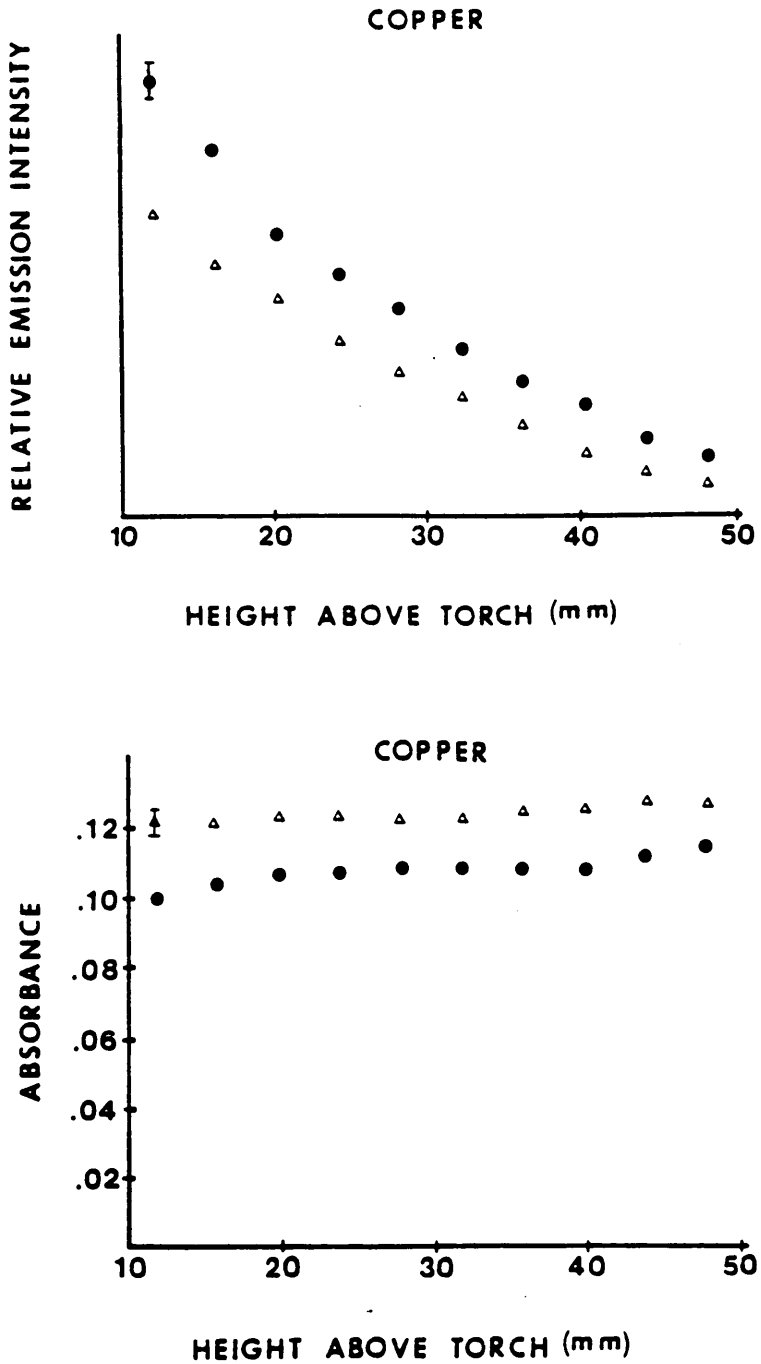

Figure 33. Emission and absorption profiles for 500 ppm Cu at 327.4 nm where circles are with the argon backfiller and the triangles are with 20 cc/min propane.

the copper excited state atom population.

A sample more energetically demanding on the plasma was barium ion. Not only does the plasma need to excite the sample to the ground state but it must ionize it and than excite it. The barium ionic emission wavelength was 455.4 nm. For this study, a 1000 ppm barium solution was observed to be in the linear portion of the barium atomic absorption working curve. It should be noted, a barium hollow cathode can be used to examine the barium ionic absorption [65]. It can be seen in Figure 34, the addition of 20 cc/min propane to the pencil plasma initially caused a 25% enhancement in the ionic absorption profile for the 1000 ppm barium solution. This enhancement decreases as one looks higher into the plasma tail plume, as might be expected for a higher energy species. While the atomic absorption profile was enhanced upon the addition of propane the atomic emission profile of the 1000 ppm barium solution at the barium ion wavelength was severely depressed. This observation indicates the barium ion ground state was enhanced upon the addition of propane while the excited state barium ion population was depressed. These results suggest that, like the previous samples (calcium and copper), the ground state was enhanced upon the addition of propane while the excited state was depressed.

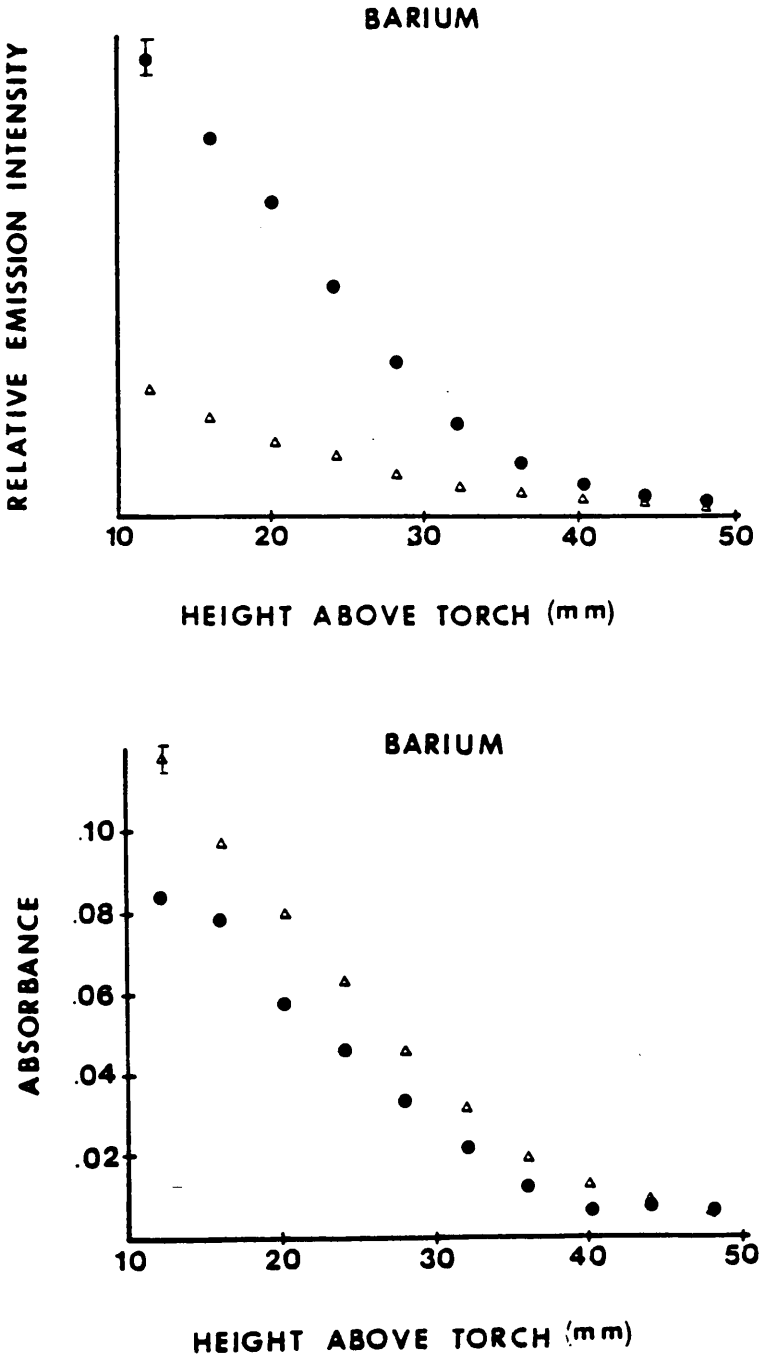

Figure 34. Emission and absorption profiles for 1000 ppm Ba at 455.4 nm where circles are with the argon backfiller and the triangles are with 20 cc/min propane.

The barium atom is less energetic than the barium ion and has previously been examined found to show enhancements in atomic emission signals upon the addition of propane. As observed with the barium ion, a 1000 ppm solution of barium fell in the linear portion of the atomic absorption working curve, thus was used for this experiment. The dots represent data points with the addition of the argon backfiller and the triangles represent data points with the addition of 20 cc/min propane in both sets of profiles. As can be seen in Figure 35, the addition of 20 cc/min propane caused an enhancement in the barium atomic emission intensity at the 553.5 nm wavelength. This observation using the filter system was consistent with previous data obtained using a monochromator. The atomic absorption profile showed a similar effect; the addition of 20 cc/min propane was observed to initially show an enhancement. These results indicated that the addition of propane increased both the excited and ground state populations for the barium atom.

Another element that exhibited similar results as did the barium atom was nickel, as can be seen in Figure 36. The profiles for nickel were obtained with a 500 ppm solution at the 352.4 nm wavelength. The dots represent data points with the argon backfiller and the triangles represent data points with the addition of 20 cc/min

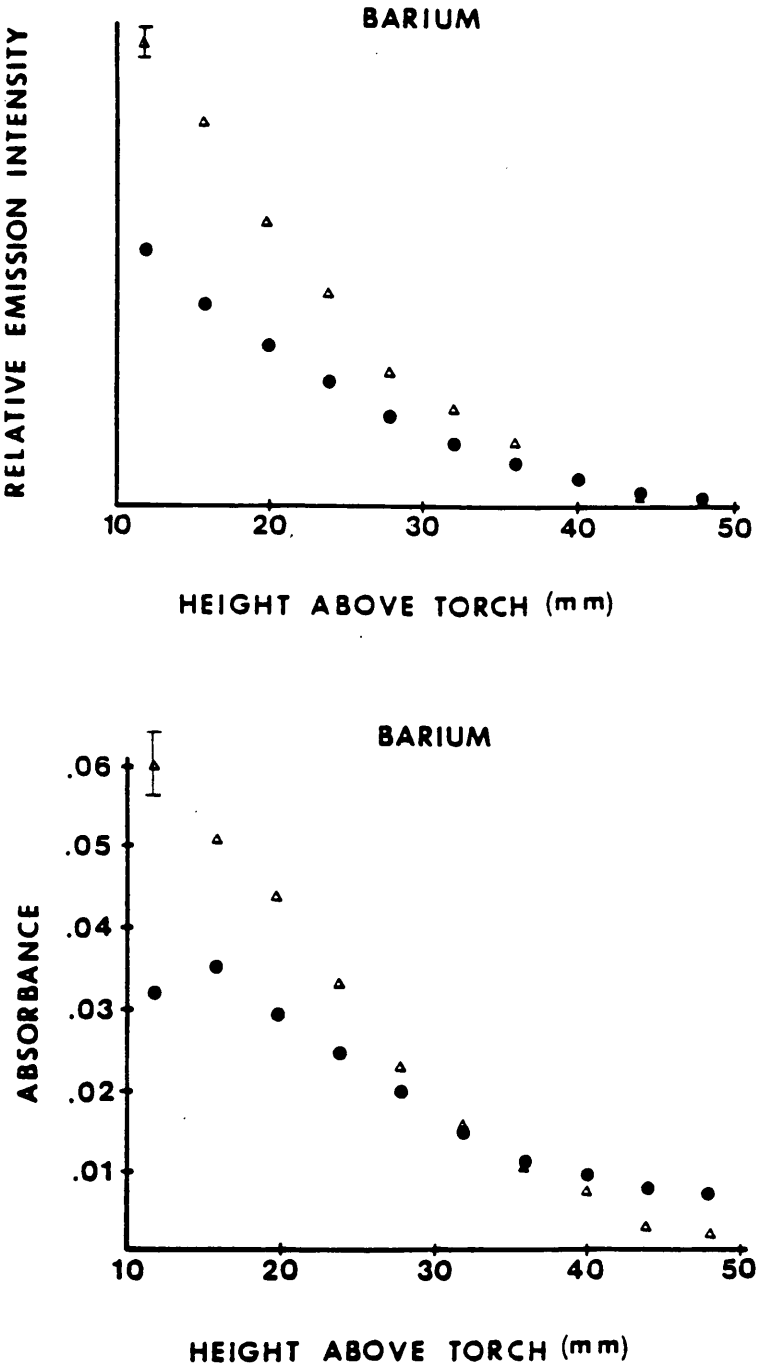

Figure 35. Emission and absorption profiles for 1000 ppm Ba at 553.5 nm where circles are with the argon backfiller and the triangles are with 20 cc/min propane.

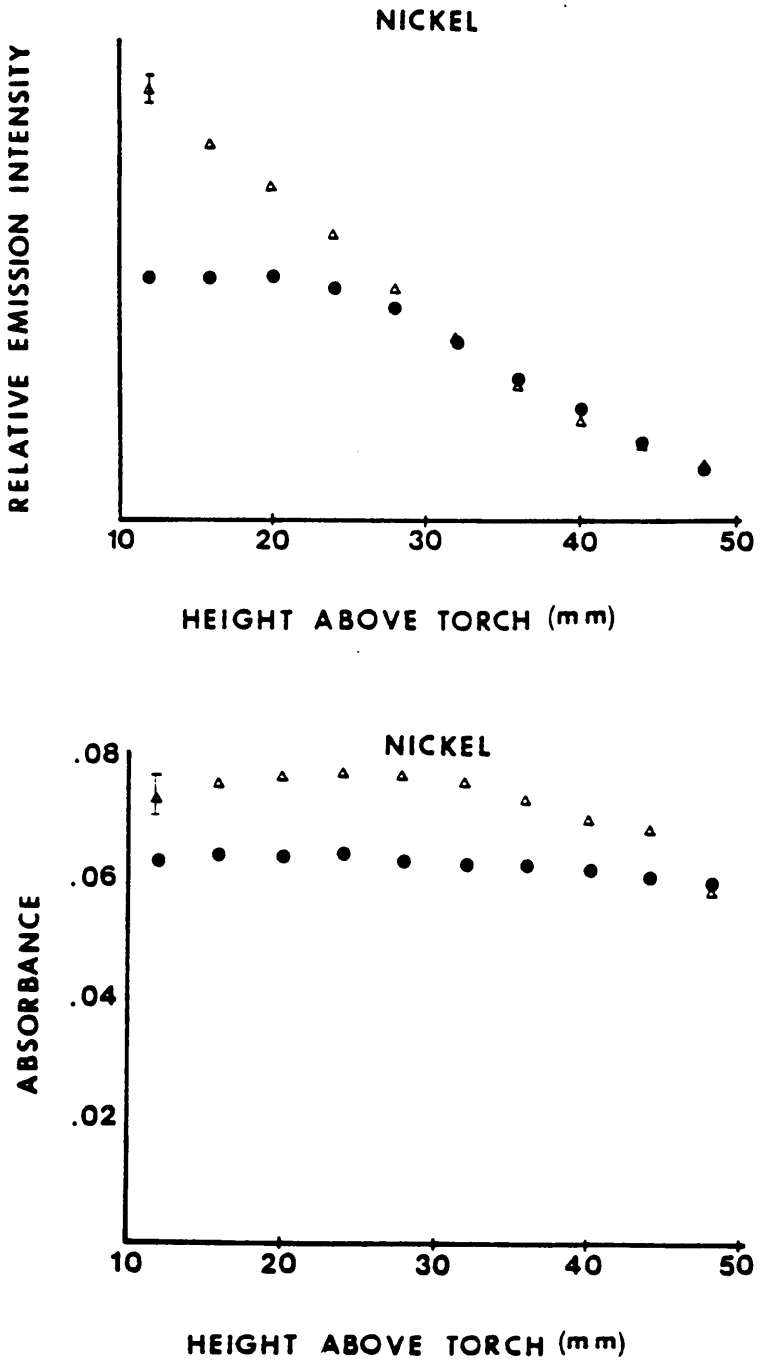

Figure 36. Emission and absorption profiles for 500 ppm Ni at 352.4 nm where circles are with the argon backfiller and the triangles are with 20 cc/min propane.

propane. As was observed with the barium atom emission, the nickel atom emission initially shows a signal enhancement upon the addition of propane. Consistently, the nickel atomic absorption at the same concentration and wavelength showed a similar enhancement upon the addition of 20 cc/min propane. Again, the same conclusion can be made for nickel as with barium which is the propane caused enhancements in both the excited and ground state atom populations.

The next two elements that were examined are both Group Ia elements. They were expected to show similar effects among themselves upon the addition of propane and were grouped together under the common name of easily ionizable elements. Both potassium and lithium ionize easily compared to the previously described elements. This makes their atom lines weak compared to their ion lines, but for this study the atom lines were used. The first of the two elements described is lithium. For lithium a 100 ppm solution was found to be in the linear portion of the atomic absorption working curve, and was used for this experiment. Both the atomic emission profiles and atomic absorption profiles for lithium were obtained at the 670.7 nm wavelength. The dots represent data points with the addition of the argon backfiller, and the triangles represent data points with the addition of 20 cc/min

propane. In Figure 37, the propane can be seen to cause an enhancement in the atomic emission profile for the lithium atom. The addition of propane also caused a slight enhancement in the atomic absorption profile for lithium. These results suggest that the addition of propane caused an increase in the lithium atom excited state population and it also caused a slight enhancement in the lithium atom ground state population.

The other easily ionizable element, potassium, was observed to show similar effects upon the addition of propane as can be seen in Figure 38. The addition of 20 cc/min propane was observed to cause an enhancement in the atomic emission profile for the potassium atom. As was observed with the lithium sample, the potassium atomic absorption profile showed a slight enhancement upon the addition of propane. These results also suggest that the addition of propane was causing an increase in the excited state for potassium as it did with lithium, and it also showed a slight enhancement in the potassium ground state population. As can be seen from the profiles of lithium and potassium, although they are from the same group, their profiles do not appear identical. An explanation for the different curves is that lithium is a higher energy element than is potassium, and the lithium reached a maximum at a more energetic region of the plasma, whereas, potassium

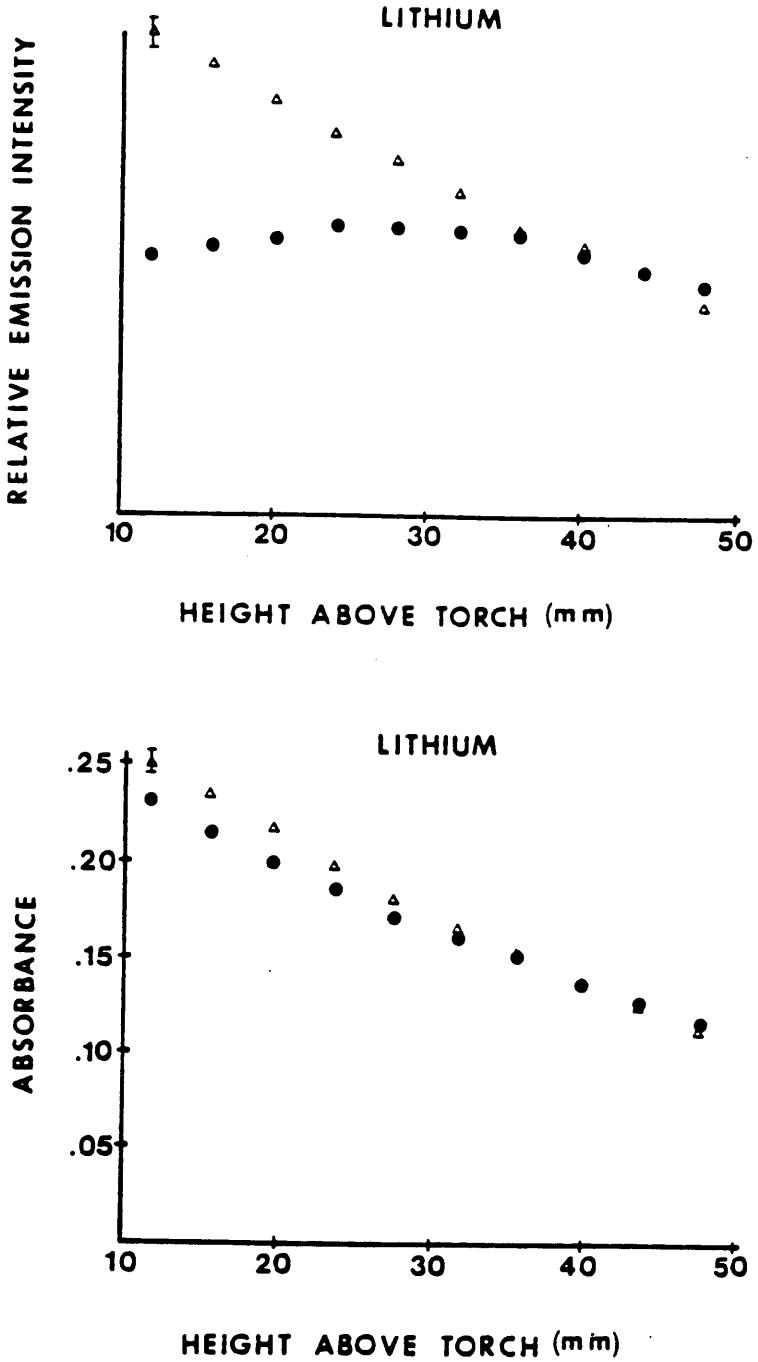

Figure 37. Emission and absorption profiles for 100 ppm Li at 670.7 nm where circles are with the argon backfiller and the triangles are with 20 cc/min propane.

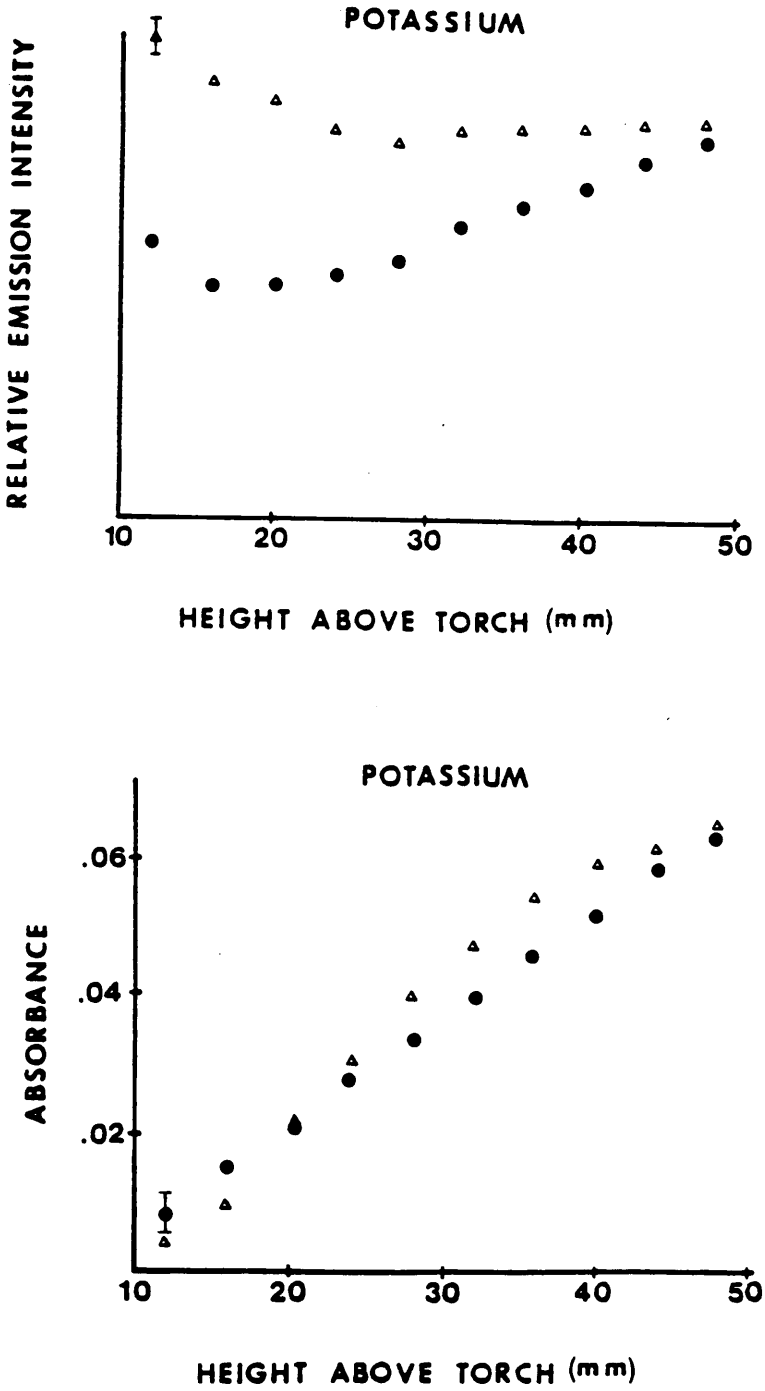

Figure 38. Emission and absorption profiles for 500 ppm K at 766.5 nm where circles are with the argon backfiller and the triangles are with 20 cc/min propane.

being a less energetic element reached a maximum at a less energetic region of the plasma. This can be observed in both the atomic emission and the atomic absorption profiles. The lithium atomic emission profiles were observed to exhibit a maximum at 30 mm above the torch, while the potassium had not reached its maximum at 50 mm above the top of the torch. The atomic absorption profile for lithium had its maximum absorbance at the top of the torch and continued to decline throughout the plasma tail plume, while potassiums absorbance continued to increase as it went higher into the plasma tail plume. Potassium still had not reached its maximum by the end of the 50 mm profile.

The last element discussed in this section is silver. Silver is last since its results were different than those previously described. At 328.1 nm, a 1000 ppm silver solution was observed to be in the linear portion of the silver atomic absorption working curve. In Figure 39, it can be seen that the addition of 20 cc/min propane, represented by the triangles, caused a severe depression in the the silver atomic emission. The silver atomic emission profile dropped off rapidly, and this can be explained by the silver being a very energetic species requiring greater energy than was available higher in the plasma tail plume. This effect can also be observed in the atomic emission

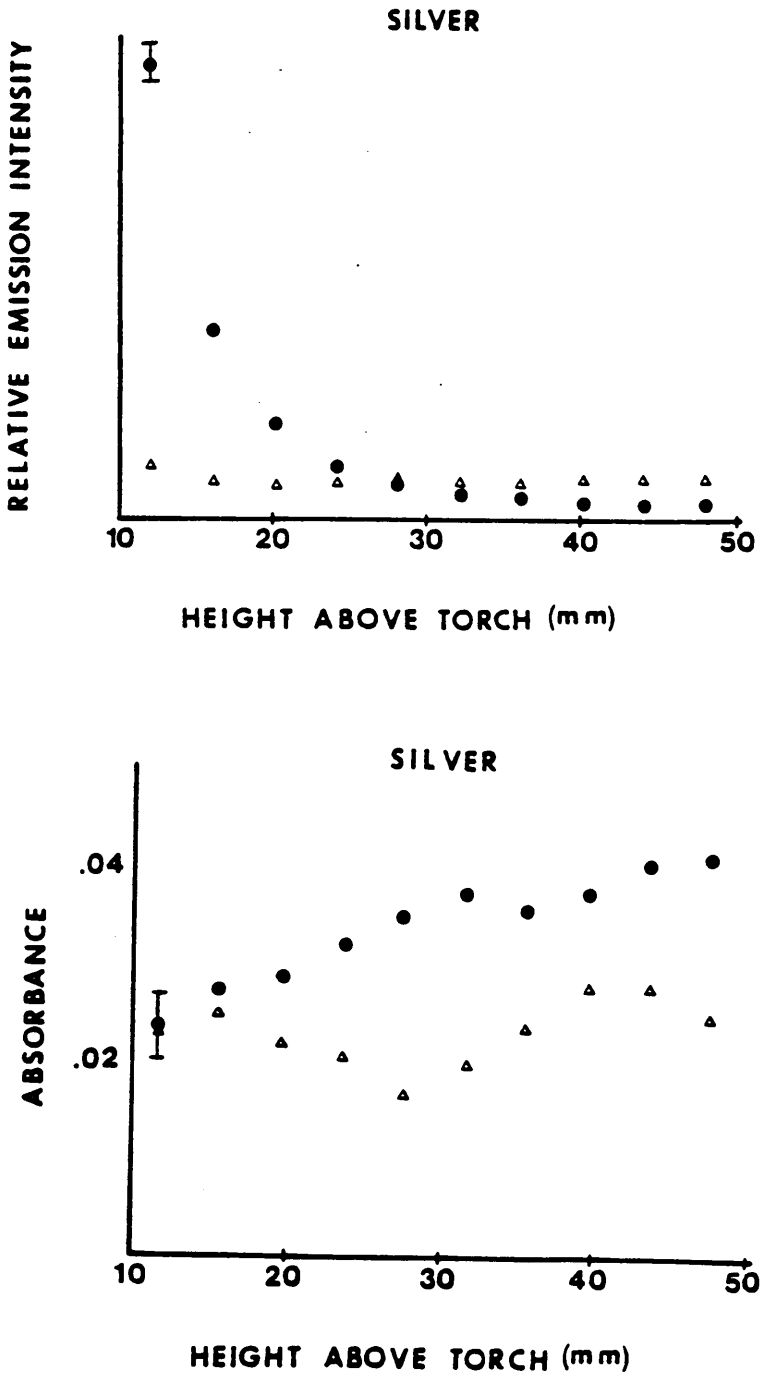

Figure 39. Emission and absorption profiles for 1000 ppm Ag at 328.1 nm where circles are with the argon backfiller and the triangles are with 20 cc/min propane.

profile. First, the values for absorbance are very low, possibly indicating there was low silver atom population, and secondly the addition of propane causes a depression in this already low absorbance profile. These two profiles indicated that the addition of propane to the plasma decreased both the silver excited and ground state populations.

Conclusions

A general conclusion can be drawn from the above results: the propane did not affect the excited state population consistently with respect to the ground state population. The ground state, being lower in energy than is the excited state, was more likely to be enhanced upon the addition of propane than was the excited state. It appeared from this study that if the ground state was enhanced the excited state could be either enhanced or depressed, but if the ground state was depressed then the excited state would also be depressed (see Table III). These data indicated that not only can molecular formations be occurring in the plasma tail plume, but the energy of the species must also be taken into consideration.

Table III - Condensed Atomic Emission and Absorption Results

Element	Conc. (ppm)	Line (nm)	MO (kcal/mole)	AES	AAS
calcium	100	422.7	92.0	-	+
copper	500	327.4	65.2	-	+
barium(II)	1000	455.4	----	-	+
barium(I)	1000	553.5	130.0	+	+
nickel	500	352.4	93.6	+	+
lithium	100	670.7	81.4	+	+
potassium	500	766.5	66.3	+	+
silver	1000	328.1	53.7	-	-

Conc. = concentration
MO = metal oxide bond
\- = depression
\+ = enhancement

Chapter 6
Energy Studies

Previously, it was shown that the addition of propane to the aerosol gas of the pencil plasma caused different effects to occur with various atomic species. In the previous chapter, barium exemplified this result. The barium excited ion population was depressed upon the addition of propane, while the ground state ion population was enhanced. Next, the barium excited atom population and barium ground state atom population were enhanced upon the addition of this organic gas. These results were typical for several other elements. In this chapter, these discrepancies are discussed and a mechanism for the results is proposed.

Experimental

The work in this chapter was performed using the experimental system described in detail in chapter 2. The only exception to this was some data was collected on a chart recorder rather than obtained by the Apple IIe computer. Another aspect of the system, that was modified to obtain further insight into the propane mechanisms, was the torch design. As can be seen in Figure 40, the long torch was modified to give a design between a long torch

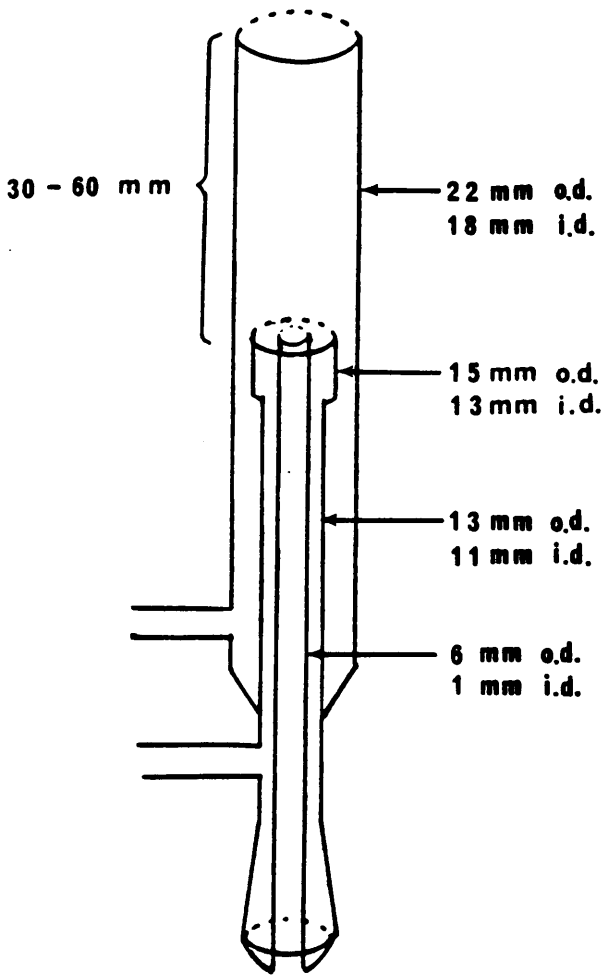

Figure 40. Schematic of a modified long sleeve torch.

and a standard ICP torch. The only change actually made to the torch was the length of the outer tube being decreased by 30 mm. The flows through this modified torch were the same as the flows, that can be seen in Table I, to maintain consistency between data.

Results and Discussion

ICP Power Reduction

The first experiment focused on the affects of propane on the atomic emission signals of a 100 ppm solution of barium. Using the chart recorder and the scanning monochromator, it was possible to scan across the barium ion line and to slew to the barium atom line to monitor the effects of propane on each signal. The results of this experiment can be seen in Figure 41. In a paper by Blades et al. [24], it was noted that the addition of an organic solvent into the ICP using a standard configuration gave what appeared to be a decrease of 500 W in a 2000 W plasma. Using the premise of this work, it was thought to be important to observe if this apparent decrease in energy upon the addition of propane was an "across the board" change or was it the result of various populations being affected differently. It can be seen in Figure 41 that the barium ion signal at 455.4 nm was about 2.5 times as large as the emission intensity for the barium atom line at 553.6

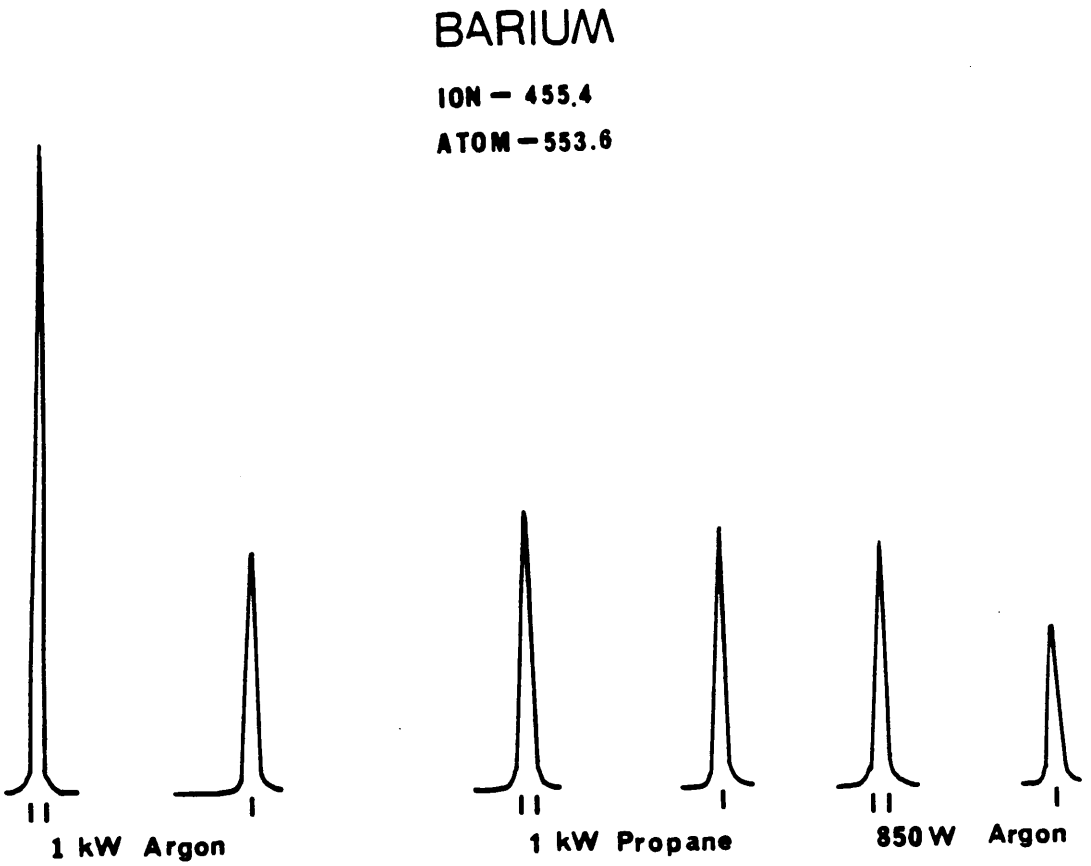

Figure 41. Barium atom and ion lines at 1 kW, 1 kW with propane, and 850 W without propane.

nm for a 1000 watt pencil plasma. In this experiment, 20 cc/min of propane was added to the 1000 W pencil plasma, and the intensity of the barium ion line dramatically decreased. The barium atom line was observed to slightly increase in intensity, and it should be noted that the two lines had roughly equal intensities as can be observed from the center set of lines on Figure 41. In order to look at the energy contribution, with respect to the addition of propane, it was necessary to assume a reference point and for this experiment the barium ion line was used. The argon backfiller was used to replace the propane. The barium ion line was monitored and the incident power was lowered until the barium ion line matched the barium ion line with the addition of propane. As can be seen from Figure 41, a reduction in power of 150 watts was required to match the barium ion emission intensities.

The next aspect of this experiment was to observe the effects of this reduction in forward power on the barium atom intensity. If there was an "across the board" change upon the addition of propane then the barium atom intensity should match that of the barium atom intensity with the addition of propane. If an "across the board" change does not occur then the barium atom intensity at 850 watts would not be the same. As it can be observed, the barium atom intensity at 850 W and at 1kW with propane was not the

same, therefore, it was concluded that the addition of propane to the plasma did not simply reduce the incident power perceive by the plasma, but it affected the various energy levels differently.

Looking at the ratio of the atom to ion intensities, it should be possible to obtain insight to certain atomic populations that are being affected differently by the addition of propane. To determine if the changes in various populations were occurring throughout the plasma tail plume a profile of atom to ion ratios was obtained. Calcium exhibits the same type pattern exhibited by barium. In Figure 42, which is a plot of the calcium atom to ion ratio, as one looks higher into the plasma tail the atom to ion ratio increases for both profiles. The lower profile is the atom to ion ratio with the argon backfiller represented by the dots, which begins at the top of the torch (60 mm above the induction coil). This plot exhibits a ratio of 0.5, corresponding to a more intense ion line with respect to the atom line. At 50 mm above the top of the torch (110 mm above the induction coil), the atom to ion ratio has reached a value of 17, indicating that the atom signal intensity was 17 times greater than the ion line relative intensity. The triangles represent atom to ion ratios with the addition of 20 cc/min propane. The ratios began with a value of 4 indicating that the atom

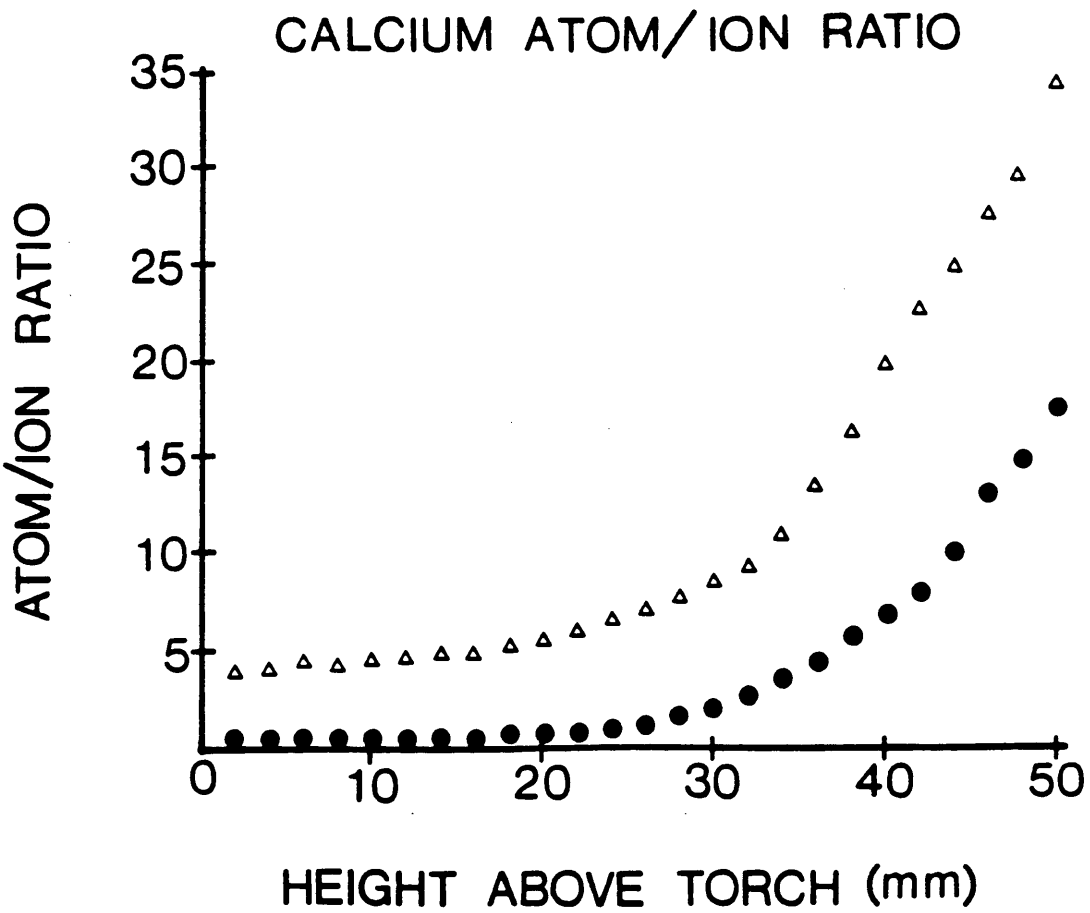

Figure 42. Profile of atom to ion ratios for Ca where the circles represent ratios with the argon backfiller and the triangles represent data points with 20 cc/min propane.

line relative intensity was 4 times as great as the ion intensity. This trend continued throughout the entire atom to ion profile. It can be concluded from this observation of increasing atom to ion ratios that the addition of propane was affecting the higher energy calcium ion to a greater extent than it was the calcium atom. To make this statement, it was necessary to ascertain that the atom and the ion intensities were both depressed upon the addition of propane. It should be noted, that the ion species was being more severly depressed than the atom species as indicated by the increased atom to ion ratio.

Modified Long Torch

As mentioned earlier in this chapter, the use of a modified long sleeve torch was used to study the effects of propane lower in the plasma tail plume. Again, calcium was used as the test element. The emission profile of the calcium ion at 393.3 nm using a 100 ppm calcium solution showed the same effect between 45 and 70 mm above the induction coil upon the addition of propane, as was observed higher in the plasma with the long sleeve torch. This effect can be seen in Figure 43, where the dots represent data points with the addition of the argon backfiller, and the boxes represent data points with the addition of 20 cc/min propane. The calcium atom line at

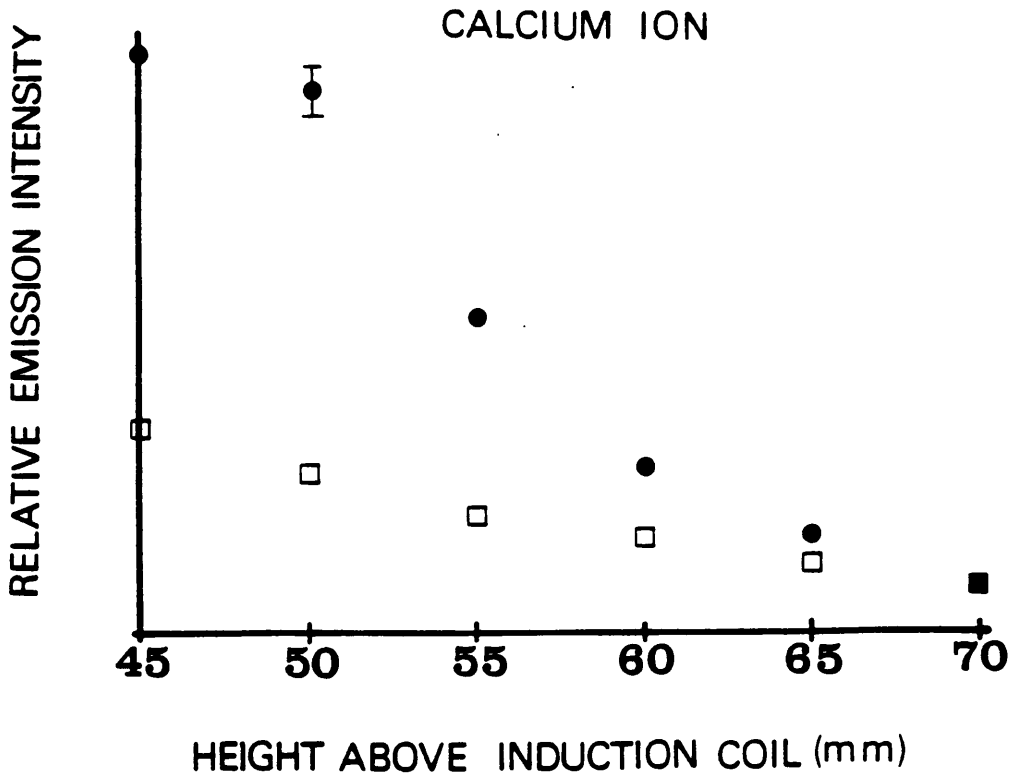

Figure 43. Profile for 100 ppm Ca(II) at 393.3 nm the circles represent data points with the addition of the argon backfiller and the boxes represent data points with the addition of 20 cc/min propane.

422.7 nm was also observed for this same 100 ppm solution. It was observed to show a similar reduction upon the addition of propane. The profiles for the calcium atom can be seen in Figure 44, where the dots represent data points with the addition of the argon backfiller and the boxes represent data points with the addition of 20 cc/min propane. It can be seen from the figures that the ion line was more severely depressed than was the atom line upon the addition of propane.

It is important to look at the excitation temperature of the plasma lower in the plasma tail plume in order to determine whether it showed the same effects that the excitation temperature in the pencil plasma tail plume showed with the long sleeve torch. The excitation temperature was obtained using the 10 line method with a 1000 ppm iron solution as the thermometric species. In Figure 45, the dots represent an excitation temperature obtained using the 10 line method with the argon backfiller, and the boxes represent the same with the addition of propane, the excitation temperature was between 3550 K and 3350 K with no more than 60 K between any two points at any height. The error for these temperature measurements was calculated to be between 2-4%. Therefore, there was no statistical difference in the excitation temperature with or without propane. This observation was

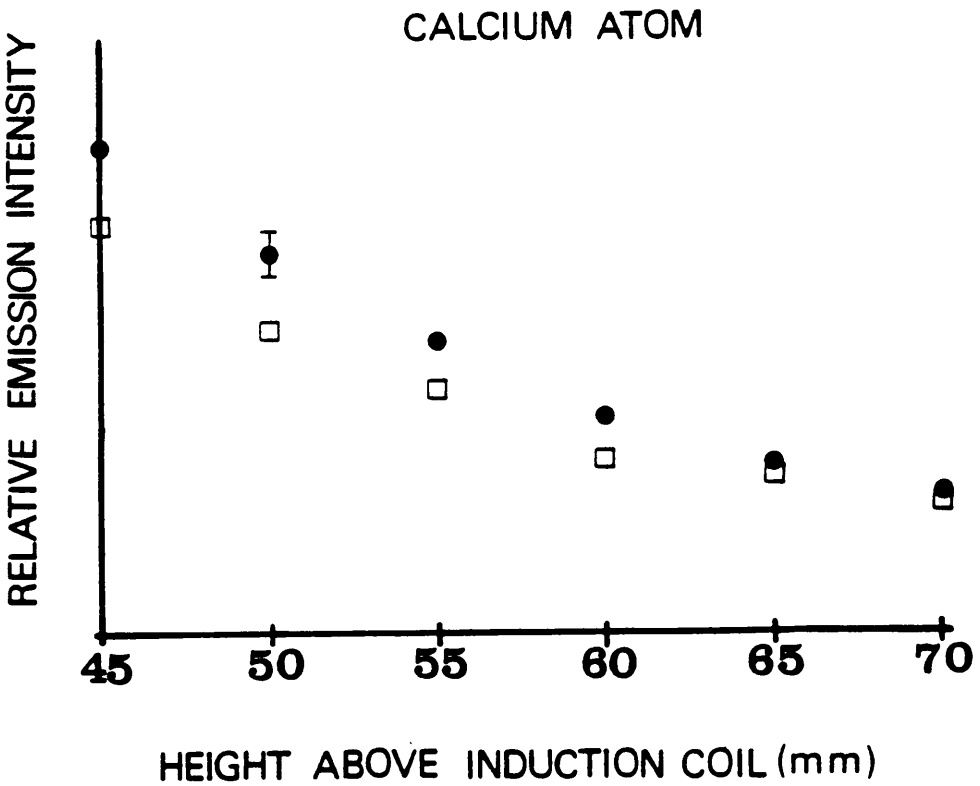

Figure 44. Profile for 100 ppm Ca(I) at 422.7 nm the circles represent data points with the addition of the argon backfiller and the boxes represent data points with the addition of 20 cc/min propane.

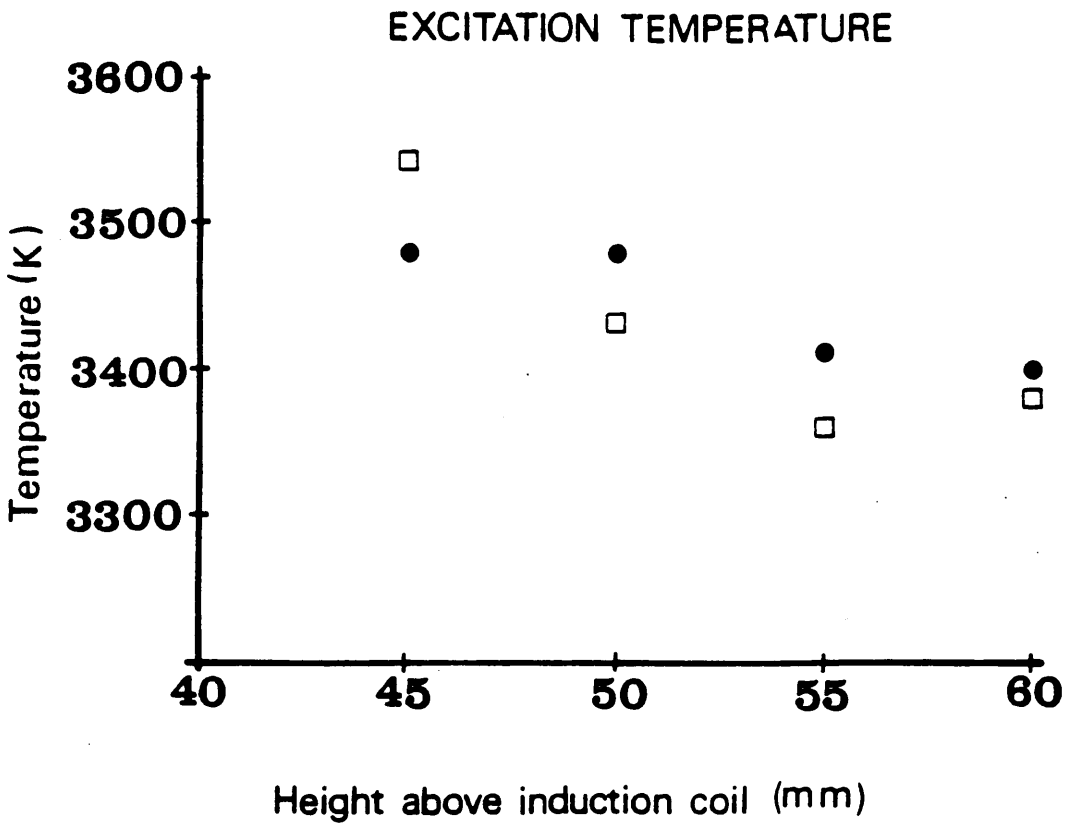

Figure 45. Excitation temperature for the modified torch using 1000 ppm Fe the circles represent data points with the addition of the argon backfiller and the boxes represent data points with the addition of 20 cc/min propane.

consistent with data previous observed with the long sleeve torch.

A comparison was conducted for the atomic signals for the same species at identical viewing heights using the two different torches to note any differences. In Figure 46, the relative intensities of the ion and atom lines for a 100 ppm calcium solution can be seen. The relative intensities for the long and short torch cannot be compared since the line intensities using the extended sleeve torch were decreased from those of the modified torch, but the ion to atom relative ratios can be compared. The viewing height for each of the two sets of lines was 60 mm above the induction coil. Looking at the two emission lines from the long torch, it can be seen that the ion line was 3.5 times more intense than the atom line. Under similar conditions using the modified (short) torch, it can be observed that the ion line was only two-thirds as intense as the atom line for calcium. A possible explanation for this difference was that the short torch had 30 mm of contact with the surrounding air, causing higher energy species (like the calcium ion versus the calcium atom) to lose energy. This result does not cause the short torch data to lose any reliability for aiding in the formulation of a mechanism that explains the effects of propane on spectrometric signals in the pencil plasma. It also gives

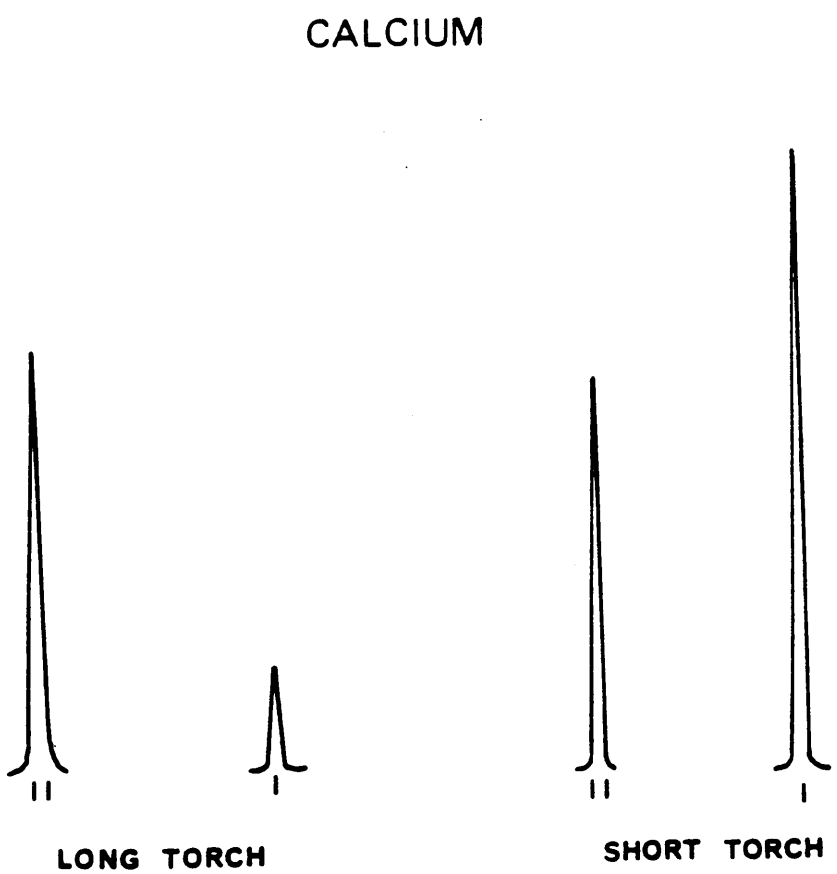

Figure 46. Calcium atom and ion lines at 60 mm above the induction coil for a long sleeve and a modified torch.

insight into possible advantages of using an extended sleeve torch.

Thermodynamic Equilibrium

This section deals with the use of several ion to atom ratios in discussing a possible energy reduction mechanism for the addition of propane to the plasma. When discussing energy, the first topic that must be covered is thermodynamic equilibrium. Since most laboratory plasmas are limited in their dimensions, it is generally accepted that they only approach thermodynamic equilibrium [67-69]. The reasoning being, it is much more likely that a photon will leave the constrains of the plasma than will any other matter. Another term was developed to described a plasma where the energy exchange between particles remains locally in equilibrium with respect to the ion, atom and electron. This condition is known as local thermodynamic equilibrium (LTE). There can be greater deviations from LTE in laboratory plasmas. This occurs when the electrons, being lighter than the other particles, are decoupled. Due to the electrons lighter mass, the energy transfer to it is much quicker than to the heavier ions and atoms. Thus, a two temperature plasma is established [54,70]. Due to this inequality, the excitation temperature and the kinetic temperature of the atoms may not be the same. This

condition has been termed partial local thermodynamic equilibrium (p-LTE).

It is possible to calculate theoretical ion to atom ratios for specific elements using a form of the Saha-Eggart equation given by Boumans and de Boer [71] (see Saha-Eggart equation). Using the spectral data from Table IV and the Saha-Eggart equation LTE ion to atom ratios for calcium, strontium, magnesium, and barium were calculated. The LTE temperature and electron number density were first necessary, and for a 1000 watt plasma the LTE excitation temperature was assumed to be 7520 with a corresponding electron number density of 7.1×10^{14} [72].

In Table V, the ion to atom ratios for these 4 elements from the pencil plasma are presented. They are noted to be much lower than was predicted if thermal equilibrium existed. It was felt that the ions must be more affected by the addition of propane than are the atoms. Another point was that all of the relative ion emission intensities decreased with respect to their relative intensities without the addition of propane. However, this trend was not true for all of the atom emission intensities. This result was not unexpected since departures from LTE are thought to occur from thermal gradients. With the pencil plasma, 2L/min of argon was pushed through the aerosol tube rather than the typical

1L//min. This increased argon flow increases the thermal gradient experienced in the plasma. As it can be seen in Figure 47, the addition of an easily ionizable element (sodium) altered the emission profiles for a 10 ppm solution of calcium. The ion line was decreased in intensity with the addition of increasing amounts of sodium, while the atom line for calcium was increased in intensity. This result was also exhibited with the addition of 20 cc/min propane. As it can be observed in Figure 48, the relative intensity of the calcium ion decreased with respect to the atom line, but the addition of sodium still caused a similar ionization interference. These results can be explained by simple ionization equilibria. However, these data indicate that the plasma was not in LTE with or without the addition of propane. Along the same line of investigation was the on the calcium phosphate depression. This depression was not observed to exist, indicating that the plasma maintained enough thermal energy to dissociate the refractory calcium phosphate molecule.

Ionization Temperature

Since the ionization temperature is said to govern the ion to atom equilibrium it was possible to use the ion to atom ratios to calculate an ion temperature [11, 47, 71].

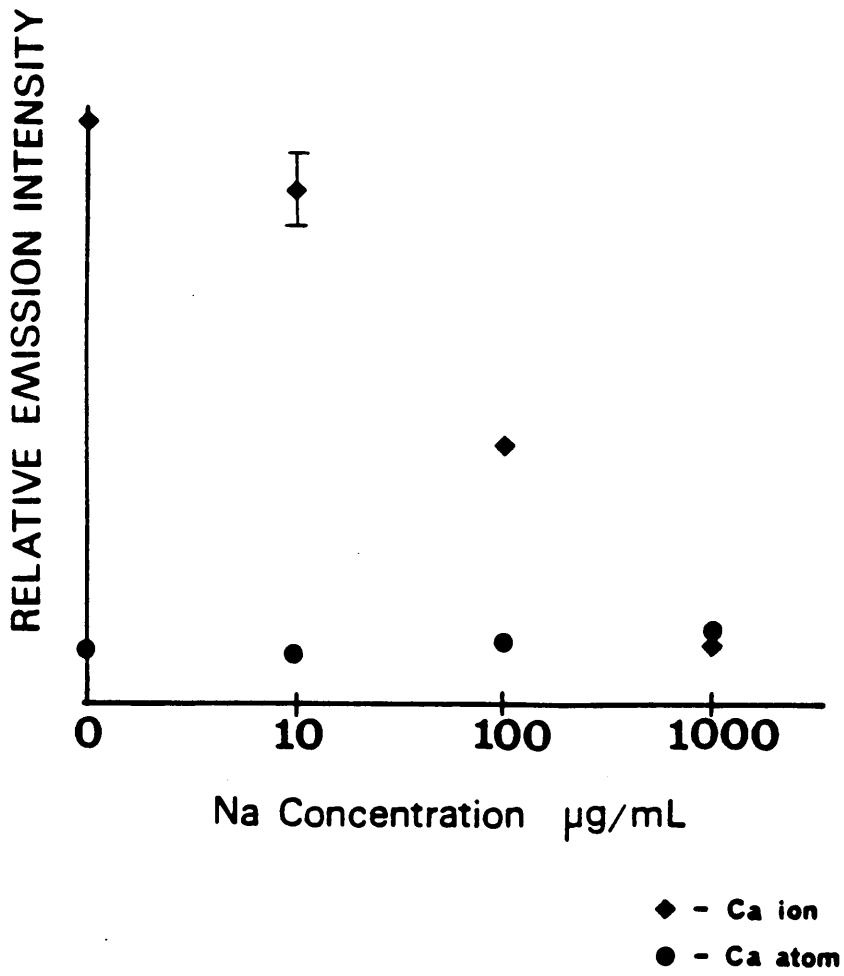

Figure 47. The effect of Na on Ca atom (the circles) and ion (the triangles).

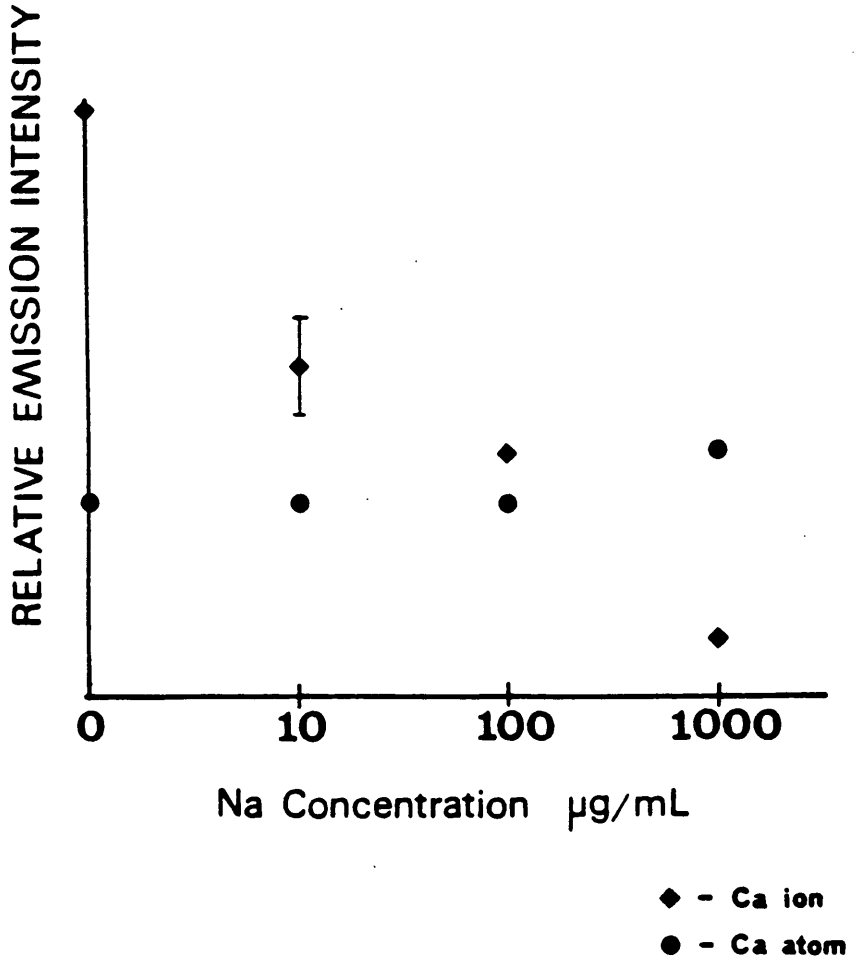

Figure 48. The effect of Na on Ca atom (the circles) and ion (the triangles) with the addition of 20 cc/min propane.

The temperature calculated needed one assumption: an electron number density. The electron number density used was the LTE value of 7.1×10^{14}, since it was lower than the value obtained with our system and was more reasonable for the corresponding excitation temperature [72]. The ion temperatures were calculated with iterations on the Apple IIe using the Saha-Eggart equation, the spectral data from Table IV, the ion to atom ratios from Table V, and the electron number density (see Appendix G). As can be seen in Table VI, the values calculated for the ionization temperature from the ion to atom ratios were between 4700 and 7100 K. These values were much higher than that of the iron excitation temperature calculated using the 10 line method. It can be noted that the higher the excitation energy of a particular line, the higher the value obtained for the ionization temperature. This result is indicative of the two temperature system that was previously described in this chapter. It can also be seen that the addition of propane caused a decrease in all of the ionization temperatures, and that the same two temperature observation can be made with these temperatures. Finally, the range of temperatures was decreasing and the values were approaching the value obtained for the iron excitation temperatures. Yet, the value obtained using the iron lines was much lower than the LTE predicted temperature of 7520 K. Compared to

Saha-Eggart Equation

$$\left(\frac{I_a}{I_a}\right)_{LTE} = \left(\frac{4.83\times10^{15}}{n_e}\right)\left(\frac{g_p A_{pq}}{\lambda_{pq}}\right)_i \left(\frac{\lambda_{pq}}{g_p A_{pq}}\right)_a T^{3/2} \exp\left[\frac{(-E_i - E_{pi} + E_{pa})}{kT}\right]$$

where:

I = relative emission intensity of the line

g_p = the statistical weight of the upper level of the transition p -> q

A_{pq} = the transition probability

λ_{pq} = the transition wavelength

E_i = ionization energy of the species (eV)

E_p = the excitation energy of the upper level of the transition p -> q

n_e = the electron number density

k = Boltzmann constant

T = the absolute temperature

(the subscripts i and a denote the ion and the atom respectively)

Table IV - Spectral Data of Ionic and Atomic Lines

Element	λ (nm)	E_p (eV)	E_i (eV)	$g_p A_{pq}$ ($10^8 s^{-1}$)
Ca I	422.7	2.936	6.111	6.54
II	393.6	3.152		5.88
Ba I	553.5	2.241	5.212	4.45
II	455.4	2.724		4.68
Sr I	460.7	2.692	5.692	6.03
II	407.8	3.042		5.68
Mg I	285.2	4.35	7.644	14.4
II	279.5	4.43		10.4

Table V - Local Thermodynamic equilibrium Ion to Atom Ratios

Element	I_{ion} / I_{atom} (LTE)	I_{ion} / I_{atom} (argon) pencil	I_{ion} / I_{atom} (propane) pencil
Barium	880	2.7	1.0
Strontium	423	6.1	1.3
Calcium	249	3.9	0.64
Magnesium	21.8	0.95	0.70

Table VI - Calculated Ionization Temperatures

Element	T_{ion} (Ar)	T_{ion} (propane)
barium	4700	4450
strontium	5360	4850
calcium	5450	5040
magnesium	7100	6000

the theoretical value, the ion temperatures showed greater deviation upon the addition of propane. However, the values of ion temperature approached the experimentally obtained excitation temperature.

Energy Reduction

To further understand the relationship propane plays in an energy reduction mechanism, ratios of an atomic emission signal with respect to the same emitting line with the addition of propane were used to comment on changes in the respective emitting populations. Then, this data was examined with respect to energy. The first aspect of this work was accomplished by using the following derived relationship:

$$I_{pq} = (1/4pi)A_{pq}hv_{pq}n_pB_{pq}$$

where:

I_{pq} = intensity of the emitted radiation
A_{pq} = transition probability of the pq transition
h = Planck's constant
v_{pq} = frequency of the pq transition
n_p = population of level p
B_{pq} = probability that photons will escape from the

emitting volume

By taking a ratio of this relation for a sample with the argon backfiller and for a sample with the addition of the propane, it can be seen that most terms will be eliminated, giving a simple method for observing the effects of propane on relative populations.

$$(I_{pq})_{propane}/(I_{pq})_{argon} = (n_p)_{propane}/(n_p)_{argon}$$

In Figure 49, which is a plot of the ratios of the atom line intensities for barium, strontium, calcium and magnesium versus the energy of the specific transition (the data can be seen in Table VII). There appears to be a relationship between the ratio and the energy. It should be noted that a ratio greater than 1.0 as observed for barium corresponds to a relative atom population increase with the addition of propane. Therefore, it is possible with this plot to describe both enhancements and depressions observed upon the addition of propane. This type of relationship can be observed in Figure 50, from the data in Table VIII, for the ion lines of these same elements. However, the ratio of ion line intensities for magnesium did not follow the trend as nicely as did the other elements.

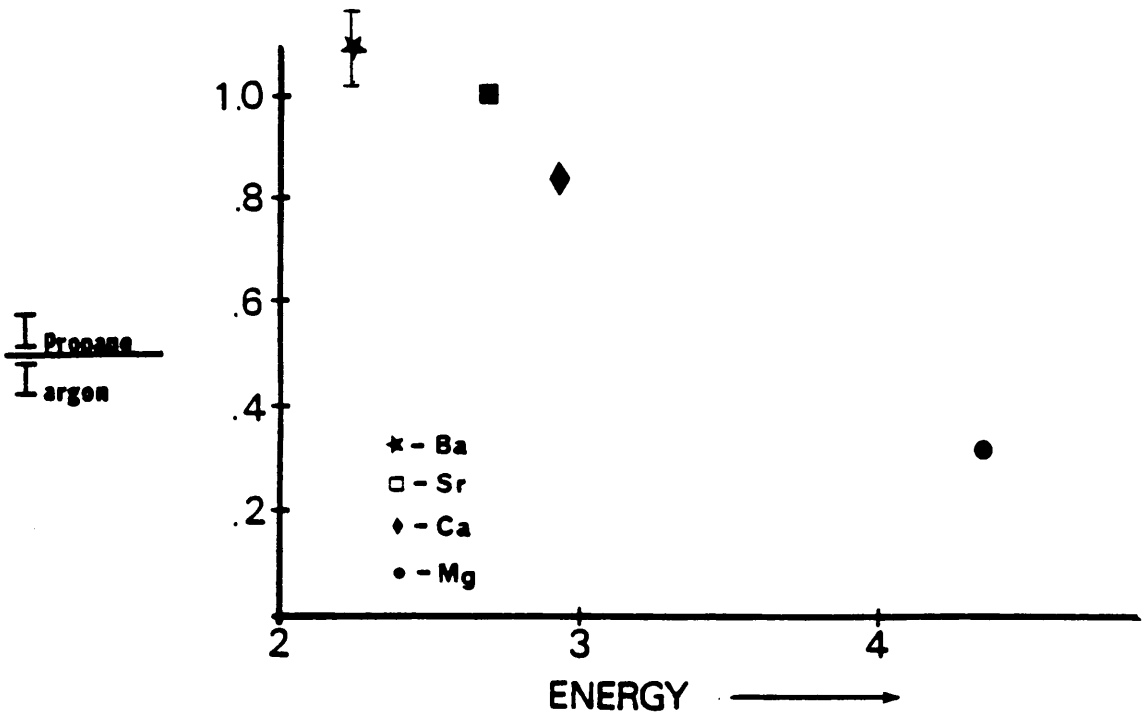

Figure 49. Ratio of atom intensities for the group IIa with propane.

Table VII - Atomic Data Using Propane for the Group IIa Atom Emission

Element	λ(nm)	Energy(qp) (eV)	$[I_{pro}/I_{ar}]$
Barium	553.5	2.241	1.10
Strontium	460.7	2.693	1.00
Calcium	422.7	2.935	.83
Magnesium	285.2	4.350	.32

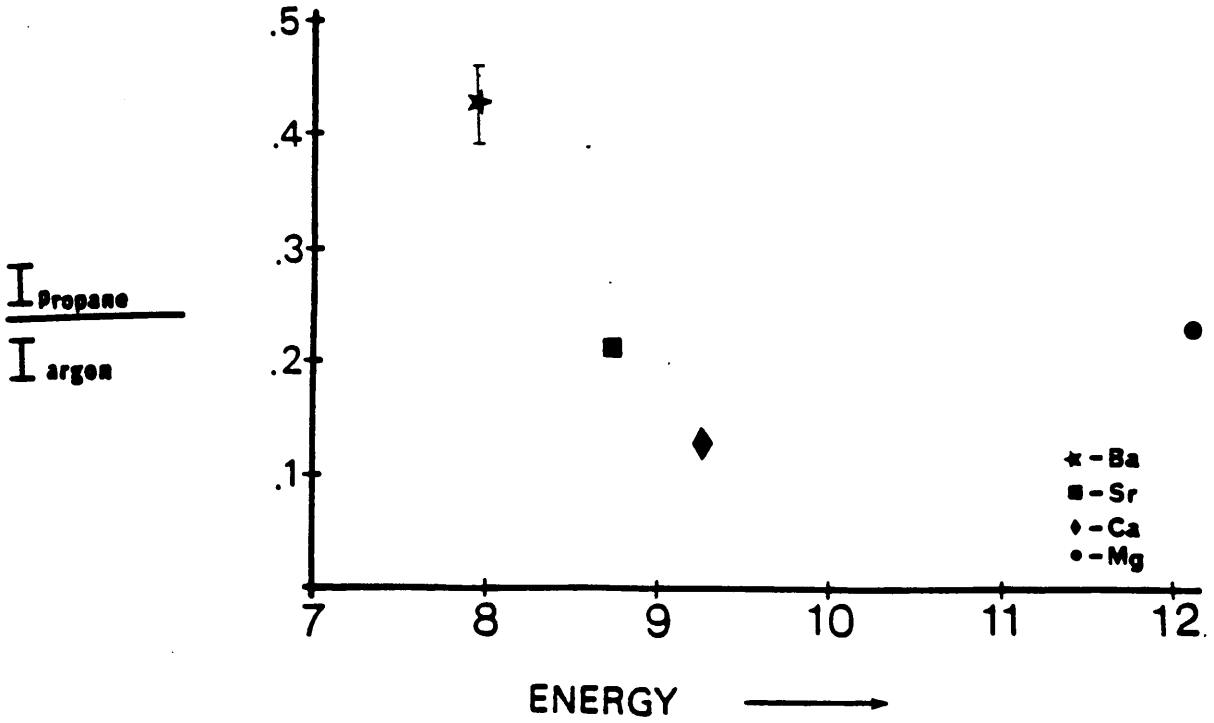

Figure 50. Ratio of ion intensities for the group IIa with propane.

Table VIII - Atomic Data Using Propane for the Group IIa Ion Emission

Element	λ(nm)	Energy(qp) (eV)	$[I_{pro}/I_{ar}]$
Barium	455.4	7.936	.427
Strontium	407.8	8.738	.211
Calcium	393.3	9.265	.127
Magnesium	279.5	12.08	.229

An identical experiment was run with butane to see whether a different organic gas gives similar results. As can be seen in Figure 51, using the data from Table IX, the atom lines appeared to follow the trend of greater depressions for a higher excitation energy. This result appeared to resemble a curve more than a straight line but it still supported the theory that the excitation energy can be used to describe the effects upon the addition of propane. The ion lines showed similar effects, illustrated in Figure 52, as were observed upon the addition of propane. Again, the magnesium ion ratio did not fall on the same curve as did the other elements (the data is from Table X). The ratios for propane and butane were not identical as can be observed in Tables VII-X. This difference may be due to the butane being much easier to add into the plasma than was propane, and therefore, probably did not disturb the plasma as much.

Transition Metals

After observing the effects of propane and butane on several Group IIa elements it was necessary to determine whether this trend continues across a row of the transition metals. To look at the transition metals, 100 ppm solutions of titanium, vanadium, chromium, iron, cobalt, nickel and copper were found to be within the linear

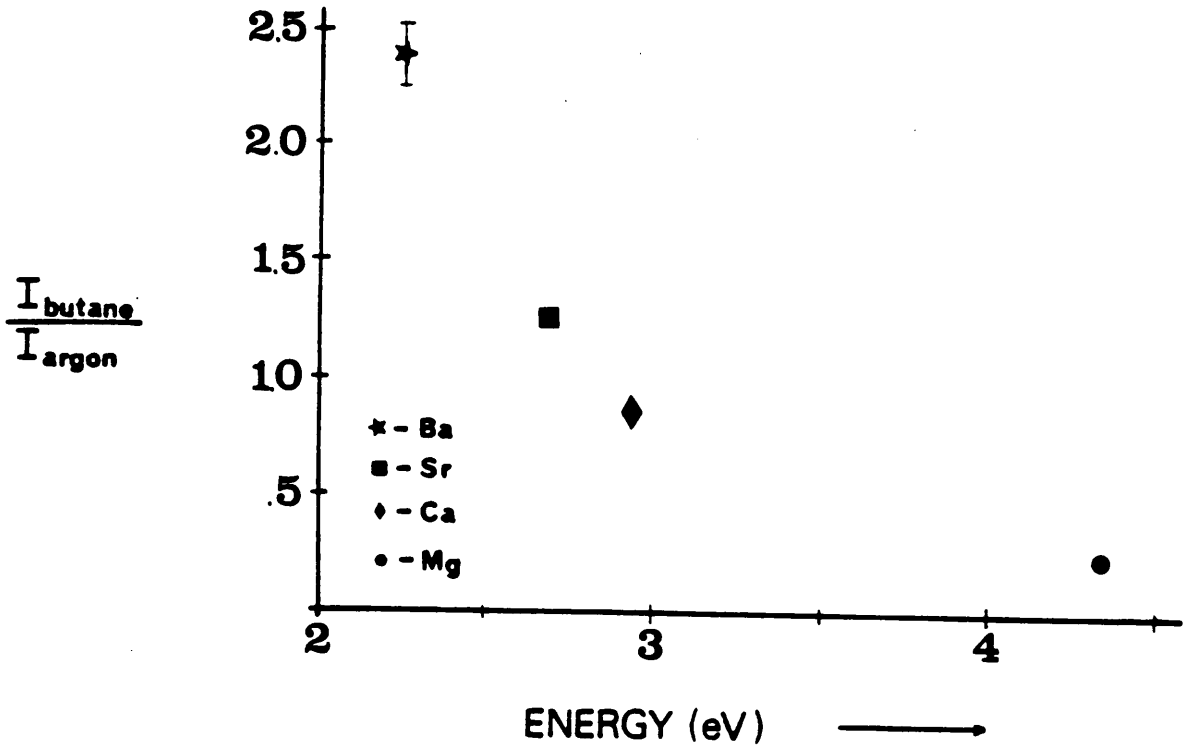

Figure 51. Ratio of atom intensities for the group IIa with butane.

Table IX - Atomic Data Using Butane for the Group IIa Atom Emission

Element	λ(nm)	Energy(qp) (eV)	$[I_{but}/I_{ar}]$
Barium	553.5	2.241	2.38
Strontium	460.7	2.693	1.25
Calcium	422.7	2.935	.84
Magnesium	285.2	4.350	.22

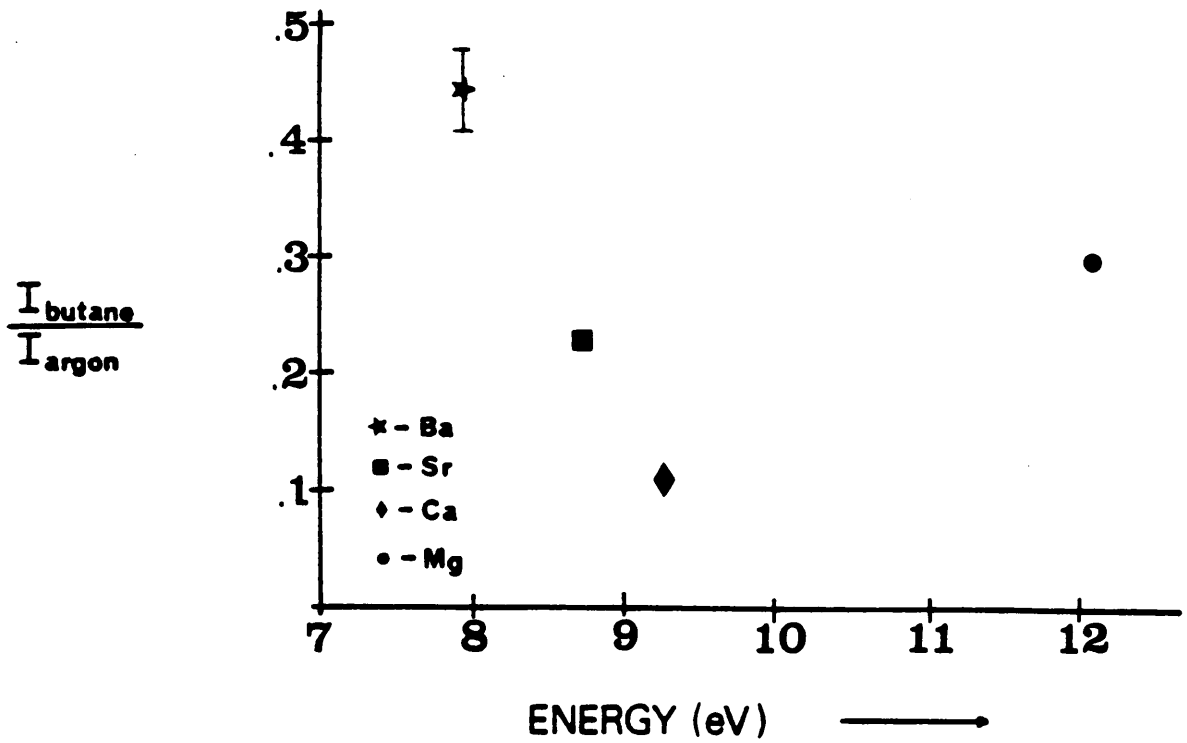

Figure 52. Ratio of ion intensities for the group IIa with butane.

Table X - Atomic Data Using Butane for the Group IIa Ion Emission

Element	λ(nm)	Energy(qp) (eV)	$[I_{but}/I_{ar}]$
Barium	455.4	7.936	.442
Strontium	407.8	8.738	.227
Calcium	393.3	9.265	.109
Magnesium	279.5	12.08	.293

working range for each element, so they were used for this study. The atom transitions were the only ones described, since most of the ionic transitions were unable to be detected with this system. The data for the above elements can be found in Table XI, where it is possible to see that two of the elements had enhancements upon the addition of propane while the other five registered depressions. It can be noted in Figure 53 that the addition of propane caused a similar effect to occur with these transition metals as it did with the Group IIa elements. There appeared to be a relationship between the excitation energy and the effect of propane on atomic emission signals. Again, the enhancements and the depressions observed upon the addition of propane can be explained by the excitation energy of the species.

Plasma Energy Density

An observation that was made while using the modified long sleeve torch (short torch) may be able to explain what appeared to be an energy loss mechanism occurring upon the addition of the organic gases. In Figure 54, the addition of the argon backfiller gives a normal shaped plasma similar to the left plasma. The addition of propane or other organic species appeared to push out the top of the plasma, depicted in the right plasma, causing a less dense

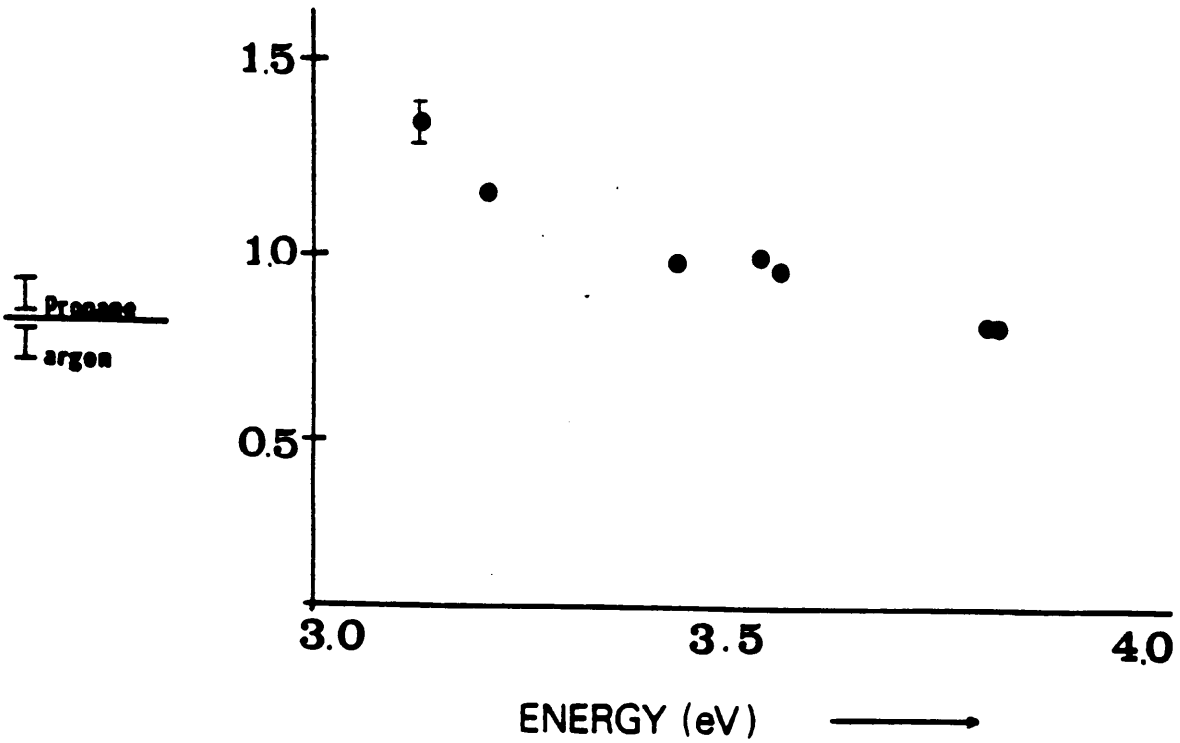

Figure 53. Ration of atom intensities for several transition metals with propane.

Table XI - Atomic Data for the Transition Metals

Element	λ(nm)	Energy(qp) (eV)	$[I_{pro}/I_{ar}]$
Titanium	365.4	3.44	.885
Vanadium	437.9	3.13	1.24
Chromium	357.9	3.46	.858
Iron	386.0	3.21	1.06
Cobalt	345.4	3.81	.72
Nickel	352.5	3.54	.90
Copper	324.8	3.82	.72

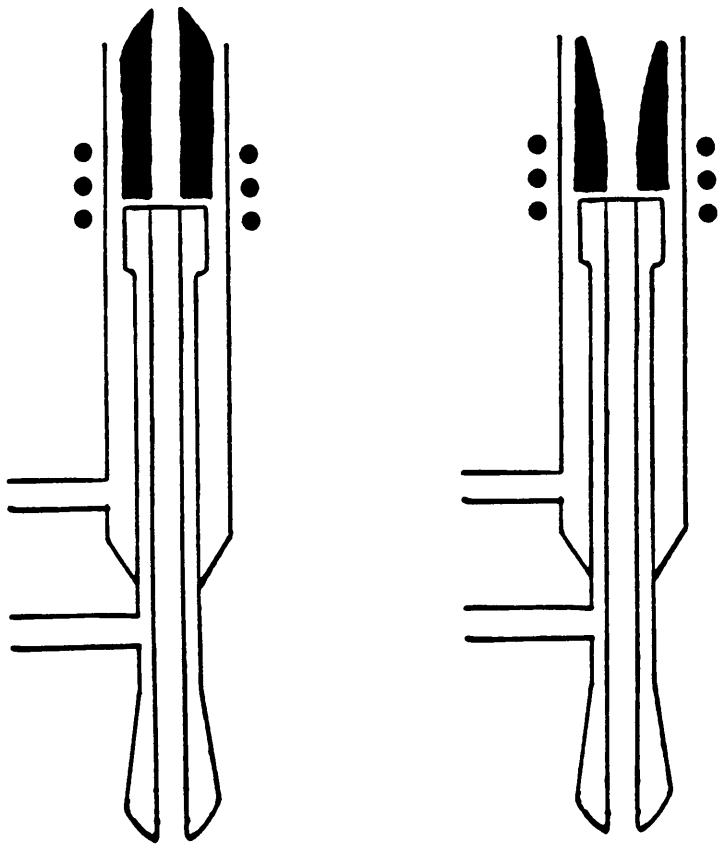

Figure 54. The effect of organics on the shape of the plasma ball.

plasma ball and possibly reducing the energy that was transferred to the analyte species. The pushing out observed upon the addition of the organic gases was likely a result of the combustion products. This observation may not have been possible using organic solvents due to the luminosity of the plasma upon the addition of organics.

Chapter 7

Conclusions

The first few experiments with the addition of propane into the pencil plasma supported the enhancements that had previously been observed with atomic fluorescence. This emission data also supported the hypothesis of reduction of metal oxides by carbon, exemplified by yttrium and lanthanum atom and oxide data. For these strong oxide formers propane was observed to enhance the atoms emission signal while reducing the oxide signal. The addition of propane was observed to cause depressions in the atomic emission signals for several elements that had previously shown enhancements with their atomic fluorescence signals under similar operating conditions. Since there was no significant change observed in the iron excitation temperature or the electron number density upon the addition of propane, a mechanism was proposed to explain the discrepancies between AFS and AES signals. The purposed mechanism was a molecular formation reaction of the metal with carbon to form a metal carbide.

To test the plausibility of molecular formation reactions, slurries were added to the plasma in order to control the elemental and molecular composition in the plasma tail. In this section, it was observed that the addition of oxygen into the plasma could enhance the

formation of metal oxides, exemplified by the yttrium and lanthanum data. The results obtained upon the addition of propane or oxygen for WO_3, WC, TiO_2 and TiC could be explained by simple molecular formation reactions. The same explanation was not possible for the effects of oxygen on an Al_2O_3 slurry and an aluminum solution. For these two samples, the addition of oxygen caused a signal enhancement rather than a predicted depression from the formation of a metal oxide. Oxygen was thought to possibly change the plasma temperature, not detected by the iron excitation temperature method. Yet, causing enhancements with the atomic emission signals of aluminum.

To further test for molecular formations and to determine if propane was actually increasing the ground state atom population as indicated by the increased AFS signals, atomic absorption measurements were attempted using the pencil plasma. The addition of propane was observed to cause enhancements in the ground state population for all elements attempted, including those that had previously shown depressions in their AES signals. Silver was the only element tested observed to show signal depressions in both atomic absorption and atomic emission upon the addition of propane. The conclusions drawn from the absorption work were that the addition of propane increased the ground state population, but did not

necessarily increase the excited state populations. It was also noted that if a depression was observed with atomic absorption then it more likely also be observed with atomic emission, but the opposite was not necessarily true.

In the final chapter, other diagnostic techniques were used to study the effects of propane on the physical properties of the plasma other than excitation temperature and electron number density. Using ion to atom ratios, in conjunction with the Saha-Eggart equation, ionization temperatures were determined for several elements. The addition of propane was observed to cause depressions in the ionization temperatures for Ca, Ba, Sr, and Mg. This change in temperature indicated that the higher energy species (ions) were more severely affected in the population of their excited states than were the lower energy species (atoms). This observations supports the two temperature system that has been described for plasmas not in LTE. This result also indicated that the use of the well accepted 10 line method to determine excitation temperature was not applicable to all studies.

To further study the effect of organic species, ratios of atom intensities with the organic gas to atom intensities without the gas were obtained, and plotted against the excitation energy. The results of this experiment indicated that a relationship exists between the

excited state atomic populations and the effects of propane. Therefore, there is a mechanism to explain both enhancements and depressions observed for various energetic species. There appeared to be an excitation energy of about 3.0 eV, where species below that value observed an enhancement in the population and above that value a depression, upon the addition of propane. It was indicated by these results that the addition of propane was hindering the excitation process of the plasma. Although the plasma has sufficient energy to desolvate and to vaporize most samples, it may not have had sufficient energy to thermally excite the higher energy transitions. This hindrance makes the pencil plasma a better atom cell with upon addition of propane. The same type of result was indicated by the susceptibility of the pencil plasma to ionization interferences, indicating a non-LTE plasma. Yet, the plasma still maintained sufficient thermal energy to dissociate the refractory calcium phosphate molecule.

Another observation made in the final chapter was that the same trends were observed with propane and butane. This result indicates that the organics effects on the plasma appear to be independent of what organic gas was being used. However, each gas may not effect all elements in the same fashion, as indicated by the absolute numbers for the ratios in Tables VII-X, but the overall trend

remains. The absolute values appear to be a result of the organic gas and the plasma operating parameters, but the trends for the various populations versus excitation energy may be due to the combustion products changing the physical shape of the plasma.

It was indicated by this work that molecular formation reactions appear to occur upon the addition of auxiliary gases, but they are not responsible for the signal enhancements of 300% observed with atomic fluorescence. It was more likely that these enhancements were due to the suppression of the excited state population. Thus, an increased ground state population of the analyte species was a result of the analyte being desolvated, vaporized but not excited due to the addition of the organic species.

Future Studies

An interesting and informative investigation would be on the effects of organic gases on the rotational temperature of the nitrogen species in the pencil plasma. Recently, there has been some work with the determination of rotational temperatures in argon ICPs using N_2 and N_2^+ rather than the more conventional OH radical [73]. This work, although still in the experimental and modeling stages shows merit as a spectroscopic technique to characterize the plasma. Other methods using diatomic molecules, (C_2), for the determination of a rotational temperature in a methane doped ICP proved to be inconclusive.

A similar line of investigation would be determination of electron temperature with and without the addition of an organic gas. Thompson scattering is an accurate way to measure the kinetic energy of the electrons and has previously accomplished this task in the argon ICP [74]. The system is still in the development stages with very few measurements to date. Based on the work presented in this dissertation, it is expected the addition of an organic gas will more severely affect electron temperature than ionization temperature.

In addition, a comparative analysis of organic gases

to organic solvents should be conducted in the pencil plasma. Again, the problem with studying organic solutions is transport efficiency. Previously, a temperature controlled spray chamber was found to remove much of the organic solvent before the analyte reached the plasma [75,76]. The use of a thermostated spray chamber may deliver a constant amount of a solvent to the plasma depending on the temperature. It would then be possible to adjust the transport efficiency of the organic solvent simply by varying the temperature. Once the temperature versus transport efficiency relationship is determined it will be possible to study several different organic solvents with respect to chemical and physical parameters in the ICP.

In this work, the use of butane as the organic gas caused similar effects to analyte signals as observed with propane. The difference, however, was the ease at which butane could be introduced into the plasma. As a result, the use of butane should be more convenient in making the pencil plasma a better atom cell for atomic fluorescence.

REFERENCES

1. D.A. Skoog, *Principles of Instrumental Analysis*, CBS College Publishing, Philadelphia (1985).

2. J.D. Winefordner, J.J. Fitzgerald, and N. Omenetto, *Appl. Spectrosc.* 29, 369 (1975).

3. P.W.J.M. Boumans and F. J. DeBoer, *Spectrochim. Acta* 30B, 309 (1975).

4. P.W.J.M. Boumans and F. J. DeBoer, *Spectrochim. Acta* 31B, 355 (1976).

5. C.E. Taylor and T.L. Floyd, *Appl. Spectrosc.* 35, 408 (1981).

6. M. Thompson, B. Pahlavanpour, and L. Thorne, *Analyst* 105, 756 (1980).

7. A. Montaser and D.W. Golightly, *Inductively Coupled Plasmas in Analytical Atomic Spectrometry*, VCH Publishers, New York (1987).

8. P.W.J.M. Boumans, *Inductively Coupled Emission Spectroscopy-Part 1*, John Wiley and Sons, New York (1987).

9. M. Thompson and J.N. Walsh, *Handbook of Inductively Coupled Plasma Spectrometry*, Blackie and Sons, Ltd., Bishbriggs, Glasgow (1983).

10. R.M. Barnes, H.S. Mahanti, M.R. Cave, and L. Fernando, *ICP Inf. Newslett.* 8, 562 (1983).

11. V.A. Fassel and R.K Kniseley, *Anal. Chem.* 46, 1110A (1974).

12. G.F. Larson, V.A. Fassel, R.K. Winge, and R.N. Kniseley, *Appl. Spectrosc.* 30, 384 (1976).

13. R.F. Browner and A.W. Boorn, *Anal. Chem.* 56, 875A (1984).

14. D.E. Dobb and D.R. Jenke, *Appl. Spectrosc.* 37, 179 (1983).

15. R.S. Babington, *Popular Sci.* May, 102 (1973).

16. C.W. Fuller, R.C. Hutton, and B. Preston, *Analyst* 106, 913 (1981).

17. J.R. Garbarino and H.E. Taylor, *Appl. Spectrosc.* 34, 584 (1980).

18. D. Truit and J.W. Robinson, *Anal. Chim. Acta* 51, 61 (1970).

19. J.F. Alder and J.M. Mermet, *Spectrochim. Acta* 28B, 421 (1973).

20. W. Nisamaneepong, D.L. Haas and J.A. Caruso, *Spectrochim. Acta* 40B, 3 (1985).

21. L.R. Layman and F.E. Lichte, *Anal. Chem.* 54, 638 (1982).

22. A.W. Boorn and R.F. Browner, *Anal. Chem.* 54, 1402 (1982).

23. P. Barrett and E. Pruszkowska, *Anal. Chem.* 56, 1927 (1984).

24. M.W. Blades and B.L. Caughlin, *Spectrochim. Acta* 40B, 579 (1985).

25. P.C. Hauser and M.W. Blades, *Appl. Spectrosc.* 42, 595 (1988).

26. G.F. Wallace, *Atomic Spectros.* 1, 38 (1980).

27. M.W. Blades and P. Hauser, *Anal. Chim. Acta* 157, 163 (1984).

28. G.L. Long and J.D. Winefordner, *Appl. Spectrosc.* 38, 563 (1984).

29. D.R. Demers, *Spectrochim. Acta* 40B, 93 (1985).

30. R.F. Browner and A.W. Boorn, *Anal. Chem.* 56, 787A (1984).

31. Plasma Therm HSF 2000D Users Manual, Plasma-Therm Inc., Kresson, New Jersey.

32. D.R. Demers and C.D. Allemand, *Anal. Chem.* 53, 1915 (1980).

33. A. Montasser and V.A. Fassel, *Anal. Chem.* 48, 1490 (1976).

34. S. Greenfield, H.McD. Mcgeachin, and P.B. Smith,

Talanta 23, 1 (1976).

35. B. Weltz, "Atomic Absorption Spectrometry," Berlag Chemie, Weinheim, New York (1976).

36. J.E. Meinhard, "Applications of Plasma Emission Spectroscopy," R.M. Barnes, Ed. Heyden, London, (1976).

37. R.H. Scott, V.A. Fassel, R.N. Kniseley, and D.E. Nixon, *Anal. Chem.* 46, 75 (1974).

38. J.W. Carr, M.W. Blades, G.M. Hieftje, *Appl. Spectrosc.* 36, 689 (1982).

39. Oriel Handbook, Vol. 2, Oriel Corp., Stratford, CT. (1985).

40. McPherson model 270 0.35 M monochromator Users Manual, McPherson Instrument, Acton, MA.

41. Pacific Instruments Model 204-10 Users Manual, Pacific Instruments, Inc., Concord, CA.

42. Adalab Users Guide, Interactive Microware, Inc., State College, PA.

43. B.W. Smith and M.C Parsons, *J. Chem. Educ.* 50, 679 (1973).

44. I. Reif, "Spectroscopic Temperature Measurements of Flames and Their Physical Significance," Ph.D. Thesis, Iowa State University, Ames (1971).

45. P.W.J.M. Boumans, Excitation Spectra in "Analytical Emission Spectrometry," E.L. Grove Ed., Marcel Decker, New York (1972).

46. A.P. Thorne, "Spectrophysics," Chapman and Hall, London (1974).

47. D.J. Kalnicky, R.N. Kniseley and V.A Fassel, *Appl. Spectrosc.* 31, 137 (1977).

48. M.W. Blades, B.L. Caughlin, Z.H. Walker and L.L. Burton, *Prog. Analyt. Spectrosc.* 10, 57 (1987).

49. H.R. Griem, "Spectral Line Broadening by Plasmas," Academic Press, New York (1974).

50. W.L. Weise, Line Broadening in "Plasma Diagnostic Techniques," R.H. Huddlestone and S.L. Leonard Eds., Academic Press (1965).

51. W.H. Gaunter, K. Visser and P.B. Zeeman, *Spectrochim. Acta* 38B, 949 (1983).

52. A. Montasser and V.A. Fassel, *Appl. Spectrosc.* 36, 613 (1982).

53. C.R. Vidal, T. Cooper, and E.W. Smith, *Astrophys. J. Suppl. Series* 25, 37 (1973).

54. J.F. Alder, R.M. Bombelka and G.F. Kirkbright, *Spectrochim. Acta* 35B, 163 (1980).

55. A. Montasser, V.A. Fassel and G. Larsen, *Appl. Spectrosc.* 35, 385 (1981).

56. L.A. deVynck, *Silicates Ind.* 31, 21 (1966).

57. I. Rubeska, *Anal. Chem.* 48, 1640 (1976).

58. A.L. Gray, *Spectrochim. Acta* 40B, 1525 (1985).

59. Aldrich Catalog, Aldrich Chemical Company, Inc., Milwaukee, WI.

60 R.C. West, Ed., "CRC Handbook of Chemistry and Physics," CRC Press, West Palm Beach, Fl (1983).

61. M.H. Abdallah, R. Diemiaszonek, J. Jarosz, J.M. Mermet, J. Robin and C. Trassy, *Anal. Chim. Acta* 84, 271, (1976).

62. L. deGalan, G.R Kornblum and M.T.C. de Loos-Vollebregt, "Recent Advances in Analytical Spectroscopy," K. Fuwa, Ed., Pergamon Press, New York (1982) p.33.

63. Current Preamplifier model 5002 Users Manual, EG & G Brookdeal Electronics Limited, Bracknell, Berkshire.

64. Lock-in Amplifier model 5104 Users Manual, EG & G Princeton Applied Research, Princeton, NJ.

65. W.R. Masamba, B.W. Smith, R.J. Krupa and J.D. Winefordner, *Appl. Spectrosc.* 42, 872 (1988).

66. P.W.J.M. Boumans, "Theory of Spectrochemical Excitation," Hilgar and Watts, London (1966).

67. H.R. Griem, *Phys. Rev.* 131, 1170 (1963).

68. H.W. Darwin, *J. Quant. Spectrosc. Rad. Trans.* 10, 33 (1970).

69. G.R. Kornblum and J. Smeyers-Verbeck, *Spectrochim. Acta* 37B, 83 (1982).

70. P.W.J.M. Boumans and F.J. DeBoer, *Spectrochim. Acta* 32B, 365 (1977).

71. M.W. Blades and B.L. Caughlin, *Spectrochim. Acta* 40B, 987 (1985).

72. N. Furuta, Y. Nojiri, and K. Fuwa, *Spectrochim. Acta* 40B, 423 (1985).

73. C.J. Seliskar, D.C Miller, and P.A. Fleitz, *Appl. Spectrosc.* 41,658 (1987).

74. M. Huang, W. Hsu, and G.M. Hieftje, Abstact of papers, Pittsburgh Conference and Exposition on Analytical Chemistry and Applied Spectroscopy, New Orleans, 1988, Abstract 722.

75. D. Hausler, and L.T. Taylor, *Anal. Chem.* 53, 1223 (1981).

76. D. Hausler, and L.T. Taylor, *Anal. Chem.* 53, 1227 (1981).

APPENDIX A
Data acquisition program to take atomic emission profiles
- by T. W. McCreary

```
 100  CLEAR : HIMEM: 36095:D% = 0:: PRINT  CHR$ (4)"BRUN QU
ICKI/O,D1"
 110  POKE 36259,1: REM  this permits data acquisition with
out timing pro
     gramming
 120  DIM D(50),B(50),S(50)
 130  PR# 0
 140  REM  The data acquisition rate will depend partly on
the size
 150  REM  of the signal.  Larger signals will take longer
to integrate
 160  REM  than will smaller signals.  Actual data acquisit
ion rates vary

 170  REM  in this program from about 20-50 points per seco
nd.  The
 180  REM  number of points taken per integration time will
 be the same;
 190  REM the actual time this takes to do will vary somewh
at.
 200  REM
 210  REM    If you wish to take more than 50 points per pr
ofile,
 220  REM   change the values in lines 120 and 390 as neede
d
 230  REM    This program was revised by Terry McCreary on
4/6/87
 240  REM
 250  REM
 260  HOME : HTAB (12): FLASH : PRINT "DCP PROFILE": NORMAL
 : PRINT : PRINT

 270  PRINT : PRINT "  This program will collect data"
 280  PRINT "for DCP profiles (up to 50 points per"
 290  PRINT "profile).  A background profile will"
 300  PRINT "be taken first, followed by a signal"
 310  PRINT "profile."
 320  PRINT : PRINT "  Data will be saved on drive 2; be"
 330  PRINT "sure to place your data disk in"
 340  PRINT "that drive.": PRINT
 350  PRINT "  Two hard copies of the data will"
 360  PRINT "be printed for the lab notebook after"
 370  PRINT "the data is saved.": PRINT
 380  PRINT : PRINT : PRINT "One moment please..."
 390  FOR I = 0 TO 50:D(I) = 0::B(I) = 0:S(I) = 0: NEXT I:F
```

```
$ = ""
 400  PRINT
 410  INPUT "File name for data";F$
 420  PRINT : INPUT "Date ";C$: INPUT "Analyte concentratio
n ";M$
 430  INPUT "Argon nebulizer flow ";R$: INPUT "Auxiliary ga
s ";X$: INPUT
      "Auxiliary gas flow ";H$: PRINT
 440  INPUT "Position of profile start ";E$
 450  INPUT "Increment size ";I$
 460  PRINT : INPUT "Other comments";K$
 470  PRINT : INPUT "Number of observations = ";N
 480  PRINT : INPUT "Length of integration in sec = ";NN
 490  PRINT : INPUT "Delay between observations in sec = ";
WT
 500 D(0) = N
 510  PRINT
 520  INPUT "HIT RETURN TO TAKE BACKGROUND";S$
 530  & AI0
 540  FOR I = 1 TO N
 550  & AI0
 560  GOSUB 1080
 570  PRINT I,( INT (IN / NN)) / 50
 580 B(I) = IN / (NN * 50)
 590  GOSUB 1140
 600  PRINT  CHR$ (7)
 610  PRINT "Hit any key to continue"
 620  GET G$: IF G$ = "" THEN 510
 630  NEXT I
 640  FOR I = 1 TO 5
 650  PRINT  CHR$ (7)
 660  NEXT I
 670  PRINT
 680  INPUT "HIT RETURN TO TAKE SIGNAL";S$
 690  PRINT
 700  FOR I = 1 TO N
 710  & AI0
 720  FOR I = 1 TO N
 730  GOSUB 1080
 740  PRINT I,( INT (IN / NN)) / 50
 750  GOSUB 1140
 760  PRINT  CHR$ (7)
 770  PRINT "Hit any key to continue"
 780  GET G$: IF G$ = "" THEN 780
 790 S(I) = ( INT (IN / NN)) / 50
 800 D(I) = S(I) - B(I)
 810  NEXT I
 820  FOR I = 1 TO 5: PRINT  CHR$ (7): NEXT I
 830  PRINT "SIGNAL MINUS BACKGROUND"
 840  FOR I = 1 TO N
 850  GOSUB 1190
 860  PRINT I,D(I)
```

```
 87Ø  NEXT I
 88Ø  PR# 3: HOME : PRINT "Data printout"
 89Ø  PR# 1: PRINT  CHR$ (27);"!" CHR$ (5): FOR J = 1 TO 2
 9ØØ  PRINT F$;"      Date ";C$;"      Analyte ppm ";M$
 91Ø  PRINT "Argon nebulizer flow  ";R$: PRINT "Auxiliary g
as  ";X$;"
      Auxiliary gas flow  ";H$
 92Ø  PRINT "Profile start at ";E$;"      Increment size  ";
I$
 93Ø  PRINT F$;"   Integration time ";NN;" sec";"   Delay t
ime ";WT;" sec
     "
 94Ø  PRINT K$: PRINT
 95Ø  PRINT  TAB( 15);"SIGNAL","BACKGROUND","S-B"
 96Ø  FOR I = 1 TO N: PRINT I,S(I),B(I),D(I): NEXT I
 97Ø  PRINT : PRINT : NEXT J: PRINT  CHR$ (12); CHR$ (27);"
@": PR# Ø
 98Ø  PRINT "DATA STORAGE ROUTINE "
 99Ø  PRINT "Saving ";F$
 1ØØØ CD$ =  CHR$ (4)
 1Ø1Ø  CALL 1ØØ2: PRINT  CHR$ (13) CHR$ (4)"OPEN "F$",D2":
PRINT  CHR$ (4
     )"WRITE"F$
 1Ø2Ø  FOR I = Ø TO N: PRINT D(I): NEXT I
 1Ø3Ø  PRINT CD$"LOCK "F$
 1Ø4Ø  PRINT CD$"CLOSE "F$
 1Ø5Ø  HOME : VTAB (6): HTAB (12): PRINT "Re-initializing p
rogram"
 1Ø6Ø  CALL 1ØØ2: GOTO 38Ø
 1Ø7Ø  END
 1Ø8Ø  REM   routine for integration of signal
 1Ø9Ø IN = Ø
 11ØØ  FOR L = 1 TO (NN * 5Ø)
 1111  & AIØ:IN = IN + D%
 1121  NEXT L
 1131  RETURN
 1141  REM  WAIT
 1151 D% = WT * 1Ø: &  TO 1
 1161  & TI1:T = D%
 1171  IF T <  > Ø THEN 1161
 1181  RETURN
 1191  REM  routine for rounding off values
 12ØØ LS = D(I) -  INT (D(I))
 1211 US =  INT (D(I)) + 1 - D(I)
 1221  IF LS >  = US THEN D(I) =  INT (D(I) + 1)
 1231  IF LS < US THEN D(I) =  INT (D(I))
 1241  RETURN
```

APPENDIX B
Fe excitation temperature using the slope method - revised by J. Bolton

```
 10  TEXT : HOME
 15  PRINT : PRINT : PRINT : PRINT
 18  DIM S(10),X(10),Y(10),E(10),G(10),A(10),V(10)
 20  PRINT "  THIS PROGRAM WILL CALCULATE THE"
 30  PRINT "TEMPERATURE OF A PLASMA BY THE SLOPE"
 40  PRINT "METHOD, FROM THE EMISSION INTENSITY"
 50  PRINT "OF SEVERAL FE LINES BETWEEN"
 60  PRINT " 367.99 nm AND 376.38 nm."
 70  FLASH : PRINT : PRINT : PRINT "PRESS ANY KEY TO CONTIN
UE"
 80  GET G$: IF G$ = "" THEN 80
 90  NORMAL : HOME
 100  PRINT "      YOU MAY CHOOSE FROM"
 110  PRINT "THE FOLLOWING LINES:"
 120  PRINT "** NUMBER **        ** WAVELENGTH (NM) **"
 130  PRINT
 140  PRINT "   1    367.99"
 150  PRINT "   2    370.56"
 160  PRINT "   3    371.99"
 170  PRINT "   4    372.26"
 180  PRINT "   5    373.49"
 190  PRINT "   6    373.71"
 200  PRINT "   7    374.83"
 210  PRINT "   8    374.95"
 220  PRINT "   9    375.82"
 230  PRINT "  10    376.38"
 260  PRINT : PRINT : PRINT "HOW MANY OF THESE LINES"
 265  INPUT "DO YOU WISH TO USE? (3-10)";L
 270  PRINT : PRINT "ENTER THE NUMBER CORRESPONDING TO EACH
"
 275  PRINT "LINE YOU WISH TO USE AND THE INTENSITY"
 280  PRINT "OF EMISSION OF THAT LINE, SEPARATED"
 290  PRINT "BY A COMMA.  'RETURN' AFTER EACH ENTRY"
 300  FOR I = 1 TO L: INPUT S(I),J(I): NEXT I
 310  FOR I = 1 TO L
 320  ON S(I) GOTO 1010,1020,1030,1040,1050,1060,1070,1080,
1090,1100
 330  NEXT I
 340 X = 0:Y = 0:XX = 0:XY = 0:YY = 0
 350  FOR I = 1 TO L
 360 X(I) = E(I) / .695
 370 Y(I) =  LOG (G(I) * A(I) * V(I) / J(I))
 380 X = X + X(I)
 390 Y = Y + Y(I)
 400 XX = XX + (X(I) * X(I))
 410 YY = YY + (Y(I) * Y(I))
```

```
 420 XY = XY + (X(I) * Y(I))
 430  NEXT I
 440 M = (((L * XY) - (X * Y)) / ((L * XX) - (X * X)))
 442 B = (Y / L) - (M * (X / L)):XO =  - 1 * (B / M)
 444 SX = XX - ((X * X) / L):SY = YY - ((Y * Y) / L):SZ = X
Y - ((X * Y) /
     L)
 446 ER = SY - (M * SZ):S =  SQR ((SY - (M * SZ)) / (L - 2)
):SM = S / ( SQR
     (SX))
 448 SB = (S * ( SQR (XX)) / ( SQR (L * SX))):R = SZ / ( SQ
R (SX * SY))
 450 T = 1 / M:TP = 1 / (M + SM):TM = 1 / (M - SM)
 452  INPUT "TITLE OF DATA";T$
 453  PR# 3: PRINT T$
 454  PR# 1
 456  PRINT T$
 457  PRINT : PRINT
 458  PRINT : PRINT "Y = MX + B"
 460  PRINT "_____________________________________________
_____________
      _______"
 462  PRINT : PRINT "SLOPE = ";M;"   Y-INTERCEPT = ";B;"
X-INTERCEPT =
     ";XO
 464  PRINT : PRINT "SLOPE UNCERTAINTY = ";SM;"   Y-INTERCE
PT UNCERTAINTY
      = ";SB
 466  PRINT : PRINT "TEMPERATURE = ";T
 468  PRINT : PRINT "TEMPERATURE RANGE FROM ";TP;" TO ";TM
 470  PRINT : PRINT "COEFFICIENT OF CORRELATION = ";R
 472  PRINT "_____________________________________________
_____________
      _____"
 474  PR# 0
 476  HOME
 478  PRINT "DO YOU WANT A TABLE OF X AND Y VALUES"
 480  PRINT "FOR PLOTTING ON SCI PLOTTER (Y/N)"
 482  GET G$: IF G$ = "" THEN 482
 484  IF G$ = "N" THEN  PRINT "GOODBYE": END
 500  PR# 1
 505  PRINT : PRINT
 510  PRINT "    X(I)         Y(I)"
 520  FOR I = 1 TO L: PRINT X(I),Y(I): NEXT I
 999  PR# 0
 1000  PRINT "GOODBYE": END
 1010 E(I) = 27167:G(I) = 9:A(I) = .0138E + 8:V(I) = 8.152E
 + 14: GOTO 33
     0
 1020 E(I) = 27395:G(I) = 7:A(I) = .0328E + 8:V(I) = 8.096E
 + 14: GOTO 33
     0
```

```
1030 E(I) = 26875:G(I) = 11:A(I) = .163E + 8:V(I) = 8.065E
+ 14: GOTO 33
    0
1040 E(I) = 27560:G(I) = 5:A(I) = .0505E + 8:V(I) = 8.059E
+ 14: GOTO 33
    0
1050 E(I) = 33695:G(I) = 11:A(I) = .886E + 8:V(I) = 8.032E
+ 14: GOTO 33
    0
1060 E(I) = 27167:G(I) = 9:A(I) = .143E + 8:V(I) = 8.028E
+ 14: GOTO 330

1070 E(I) = 27560:G(I) = 5:A(I) = .0904E + 8:V(I) = 8.004E
+ 14: GOTO 33
    0
1080 E(I) = 34040:G(I) = 9:A(I) = .744E + 8:V(I) = 8.001E
+ 14: GOTO 330

1090 E(I) = 34329:G(I) = 7:A(I) = .611E + 8:V(I) = 7.982E
+ 14: GOTO 330

1100 E(I) = 34547:G(I) = 5:A(I) = .523E + 8:V(I) = 7.971E
+ 14: GOTO 330
```

APPENDIX C

Proof for scatter

Fluorescence vs. Absorption

First it is necessary to calculate values for d using values for R and l:

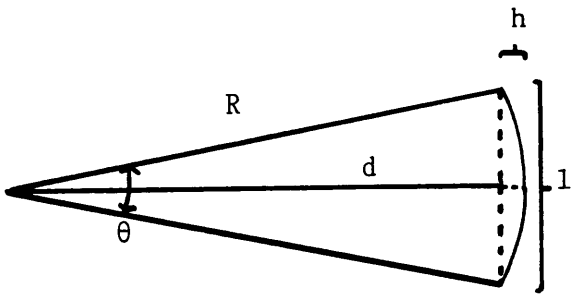

$$d = (R^2 - (l/2)^2)^{.5} = (6^2 - .75^2)^{.5} = 5.95$$

For a 1.5" diameter f#2 lens placed 6" from the source the total solid angle collected is equal to:

$$\theta = 2\tan^{-1}(1.5"/2X5.95) = 14.38^{o}$$

For absorption this entire angle will contain all of the absorbed light (I_A)

Assuming 100% efficiency all light which is absorbed will be re-emitted as fluorescence (I_F):

$$(I_A)_{TOTAL} = (I_F)_{TOTAL}$$

But, the fluorescence will be emitted over an entire sphere

therefore, with our lens system we will only collect 14.38^{o} of the sphere for the fluorescence:

The area of the sphere is:

$A = 2R^2\theta$ (θ in radians)

$A = 452.2"$

The area of the cone subtended:

$A = 2\pi Rh$ (where $h = R - d$)

$A = 1.88"$

$(I_F)_{collected} = (1.88/452.2)(I_F)_{TOTAL}$

substituting $(I_A)_{TOTAL}$ for $(I_F)_{TOTAL}$:

$(I_F)_{collected} = (1.88/452.2)(I_A)_{TOTAL}$

For comparison of the scatter effects assume 1% scatter with respect to $(I_A)_{TOTAL}$

$scatter = 0.01(I_A)_{TOTAL}$

Scatter for absorbance:

$(0.01(I_A)_{TOTAL}/(I_A)_{TOTAL})X100\% = 1.0\%$

Scatter for fluorescence:

$(0.01(I_A)_{TOTAL}/(1.88/452.2)(I_A)_{TOTAL})X100\% = 240.6\%$

APPENDIX D
Atomic Absorption translation stage

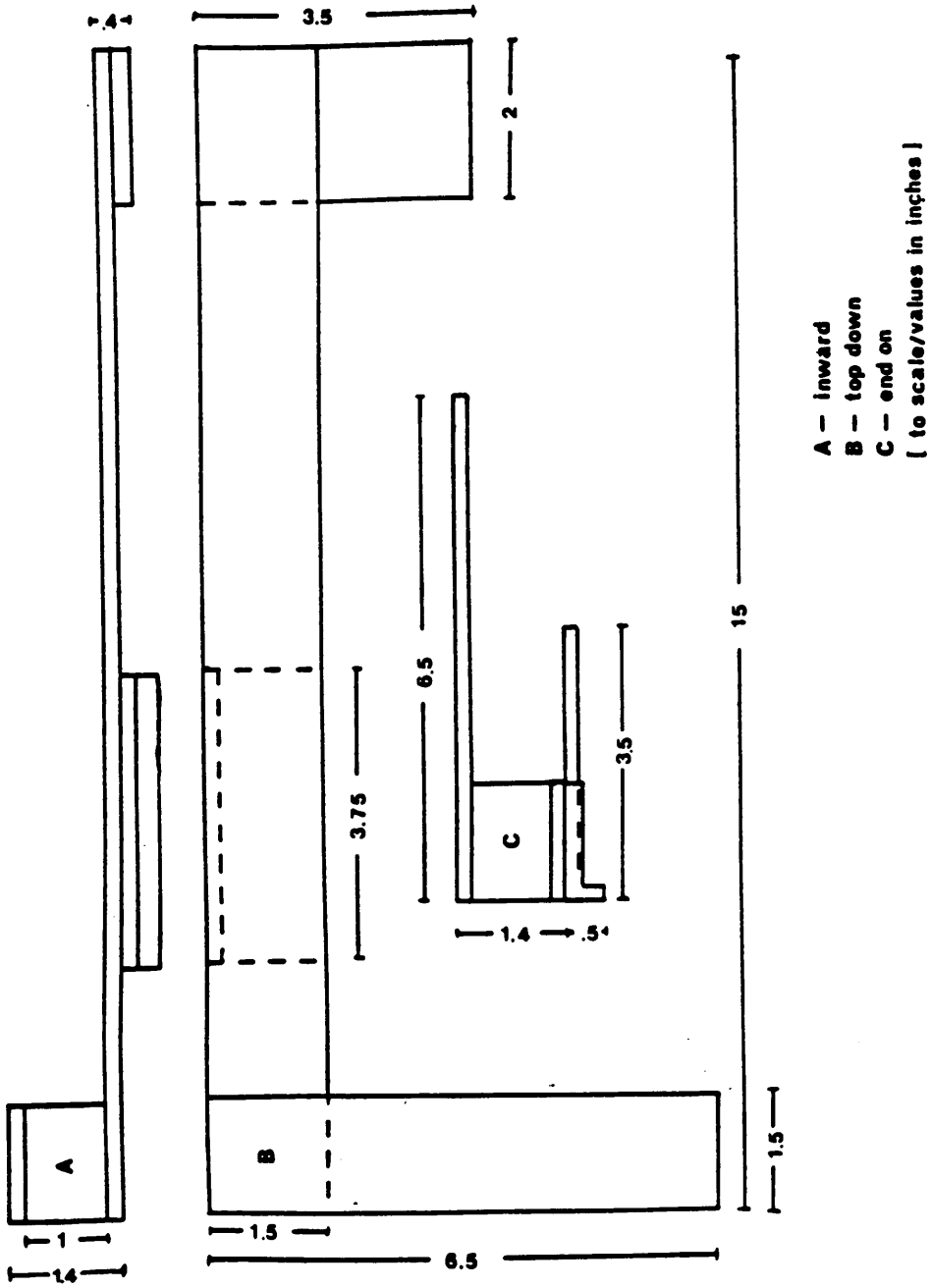

Figure 55. Schematic diagram of the AAS translation system.

APPENDIX E
HCL Pulsing Supply

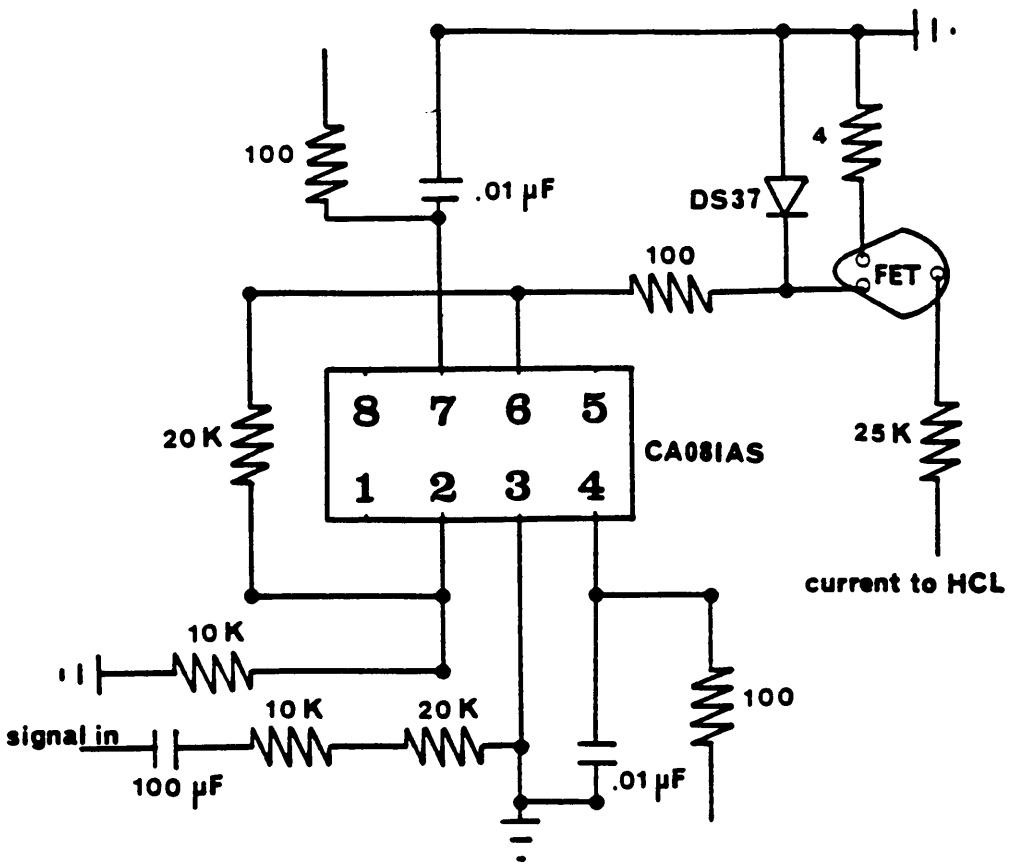

Figure 56. Schematic diagram of the HCL pulsing supply.

APPENDIX F
Data acquisition program for atomic absorption profiles

```
 10  CLEAR : HIMEM: 36095:D% = Ø: DIM D%(3ØØ): PRINT  CHR$
(4)"BRUN QUICK
     I/O,D1"
 20  DIM D(3ØØ),B(3ØØ),S(3ØØ),A(3ØØ)
 30  PR# Ø
 40  HOME : HTAB (12): FLASH : PRINT "ICP ABSORBANCE": NORM
AL : PRINT : PRINT

 50  PRINT : PRINT "  This program combines STUFFER"
 60  PRINT "and a variable integration subroutine"
 70  PRINT "using the Adalab A/D converter.
 80  PRINT "This program will take background"
 90  PRINT "data first and then signal data."
 100  PRINT : PRINT "  Data will be saved on drive 2; be"
 110  PRINT "sure to place your data disk in"
 120  PRINT "that drive.": PRINT
 130  PRINT "  Two hard copies of the data will"
 140  PRINT "be printed for the lab notebook after"
 150  PRINT "the data is saved.": PRINT
 160  PRINT : PRINT : PRINT "One moment please..."
 170  FOR I = Ø TO 3ØØ:D(I) = Ø:D%(I) = Ø:B(I) = Ø:S(I) = Ø
:A(I) = Ø: NEXT
     I:F$ = ""
 180  HOME
 190  INPUT "File name for data";F$
 200  PRINT : INPUT "Date ";C$: INPUT "Analyte concentratio
n ";M$
 210  INPUT "Argon nebulizer flow ";R$: INPUT "Auxiliary ga
s ";X$: INPUT
     "Auxiliary gas flow ";H$: PRINT
 220  INPUT "Position of profile start ";E$
 225  INPUT "Increment size ";I$
 230  PRINT : INPUT "Other comments";K$
 240  PRINT : INPUT "Number of observations = ";N
 250  PRINT : INPUT "Length of integration in sec = ";NN
 260  PRINT : INPUT "Delay between observations in sec = ";
WT
 270 D(Ø) = N
 271 A(Ø) = N
```

```
 280  PRINT
 290  INPUT "HIT RETURN TO TAKE BACKGROUND";S$
 300  & AI0:DMP = D%:D% = 10: &  TO 1
 310  & TI1:T = D%: IF T <  > 0 THEN 310
 320  FOR I = 1 TO N
 330  GOSUB 870
 340  PRINT I,( INT (IN / NN)) / 10
 350 B(I) = IN / (NN * 10)
 360  GOSUB 980
 370  PRINT  CHR$ (7)
 380  PRINT "Hit any key to continue"
 390  GET G$: IF G$ = "" THEN 280
 400  NEXT I
 410  FOR I = 1 TO 5
 420  PRINT  CHR$ (7)
 430  NEXT I
 440  PRINT
 450  INPUT "HIT RETURN TO TAKE SIGNAL";S$
 460  PRINT
 470  & AIO:DMP = D%:D% = 10: &  TO 1
 480  & TI1:T = D%: IF T <  > 0 THEN 480
 490  FOR I = 1 TO N
 500  GOSUB 870
 510  PRINT I,( INT (IN / NN)) / 10
 520  GOSUB 980
 530  PRINT  CHR$ (7)
 540  PRINT "Hit any key to continue"
 550  GET G$: IF G$ = "" THEN 550
 560 S(I) = ( INT (IN / NN)) / 10
 570 D(I) =  LOG (B(I) / S(I)) / 2.30259
 571 D(I) = D(I) * 1000
 572 A(I) = D(I) / 1000
 580  NEXT I
 590  FOR I = 1 TO 5: PRINT  CHR$ (7): NEXT I
 600  PRINT "ABSORBANCE"
 610  FOR I = 1 TO N
 620  GOSUB 1030
 630  PRINT I,A(I)
 640  NEXT I
 650  PRINT "DATA STORAGE ROUTINE "
 660  PRINT "Saving ";F$
 670 CD$ =  CHR$ (4)
 680  PRINT CD$"OPEN "F$",D2": PRINT CD$"WRITE "F$
 690  FOR I = 0 TO N: PRINT A(I): NEXT I
 700  PRINT CD$"LOCK "F$
 710  PRINT CD$"CLOSE "F$
 720  PR# 3: HOME : PRINT "Data printout"
 750  PR# 1: PRINT  CHR$ (27);"!" CHR$ (5): FOR J = 1 TO 2
 760  PRINT F$;"     Date ";C$;"     Analyte ppm ";M$
 770  PRINT "Argon nebulizer flow  ";R$: PRINT "Auxiliary g
as  ";X$;"
      Auxiliary gas flow  ";H$
```

```
 78Ø  PRINT "Profile start at ";E$;"      Increment size  ";
I$
 79Ø  PRINT F$;"   Integration time ";NN;" sec";"   Delay t
ime ";WT;" sec
     "
 8ØØ  PRINT K$: PRINT
 81Ø  PRINT  TAB( 15);"SIGNAL","BACKGROUND","ABSORBANCE"
 82Ø  FOR I = 1 TO N: PRINT I,S(I),B(I),A(I): NEXT I
 83Ø  PRINT : PRINT : NEXT J: PRINT  CHR$ (12); CHR$ (27);"
@": PR# Ø
 84Ø  HOME : VTAB (6): HTAB (12): PRINT "Re-initializing pr
ogram"
 85Ø  CALL 1ØØ2: GOTO 16Ø
 86Ø  END
 87Ø  REM  1Ø SEC INTEGRATION
 88Ø IN = Ø
 89Ø DLAY = .1
 9ØØ  FOR L = 1 TO (NN * 1Ø)
 91Ø  & AIØ:DTA = D%
 92Ø IN = IN + DTA
 93Ø D% = DLAY * 1Ø: &  TO 1
 94Ø  & TI1:T = D%
 95Ø  IF T <  > Ø THEN 94Ø
 96Ø  NEXT L
 97Ø  RETURN
 98Ø  REM  WAIT
 99Ø D% = WT * 1Ø: &  TO 1
 1ØØØ  & TI1:T = D%
 1Ø1Ø  IF T <  > Ø THEN 1ØØØ
 1Ø2Ø  RETURN
 1Ø3Ø LS = D(I) -  INT (D(I))
 1Ø4Ø US =  INT (D(I)) + 1 - D(I)
 1Ø5Ø  IF LS >  = US THEN D(I) =  INT (D(I) + 1)
 1Ø6Ø  IF LS < US THEN D(I) =  INT (D(I))
 1Ø7Ø  RETURN
```

APPENDIX G
Ion temperature program
- J. Bolton & L. Perkins

```
10  PRINT "THIS PROGRAM BY J. BOLTON AND L. PERKINS"
20  PRINT "WILL TAKE EXPERIMENTAL ION/ATOM RATIOS"
30  PRINT "AND CALCULATE A CORRESPONDING T(ION)"
40  PRINT "       1    CA          4    CD"
50  PRINT "       2    BA          5    ZN"
60  PRINT "       3    MG          6    SR"
70  GET G$: IF G$ = "" THEN 70
80  IF G$ = "1" THEN 630
90  IF G$ = "2" THEN 640
100  IF G$ = "3" THEN 650
110  IF G$ = "4" THEN 660
120  IF G$ = "5" THEN 670
130  IF G$ = "6" THEN 680
140  INPUT "ENTER EXCITATION TEMPERATURE";T
145 S = T
150  INPUT "ION/ATOM RATIO";I
160  INPUT "ELECTRON DENSITY";N
170 Y = G(1) * G(2)
180 J = (V(1) - V(2) + V(3))
190 K = J / T
200 M =  - 11600 * K
210 L =  EXP (M)
220 X = ((4.83E15) / (N)) * Y * (T ^ 1.5) * L
230  IF (I - X) > 20 THEN 470
240  IF (I - X) > 10 THEN 480
250  IF (I - X) > 5 THEN 490
260  IF (I - X) > 1 THEN 500
270  IF (I - X) > .1 THEN 510
280  IF (I - X) <  - 20 THEN 550
290  IF (I - X) <  - 10 THEN 560
300  IF (I - X) <  - 5 THEN 570
310  IF (I - X) <  - 1 THEN 580
320  IF (I - X) <  - .1 THEN 590
330  PR# 1
340  PRINT "FROM THE DATA ENTERED"
350  PRINT "TEMPERATURE ";S
360  PRINT "ION/ATOM RATIO ";I
370  PRINT "ELECTRON NUMBER DENSITY ";N
380  PRINT "THE EXPERIMENTAL TEMPERATURE IS ";T
390  PRINT "THE EXPERIMENTAL ION TO ATOM RATIO IS     ";X
400  PR# 3
410  PRINT "DO YOU WANT TO MAKE ANOTHER RUN?"
420  GET A$: IF A$ = "" THEN 420
430  IF A$ = "N" THEN 450
440  IF A$ = "Y" THEN 10
450  PRINT "GOOD BYE"
```

```
 460  END
 470 Z = 20: GOTO 520
 480 Z = 10: GOTO 520
 490 Z = 5: GOTO 520
 500 Z = 1: GOTO 520
 510 Z = .1: GOTO 520
 520 T = T + Z
 530  PR# 3
 540  PRINT "T=";T,"X=";X: GOTO 170
 550 Z = 20: GOTO 600
 560 Z = 10: GOTO 600
 570 Z = 5: GOTO 600
 580 Z = 1: GOTO 600
 590 Z = .1: GOTO 600
 600 T = T - Z
 610  PR# 3
 620  PRINT "T=";T,"X=";X: GOTO 170
 630 V(1) = 6.111:V(2) = 2.936:V(3) = 3.152:G(1) = 64.63:G(
2) = 1.495E -
     2: GOTO 140
 640 V(1) = 5.212:V(2) = 2.241:V(3) = 2.724:G(1) = 124.4:G(
2) = 1.028E -
     2: GOTO 140
 650 V(1) = 7.644:V(2) = 4.350:V(3) = 4.43:G(1) = 19.81:G(2
) = 3.721E - 2
     : GOTO 140
 660 V(1) = 8.991:V(2) = 5.420:V(3) = 5.470:G(1) = 14.39:G(
2) = 2.649E -
     2: GOTO 140
 670 V(1) = 9.391:V(2) = 5.800:V(3) = 6.130:G(1) = 10.06:G(
2) = 6.519E -
     2: GOTO 140
 680 V(1) = 5.692:V(2) = 2.692:V(3) = 3.040:G(1) = 76.40:G(
2) = 1.393E -
     2: GOTO 140
```

The vita has been removed from the scanned document